2004-01-22

Derivation of Moving-Coil Loudspeaker Parameters Using Plane Wave Tube Techniques

Brian Eric Anderson
Brigham Young University - Provo

DERIVATION OF MOVING-COIL LOUDSPEAKER PARAMETERS USING PLANE WAVE TUBE TECHNIQUES

by

Brian E. Anderson

A thesis submitted to the faculty of

Brigham Young University

in partial fulfillment of the requirements for the degree of

Master of Science

Department of Physics and Astronomy

Brigham Young University

December 2003

BRIGHAM YOUNG UNIVERSITY

GRADUATE COMMITTEE APPROVAL

of a thesis submitted by

Brian E. Anderson

This thesis has been read by each member of the following graduate committee and by majority vote has been found to be satisfactory.

_____	_____
Date	Timothy W. Leishman, Chair
_____	_____
Date	Scott D. Sommerfeldt
_____	_____
Date	Jonathan D. Blotter

BRIGHAM YOUNG UNIVERSITY

As chair of the candidate's graduate committee, I have read the thesis of Brian E. Anderson in its final form and have found that (1) its format, citations, and bibliographical style are consistent and acceptable and fulfill university and department style requirements; (2) its illustrative materials including figures, tables, and charts are in place; and (3) the final manuscript is satisfactory to the graduate committee and is ready for submission to the university library.

_____ _____

Date

Timothy W. Leishman
Chair, Graduate Committee

Accepted for the Department

_____

Scott D. Sommerfeldt, Chair
Department of Physics and Astronomy

Accepted for the College

_____

Earl M. Woolley, Dean
College of Physical and Mathematical Sciences

ABSTRACT

DERIVATION OF MOVING-COIL LOUDSPEAKER PARAMETERS

USING PLANE WAVE TUBE TECHNIQUES

Brian E. Anderson

Department of Physics and Astronomy

Master of Science

Small-signal moving-coil loudspeaker driver parameters are traditionally derived through electrical impedance measurement techniques. These parameters are commonly called Thiele/Small parameters, after Neville Thiele and Richard Small who are credited with developing industry-standard loudspeaker modeling techniques. However, because loudspeaker drivers are electro-mechano-acoustical transducers, it should be possible to measure their parameters in physical domains other than the electrical domain. A method of measuring loudspeaker parameters from the acoustical domain will be developed. The technique uses a plane wave tube to measure acoustical properties of a baffled driver under test. Quantities such as the transmission loss through the driver are measured for a driver placed in the tube using the two-microphone transfer-function technique. Models have been developed to curve fit the resulting data, from which small-signal loudspeaker

parameters are subsequently derived. This thesis discusses the acoustical measurement theory, apparatus, and system modeling methods (via equivalent circuits). It also compares measured parameters to those derived using electrical techniques. Parameters derived from both approaches are compared with reference values to establish bias errors. Sequential measurements are also compared to reveal random errors in the derivation processes.

ACKNOWLEDGMENTS

Many thanks are due to many people. I could not have completed this work without the help that was freely offered. Help was given throughout many stages of this research project.

- First I must thank my loving wife Angela who has been supportive of me throughout the project. She has also sacrificed much of her time to help me do some of the laborious tasks of this work. From mowing the lawns to bringing me dinners she has been my biggest support.
- Many thanks are due to Dr. Timothy Leishman who developed the original idea for this project. He has devoted a good portion of his busy schedule to assist me in this work. He has answered many questions I have had and given encouragement throughout. Thanks are also due to his understanding wife and family.
- Dr. Scott Sommerfeldt has answered many questions for me and has given me many good suggestions in areas of his expertise.
- Dr. Jonathan Blotter has also answered questions and advised me in the mechanical engineering aspects of this work.
- Wes Lifereth must be thanked for his advice and tutorials in assisting with wood working, and machining.

- Students who have helped and answered questions include: Garth Braithwaite, Xi Chen, Steve Davis, Gordon Dix, Ben Faber, Kent Gee, John Heiner, Laralee Ireland, Lance Locey, Sarah Rollins, and Heather Smith.
- Thanks are due to the Brigham Young University, Physics and Astronomy Department, which funded a large portion of this research project and provided facilities in which the measurements and processing were accomplished.
- Facilities were also used in the Mechanical Engineering Department of Brigham Young University.
- SoundTube Entertainment Inc. provided many drivers for this research study, of which, five were employed in this research study.
- Poll Sound, specifically Deward Timothy, provided the use of the LMS analyzer and various boxes used in the closed-box technique measurements.

TABLE OF CONTENTS

LIST OF TABLES

Chapter 8

Chapter 9

LIST OF FIGURES

Chapter 1

Chapter 2

Chapter 3

Chapter 4

Chapter 5

Chapter 6

Chapter 7

Chapter 8

GLOSSARY OF SYMBOLS

This glossary contains variables that are used repeatedly in the thesis.

B	Magnetic flux density in the driver gap
Bl	Motor strength or strength factor (the product of B and l)
c	Speed of sound in air (344 m/s)
C_{MS}	Mechanical compliance of driver suspension
e	Electrical voltage
f	Frequency, in Hz
f_c	Cutoff frequency for the first cross mode of the plane wave tube
f_0	*In vacuo* resonance frequency of driver
f_s	Free-air resonance frequency of driver
i	Electrical current
j	Imaginary number $\sqrt{-1}$
k	Wave number (ω divided by c)
l	Length of voice coil in magnet air gap
L_{VC}	Inductance of driver voice coil
M_{AR}	Effective acoustic mass loading seen by driver cone
M_{MD}	Moving mass of driver diaphragm assembly
M_{MS}	Moving mass of driver diaphragm assembly including air load
p_B	Blocked sound pressure

p_i	Sound pressure incident upon driver
p_r	Sound pressure reflected from driver
p_t	Sound pressure transmitted past driver
Q_{ES}	Electrical quality factor
Q_{MS}	Mechanical quality factor
Q_{TS}	Total system quality factor
R	Complex reflection coefficient
$R_{\max}$	Value of electrical resistance at resonance frequency
R_{MS}	Mechanical resistance of driver suspension
R_{MT}	Mechanical resistance of termination impedance
R_{VC}	DC resistance of driver voice coil
S	Cross-sectional area of plane wave tube
S_D	Effective radiating surface area of driver
TL	Transmission loss
U	Volume velocity, particle velocity multiplied by surface area
V_{AS}	Volume of air having the same acoustic compliance as the driver suspension
W_i	Sound power incident upon driver
W_t	Sound power transmitted past driver
x	Position in the plane wave tube
X_E	Electrical reactance of driver electrical system
X_M	Mechanical reactance of driver mechanical system

X_{MT} Mechanical reactance of termination impedance translated up to the back of the driver diaphragm

Z_{AR} Acoustic radiation impedance seen by driver

Z_{AT} Acoustic impedance of termination translated to the back of the partition

Z'_{AT} Acoustic impedance of termination translated to the back of the driver diaphragm including filtering effects due to magnet structure and frame

Z_E Electrical impedance of the driver voice coil

Z_M Mechanical impedance of the driver mechanical system

$Z_{M,BB}$ Mechanical impedance of a black box

Z_{MT} Mechanical termination impedance translated up to the back of the driver diaphragm

α Sound absorption coefficient

ρ_0 Ambient density of air ($1.21\ kg/m^3$)

τ Sound power transmission coefficient

τ_{CC} Closed-circuit transmission coefficient of driver under test

τ_{OC} Open-circuit transmission coefficient of driver under test

ω Angular frequency, in rad/s

CHAPTER 1

INTRODUCTION

1.1 Moving-Coil Loudspeakers

Moving-coil loudspeaker drivers have been in use for several decades. They were originally invented by Kellogg and Rice (circa 1920) [1]. A cutaway view of a moving-coil loudspeaker driver typical of modern designs is shown in Fig. 1.1. A cross-sectional diagram is shown in Fig. 1.2. The behavior of a driver is governed by basic principles of physics. An alternating current is supplied to the leads of the driver. These leads are connected to a wire that wraps around a coil former, creating what is known as the voice coil. The coil has an electrical resistance and inductance associated with it. It is positioned within the gap created between a hollow cylindrical magnet (e.g., north pole) and a solid cylindrical pole piece (e.g., south pole). The latter is located within the hollow coil former. Current applied to the voice coil flows in a circular direction around the windings. The magnet structure provides magnetic flux through the coil with field lines running perpendicular to the direction of current flow.

As is well known in the study of electromagnetism, if a current flows in the presence of a magnetic field, a Lorentz force is created. When applied to the geometry of a moving-coil loudspeaker driver, the orthogonally oriented Lorentz Force simplifies to the product of the effective magnetic flux density, the effective length of the coil in the field, and the current flowing in the coil. Since the applied current alternates, the Lorentz force likewise alternates, causing the voice coil (and anything attached to it) to oscillate in an analogous manner.

The voice coil is attached to the former, which is attached to a cone or diaphragm. This diaphragm assembly is held in place by a suspension system that centers the voice coil in the magnet gap. Suspension systems typically consist of two separate flexible components: the surround and the spider. These spaced components serve to constrain the cone vibrations to motion along a single axis and supply a restoring force to return the cone to its rest position. The suspension system has a compliance and resistance associated with it. The cone, coil former, voice coil, parts of the suspension system, and lead wires ideally move in phase as lumped elements with a certain effective mass. Oscillations of the cone produce fluctuations in air pressure that radiate away from the driver as sound waves.

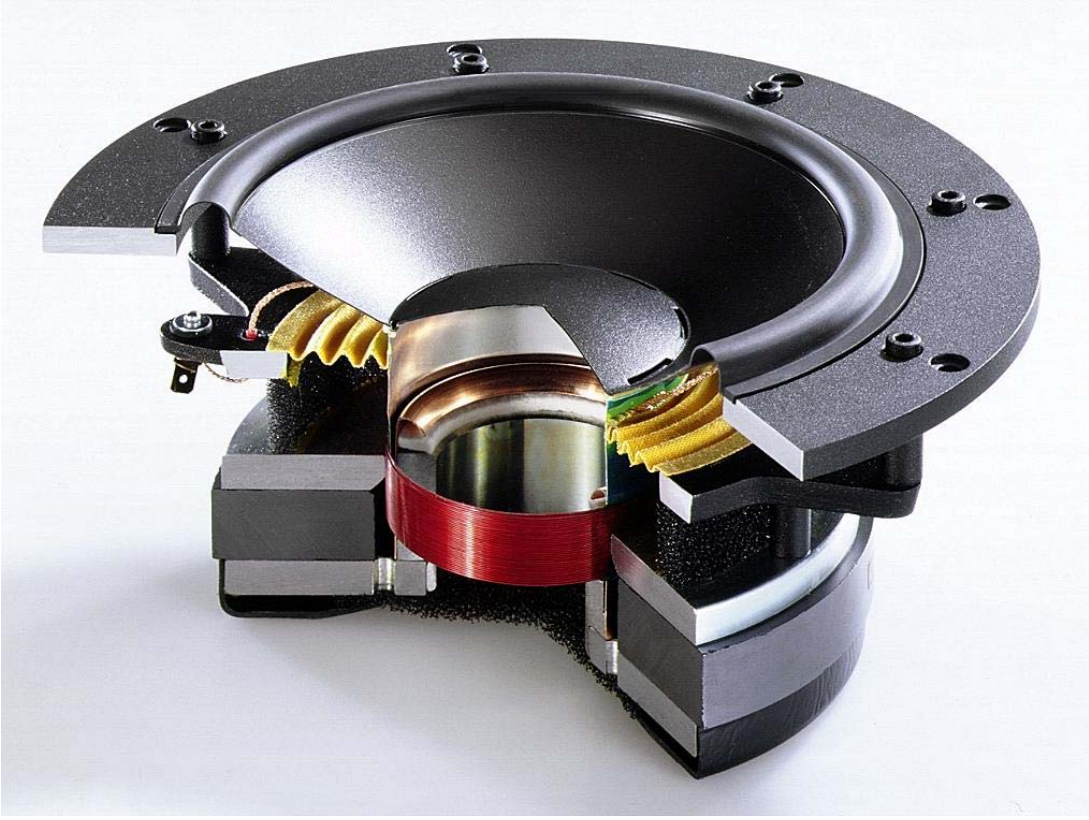

Fig. 1.1. Cutaway view of a typical moving-coil loudspeaker driver. Figure used with permission from www.flexunits.com.

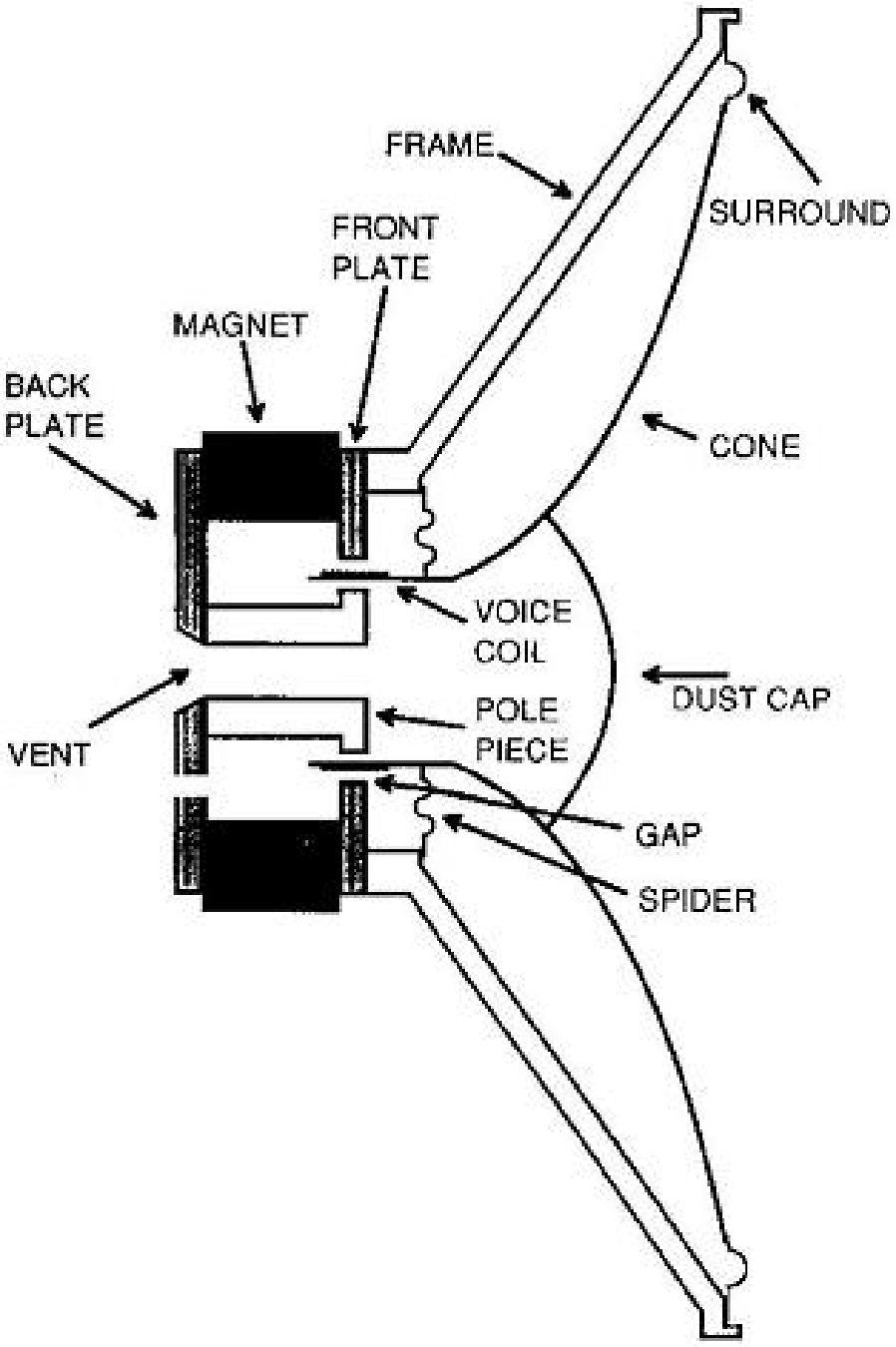

Fig. 1.2. Cross-sectional view of a typical moving-coil loudspeaker driver. Reprinted, with permission of Amateur Audio Press, from *The Loudspeaker Design Cookbook*, Sixth Edition, 2000, by Vance Dickason, p. 3 . © Copyright 2000 by Vance Dickason, Audio Amateur Corporation, P.O. Box 876, Peterborough, NH 03458, USA. All rights reserved.

1.2 Brief History of Moving-Coil Loudspeaker Modeling Development

Moving-coil loudspeaker drivers have been studied for years. McLachan first developed equations governing moving-coil loudspeakers in the 1930s [2]. In the 1940s, Olson presented analogous circuits that represent the multiple domains of the moving-coil driver [3]-[4]. Later, in 1954, Beranek furthered the developments of Olson in his development of a partial solution to the response of a bass-reflex loudspeaker system [5, p.239]. In 1958, Novak presented a generalized theory on the design and performance of vented and closed-box loudspeaker enclosures [6]. However, Thiele is generally thought of as the first to develop a complete synthesis procedure for direct radiator loudspeakers. Thiele's work was initially published in the 1961 Proceedings of the Institution of Radio Engineers [7]. It was then reprinted in the 1971 Journal of the Audio Engineering Society (*JAES*). Between 1968 and 1972, Benson [8] published a series of papers building on previous work. Work done by Benson was not well known until Small referenced his work. Small published papers [9]-[11] in the internationally published *JAES*, which brought recognition to both Benson's and Small's efforts [9]-[11].

A fundamental set of parameters that describe the lumped element model of a moving-coil loudspeaker have been given the name *Thiele/Small Parameters* in recognition of their work. Knowledge of these parameters is essential in the design of complete loudspeaker systems [12], [13]. A more complete history of the development of moving-coil loudspeakers may be found in *Testing Loudspeakers*, by D'Appolito [14, p.9].

1.3 Electrical Impedance Measurement Techniques

The parameters of moving-coil loudspeaker drivers have traditionally been characterized through the electrical impedances measured at their terminals. Determination of all mechanical parameters requires one to also measure this impedance under a perturbed condition. Alternatively, the simultaneous measurement of cone velocity or the use of optimization techniques is required. Despite the drawbacks of using both unperturbed and perturbed impedance curves, the perturbation technique continues to be the most commonly used method for determination of mechanical parameters. The most common types of perturbed measurement conditions are the added-mass technique and the closed-box technique [7], [10], [12]-[24].

If one employs simultaneous cone velocity measurements, the sensors that may be used include accelerometers, laser vibrometers, and microphones [25]-[28]. Techniques have also been developed to allow driver parameters to be measured using only an unperturbed electrical impedance curve [29]-[34].

Examples of parameter extraction methods include the three-point method, impedance magnitude curve fitting, complex impedance curve fitting, system identification, and nonlinear optimization. A more complete discussion of methods related to electrical impedance measurements and their limitations may be found in Chapter 3.

1.4 Electro-Mechano-Acoustical Devices

Fortunately, because drivers are electro-mechano-acoustical transducers, they should not only allow electrical interrogation, but should lend themselves to acoustical

interrogation. It is well known that many acoustical materials may be characterized by impedance, reflection, transmission, and absorption properties when plane waves are incident upon their surfaces. If a surface terminates a plane wave tube, these characteristics may be found using a two-microphone technique that decomposes the adjacent one-dimensional sound field into incident and reflected components. Properties of drivers incorporated as bounding surface elements of plane wave tubes could therefore be derived from field characteristics they produce under different conditions (e.g., with open or closed circuits). Because electrical conditions are easily controlled and automated, this unique application of plane wave tube measurements should provide an important option in the practical characterization of drivers.

1.5 Capabilities of a Plane Wave Tube

It has been shown that if a mechano-acoustical filter is placed between a plane wave source tube and an anechoically terminated receiving tube, several of its acoustical properties may be ascertained from the measurement and decomposition of the source and receiving tube fields [35]-[41]. Knowledge of these incident and reflected components allows derivation of several important quantities: incident and reflected pressures, particle velocities, intensities, sound powers, energy densities, acoustic impedances, etc. Reflection and transmission coefficients may also be determined, along with frequency-dependent driver impedance data.

An ideal anechoic receiving space has only a transmitted component of sound. However, if an anechoic termination provides insufficient absorption at the lowest frequencies of interest, the receiving space sound field may also be decomposed.

1.6 Moving-Coil Driver Characterization

If a moving-coil loudspeaker is to be tested in a plane wave tube transmission loss arrangement, it must typically be mounted in a baffle, then inserted between a source tube and receiving tube. This arrangement may also be conveniently modeled using an equivalent circuit. If the loudspeaker driver does not fill the cross section of the tube, the impedance of the baffle must also be included in the circuit. However, this unnecessarily complicates matters. If the impedance of the baffle is very large (i.e., if the baffle is nearly rigid), the circuit reduces to a very manageable form. Using basic circuit analysis techniques, expressions can be derived in terms of standard plane wave tube measurement quantities. However, many Thiele/Small parameters must be obtained by curve fitting measured data to match analytical expressions.

1.7 Effectiveness of Techniques

The effectiveness of the plane wave tube measurement technique will be evaluated by comparing parameters derived by the technique to those derived by several electrical impedance measurement techniques. In addition, it will also be evaluated by comparing some of the parameters to those derived through more direct procedures. Reference parameter values are used to determine bias errors of the various techniques. Mason *et al* explained that relative standard deviation may be a useful quantity in determining random errors: "Occasionally several data sets of similar requirements are to be compared and the relative magnitudes of the standard deviations provide valuable information on differences in variability of the processes that generated the data sets"

[42]. Random errors are thus determined by the relative standard deviation of parameters determined over consecutive measurement runs.

Many drivers are studied to determine the effectiveness of each technique as a function of driver size (see Fig. 1.3).

Fig. 1.3. Photograph of the nine drivers used in the research study.

Table 1.1 contains a few characteristic values for the nine drivers. The drivers are numbered according to their effective radiating surface areas.

Driver	Effective Diameter (cm)	Surface Area (m^2)	DC Resistance (ohms)
1	24.7	0.04792	4.666
2	20.9	0.03431	3.2194
3	16.8	0.02217	5.8692
4	16.5	0.02138	6.585
5	16.5	0.02138	6.151
6	16.5	0.02138	6.204
7	13	0.01327	6.3455
8	8.7	0.00594	5.8407
9	6.2	0.00302	6.872

Table 1.1. Characteristics of each of the nine drivers under test. The effective cone diameter of each driver was determined including half the surround with the cone diameter. The surface area S_D was computed from the measured diameters. Finally, the DC resistance R_{VC} of the each driver voice coil is given in ohms.

1.8 Objectives

The goal of this research was to develop a procedure for the determination of moving-coil loudspeaker parameters using plane wave tube techniques. A model is that allows analytical expressions to be derived for parameter estimation from plane wave tube data. Parameters derived from plane wave tube techniques are compared to parameters derived from several electrical impedance measurement techniques. It was anticipated that parameter estimates from both types of techniques would give comparable results. Reference values are determined to aid in the comparison study. Comparison of relative bias errors and random errors demonstrate the effectiveness of the plane wave tube parameter estimations.

1.9 Plan of Development

The chapters in the thesis will proceed as follows. Reference parameter values will be discussed in Chapter 2. Chapter 3 will discuss the theory of parameter measurements using electrical impedance techniques. Chapter 4 will present experimentally determined values for some of these techniques. A discussion of basic

plane wave tube theory and practical applications will be given in Chapter 5. Development of equivalent circuit models for a driver mounted in a plane wave tube transmission loss configuration will be given in Chapter 6. Chapter 7 will discuss the theory of driver parameter derivations using transmission loss measurements. Chapter 8 will discuss experimental aspects of the parameter derivations and present experimentally determined values. Chapter 9 will compare results of reference values, electrically determined parameters, and acoustically determined parameters. Chapter 10 will provide conclusions and present recommendations for future research in plane wave tube measurement techniques.

CHAPTER 2

REFERENCE PARAMETER MEASUREMENTS OF MOVING-COIL LOUDSPEAKER DRIVERS

In order to characterize the effectiveness of both electrical impedance parameter measurements and acoustical plane wave tube parameter measurements, reference parameter values must be determined directly if possible. However, many parameters do not lend themselves to practical direct measurement. For example, the moving mechanical mass M_{MD} cannot be measured directly unless one destructively detaches the moving cone system and weighs it. Similarly, the magnetic strength factor Bl cannot be measured directly unless one disassembles the moving coil system then measures the magnetic field in the magnet gap and the voice coil length in the gap. Even then, the effective values of B and l are difficult to surmise because of field line fringing. Furthermore, the mechanical resistance R_{MS} of the driver suspension system cannot be directly measured in a simple fashion. This chapter discusses direct measurements taken to produce reference values for the static mechanical suspension compliance C_{MS} and the moving mass M_{MD}.

2.1 Static Mechanical Compliance of the Driver Suspension System

The mechanical compliance parameter C_{MS} (or V_{AS}, which is the volume of air having the same acoustic compliance as the driver suspension system) is the most difficult parameter to measure using electrical impedance measurement techniques [24], [27], [33], [43]-[46]. Notably, V_{AS} is sensitive to measurement conditions such as

temperature, atmospheric density, and driver orientation [14, p.22 and p.27], [43], [47]. Furthermore, some authors have shown that the value for the static compliance of the suspension system is different than a value obtained using dynamic determination methods (through the driver resonance frequency) [15], [46, Fig.1]. The difference between static and dynamic values for C_{MS} is apparently due to suspension creep and hysteresis effects [24], [27], [33], [43]-[46]. Reference values for static compliance were determined as part of this work to verify this effect.

Ashley and Swan suggested a method to determine mechanical compliance of a driver suspension system from the displacement of a cone when a known force is applied to it [48]. In order to displace the cone enough to get accurate readings with a vernier caliper, they had to apply a significant load. Others have used similar types of measurement procedures [5, p.230], [12], [45].

2.1.1 Measurement Theory

The cone and suspension system of a moving-coil loudspeaker driver may be modeled as a simple mass-spring system. If a loudspeaker is oriented with its cone facing upward, the sum of the forces acting on the cone yields the following equation:

$$\sum F_y = -M_{MD} g + \frac{y_{rest}}{C_{MS}} = 0, \tag{2.1}$$

where F_y represents a generic force in the y direction, g is the acceleration due to gravity, and y_{rest} is the rest position.

The static compliance may be easily determined by adding a known load to the cone then accurately assessing the resulting displacement. For example, if a known mass

were placed on the cone, the resulting displacement would be due only to the added weight. The new sum of forces (not including the equilibrium forces) would allow for determination of the static suspension compliance as follows,

$$\sum F_y = -M_{add} g + \frac{y_{add}}{C_{MS}} = 0 \tag{2.2}$$

or

$$y_{add} = C_{MS} g M_{add} \tag{2.3}$$

where M_{add} is the mass added, and y_{add} is the resulting shift in position from the original rest position.

If M_{add} varies, a plot of y_{add} versus gM_{add} should yield a straight line with C_{MS} as the slope of that line. As long as the added masses are small enough that the suspension remains in its linear compliance region, one may thereby determine static C_{MS} for the driver under test. However, it should be noted that an accurate value for acceleration due to gravity must be used to instill confidence in such static compliance measurements.

A graph for determination of local acceleration due to gravity was obtained from a formula given by Moreland [49]. One only needs to know the north latitude (φ) and the elevation (H) relative to sea level of their position to obtain a value for local gravity to 0.01% accuracy:

$$g\left(m/s^2\right) = 9.780556\left[1 + 0.0052885\sin^2(\varphi) - 0.0000059\sin^2(2\varphi)\right] - 0.0000020H \tag{2.4}$$

The north latitude of Provo, Utah is 40.2°, and its elevation is 1370m. Using these values in Eq. (2.5) yields the following value for local gravity: $9.7993 \pm 0.00098\, m/s^2$.

2.1.2 Experimental Apparatus and Procedure

A Brown and Sharpe Coordinate Measurement Machine (CMM) was used to help experimentally determine the static suspension compliances for the drivers under test. A photograph of the apparatus is shown in Fig. 2.1. The CMM has a Renishaw SP600M probe head with a 2mm Renishaw probe stylus made of sapphire. The CMM is normally used for highly accurate x-y-z coordinate measurement of machined parts. The probe stylus is maneuvered using a joystick. Measurement points are recorded when the probe stylus encounters a boundary surface. However, the probe stylus must encounter a sufficient, user-defined triggering force for a measurement point to be recorded.

Special aluminum weights were machined in order to apply evenly distributed loads to the cones of the drivers under test. They were essentially aluminum cylinders with one end closed (i.e., in the form of inverted cups). The cylinders were designed to spread the mass load symmetrically around the diaphragm above the voice coil (see Figs. 2.2 and 2.3). The triggering force of the CMM was applied at a point in the center of the closed end of the cylinder. A triggering force of 0.2 N was judged to be sufficient for static suspension compliance determination. The distribution of forces produced by the cylinders thus prevented unwanted deflection of the driver dust caps that would have resulted from force concentrations, causing misleading results in overall cone displacement measurements. Other cylindrical test weights were added to the arrangement to produce grater displacements while allowing the probe stylus to trigger off of the original reference point on the closed end of the inverted cup mass (see Fig. 2.4).

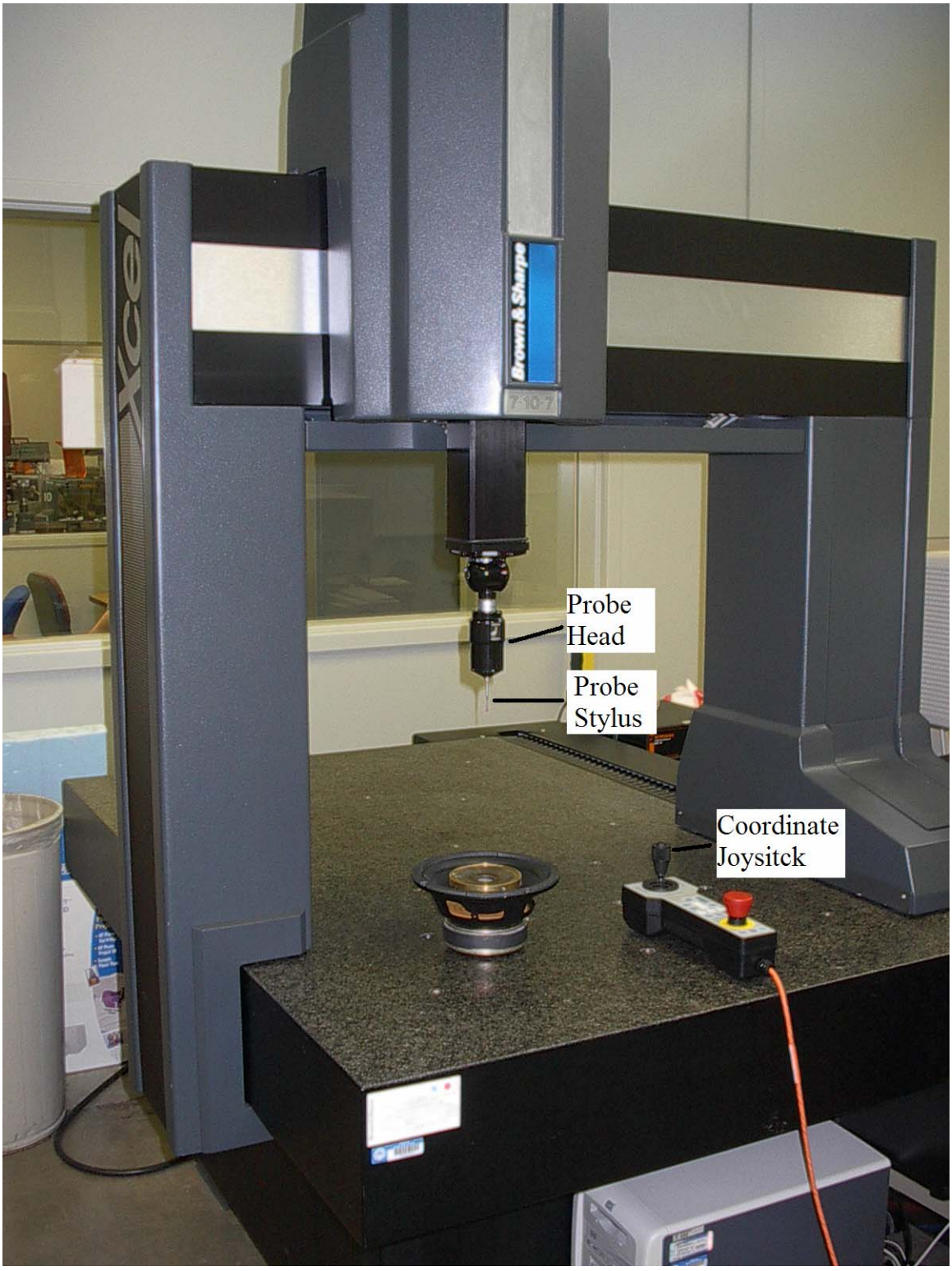

Fig. 2.1. Photograph of the Brown and Sharpe CMM with a sample driver under test. The CMM was used to determine static compliance estimates using force versus displacement data.

Fig. 2.2. Photograph of a sample driver under test.

Fig. 2.3. Photograph of the aluminum cylinder placed on the driver under test. The cylinder provided an even load distribution to the driver diaphragm.

Fig. 2.4. Photograph of an additional known weight, which results in a measurable displacement using the CMM. The added weight contains a hollow center allowing a point of reference to be maintained.

Various cylindrical weights were placed on the inverted cup and displacement measurement points were recorded for each addition. The masses of the applied test weights were known to within a hundredth of a gram. The triggering force of 0.2 N was accounted for in the cone loading. An attempt was made to apply equal increments of weight and to stay within the linear region of the suspension compliance.

As indicated above, the static suspension compliance may be determined by curve-fitting the slope of gM_{add} vs. y_{add} data. A sample plot for one of the drivers under test (driver #1) is shown in Fig. 2.5. Plots for the other drivers are also very linear, and result in low statistical deviation. Compliance values for each of the drivers under test and the relative uncertainties [50] of each data set are listed in Table 2.1. Due to the additional displacement from equilibrium caused by the inverted cup weights, an accurate

determination of the unloaded rest position could not be obtained. However, this does not create a problem since the additional weights were applied in the linear region of the suspension compliance, resulting only in an offset shift of the weight versus displacement lines (i.e., not affecting the slope of the line). These static values for suspension compliance are included in the comparisons made in Chapter 9, but were not used as reference values because of the inherent difference between statically and dynamically obtained compliance estimates [15], [46, Fig.1].

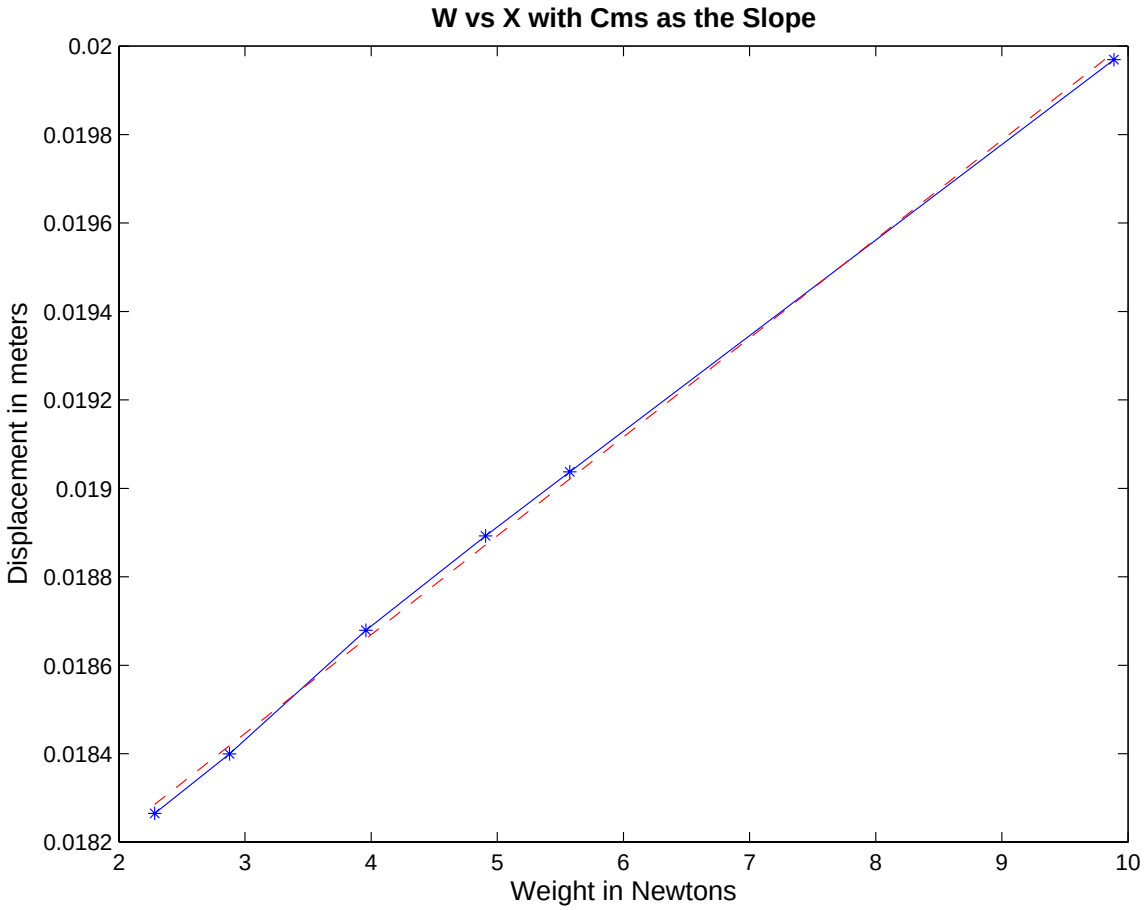

Fig. 2.5. Example force versus displacement data (*) taken from the CMM, along with the curve fit line (dashed line) for driver #1.

Driver	Static Cms	Correlation Coeff.	% Relative Uncertainty
1	223.664	0.9994	1.67
2	1035.46	0.9997	1.50
3	846.989	0.9919	6.41
4	508.421	0.9954	4.83
5	522.092	0.9971	3.78
6	505.334	0.9909	6.78
7	793.906	0.9996	1.42
8	622.762	0.9970	3.86
9	659.631	0.9985	2.74

Table 2.1. Table of static C_{MS} ($\mu m / N$) values, determined by using curve fitting force versus displacement data from the CMM. Associated statistical uncertainties in the curve fit are also included.

2.2 Mechanical Moving Mass of the Driver Suspension System

The most straightforward physical method to determine the mechanical moving mass of the diaphragm assembly is to weigh the assembly directly [15], [27]. However, in this process, an important question must be addressed: how much of the suspension and lead wires should be included in the measurement? When the diaphragm vibrates, do half of the surround, spider, and lead wires effectively move in unison with it? Clark suggests that half of the suspension system should be included [27]. However, to be certain, one could destructively remove the diaphragm assembly with its entire suspension system and lead wires. The mass of the complete assembly would then represent an upper limit to the allowable moving mass value. On the other hand, if all of the suspension system and lead wires were cut off (so that only the cone, voice coil former, voice coil, dust cap, and adhesives remained), the reduced mass would represent the lower allowable limit.

This destructive measurement technique has significant value for establishing basic reliability of the various parameter measurement techniques. If an electrical measurement technique or the plane wave tube technique fail to yield a moving mass

value that falls between the established upper and lower limits, the method has been shown to produce an unreliable estimation and should only be used with reservation.

Figures. 2.6 and 2.7 demonstrate how the five drivers were disassembled for the moving mass destructive evaluation technique. The upper and lower mass limits are shown for the five drivers under test in Table 2.2, along with the masses of their surrounds, spiders, and lead wires. The estimated moving mass of each complete assembly, including one half or one third of the mass of its surround, spider and lead wires is also included in the table.

Fig. 2.6. Photograph of cone assemblies and suspension system pieces of drivers used in the destructive evaluation technique for M_{MD}.

Fig. 2.7. Photograph of driver frames and magnet structures remaining after the destructive evaluation technique.

Driver Number	Upper Limit	Lower Limit	Surround	Spider	Lead Wires	1/2 Assembly	1/3 Assembly
1	174.42	124.53	43.22	6.21	0.44	149.48	141.16
3	27.37	19.4	7.19	0.67	0.12	23.39	22.06
7	9.95	6.76	2.03	0.85	0.32	8.36	7.82
8	4.16	2.96	0.77	0.33	0.09	3.56	3.36
9	2.25	1.77	0.25	0.18	0.05	2.01	1.93

Table 2.2. Measured values for moving mass M_{MD} (gm) using destructive evaluation. Upper and lower limits include the diaphragm assembly with and without the suspension system and lead wires respectively. Values are also given for the mass of various parts of the drivers under test. Values for moving mass estimates, which include one half and one third of the suspension system are also given.

CHAPTER 3

ELECTRICAL IMPEDANCE MEASUREMENTS: THEORETICAL BASIS

This chapter discusses moving-coil loudspeaker driver modeling and challenges encountered in parameter derivations based on electrical measurements. It provides an explanation of the original three-point parameter derivation method, an explanation of a procedure developed by Garrett, and a brief description of other electrical impedance techniques. While loudspeaker driver modeling has been relatively consistent for decades, experimental aspects of parameter derivations have been inconsistent, to the point that researchers often state conflicting conclusions. The chapter will conclude with a description of perturbation techniques, velocity sensing techniques, and optimization techniques.

3.1 Moving-Coil Loudspeaker Driver Modeling

A moving-coil loudspeaker driver can be modeled to a first approximation with lumped-parameter characteristics and with coupling between the electrical, mechanical, and acoustical domains. Equivalent circuits are most commonly used for this type of modeling, with transformers and gyrators representing the coupling [13], [51], [52, p.1-48]. Coupling between the electrical domain and the mechanical domain is due to the alternating Lorentz force acting on the voice coil. Coupling between the mechanical and acoustical domains is due to the motional coupling of the cone and the air adjacent to the cone.

The voice coil of a driver is initially modeled as a resistor R_{VC} in series with an inductor L_{VC} in the electrical impedance analogy. The diaphragm and suspension system are modeled in the mechanical mobility analogy as a damped mass-spring system (with mass M_{MD}, compliance C_{MS}, and resistance R_{MS}). The radiation loading Z_{AR} on the cone of the driver is represented in the acoustic impedance analogy. A multiple-domain equivalent circuit representation [12], [20], [52, p.6-2] of a moving-coil driver combines these analogies as shown in Fig. 3.1. (The circumflex mark over the voltage and current variables denotes a complex frequency-domain signal amplitude.)

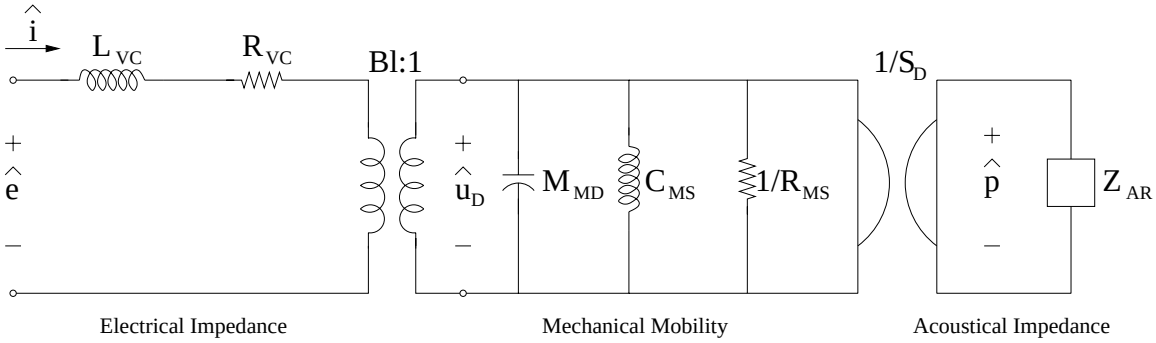

Fig. 3.1. Multiple-domain equivalent circuit representation of a moving-coil loudspeaker driver. (Refer to the Glossary of Symbols.)

This circuit can be simplified to a single-domain representation by carrying the acoustic radiation impedance through the area gyrator into the mechanical mobility analogy then carrying the mechanical mobility elements through the transformer into the electrical impedance analogy. The result is shown in Fig. 3.2.

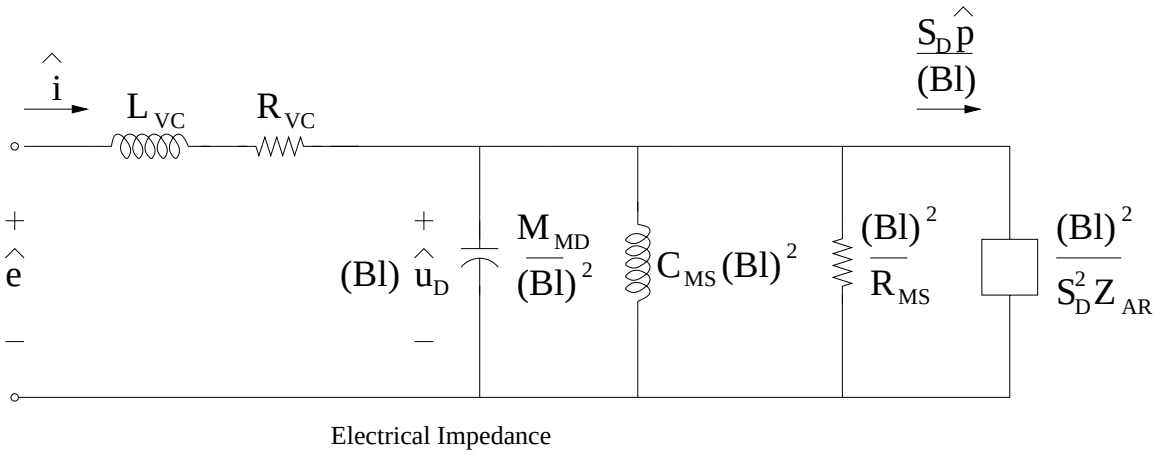

Fig. 3.2. Electrical impedance representation of a moving-coil loudspeaker driver.

The radiation impedance may be modeled as a radiation mass loading M_{AR} plus a radiation resistance R_{AR}. Combining the radiation mass loading with the moving mass yields an effective moving mass [5, p.122], [14, p.12], [47, p.160]

$$M_{MS} = M_{MD} + S_D^2 M_{AR} = M_{MD} + \frac{8}{3}\rho_0 \left(\frac{S_D}{\pi}\right)^{1.5}, \tag{3.1}$$

which may be represented as shown in Fig. 3.3.

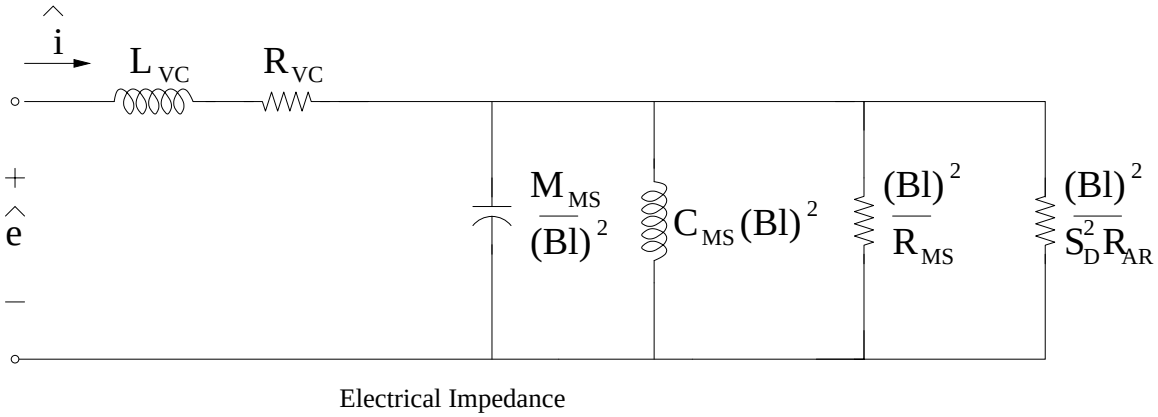

Fig. 3.3. Equivalent circuit for a loudspeaker driver with the fluid mass loading combined with the physical moving mass to form M_{MS}.

Since at low frequencies the reactance due to the inductance of the voice coil ($X_E = j\omega L_{VC}$) is very small when compared to the resistance of the voice coil, it is common to neglect its value [7], [13], [15], [26], [32]-[33]. This step makes it easier to determine the mechanical parameters.

3.2 Overview of Electrical Impedance Measurements

Unfortunately, the electrical measurement process can be time consuming and problematic. Bias errors for a given parameter have been shown to be as great as 10% between the two perturbation techniques [53]. Measured parameters can be quite sensitive to the exact setup configuration employed. Measurements should not be made in noisy environments with high background levels [14, p.18], [24, p.303]. Measurements should ideally be made in a free-field environment to agree with assumptions made in circuit modeling [5, p.229], [18], [25], [31]. The orientation of the driver (horizontal or vertical) can also affect the accuracy of derived parameters [12], [14, p.22], [24, p.303], [46]. Some authors have stated that altitude can affect derived parameters [12], [14, p.27] while others believe that altitude has no effect [53]. Some have stated that parameter values depend upon whether the suspension has been "broken in" or not [14, p.17], [27], [47]. In short, derived parameters are expected to vary according to the specific procedures used in the electrical measurements [27], [43], [46], [53].

Due to electroacoustic reciprocity, a moving-coil loudspeaker driver also acts as a receiver. Pressure fluctuations created by background noise will affect the motion of the cone. Because electrical impedance measurements are generally made in the small-signal

domain, background noise can have a significant effect on a driver under test. Large background noise levels near the resonance frequency of the driver under test could result in particularly troubling errors in the determination of its resonance frequency.

The circuit modeling in Section 3.1 assumes that the frame of the driver under test is rigidly mounted without a baffle or enclosure and that the diaphragm radiates into a free field. However, it is a difficult matter to simultaneously produce rigid mounting and a free-field condition during impedance measurements. Some authors have suggested using a large room for impedance measurements with the driver far from reflecting surfaces [14, p.16], [24, p.303], [47, p.156]. This suggestion also assumes that one can create a setup that allows the frame of the driver under test to be held rigidly without creating undesirable baffling effects.

The orientation of the driver under test may cause a shift in measured parameter values. When a driver axis is oriented vertically, the cone has a different rest position than when its axis is oriented horizontally (see Fig. 3.4). The shift in the cone rest position is due to the force of gravity acting on the cone assembly. Although such a shift is insufficient to displace a cone assembly out of its linear C_{MS} region, it can be sufficient to notably affect the force factor *Bl*. Such variation of the force factor should be considered when performing impedance measurements.

Fig. 3.4. The orientation of the driver under test with its axis vertical (left) and horizontal (right). Driver photos used with permission from the Sonicraft line of drivers offered by Madisound Speaker Components.

3.3 Determination of Moving Mass and Suspension Compliance

Several types of electrical measurement procedures have been used to derive driver parameters. One requires both a free-air impedance curve and a perturbation impedance curve (with a shift in the driver resonance frequency f_s). Another is to measure cone velocity simultaneously with impedance data to obtain necessary transfer functions. A third is to use complex optimization techniques on a single impedance curve. Despite the obvious advantages of the latter two techniques, the most common method is still the original perturbation method. The perturbation of the system typically results from the use of either the added-mass technique or the closed-box technique. The added-mass technique requires a known mass to be attached to the diaphragm of the driver under test, causing a downward shift in f_s. Some research suggests that non-magnetic weights should be used in the added-mass procedure [5, p.229], [18], [27]. Other research suggests that the added mass technique has inherent fundamental

problems [46], [53]. The closed-box technique requires the driver under test to be mounted onto a box of known volume (an acoustic compliance), causing an upward shift in f_s. Either technique leads to a solution for M_{MS} and C_{MS} from two equations and two unknowns.

In the past, authors have differed in their methods of dealing with the measurement of suspension compliance and moving mass. However, several agree that determination of the compliance cannot produce an accurate or repeatable resulting value, due to suspension creep and hysteresis [43], [45]-[46]. Many also state that accurate determination of suspension compliance is not critical to complete loudspeaker system performance [7], [11], [14, p.27], [54]-[55].

3.4 Original Three-Point Method for Parameter Derivation

Perhaps the most basic method to determine loudspeaker driver parameters is the original three-point method proposed by Thiele [7]. The method relies upon the accuracy of obtaining three points from an electrical impedance measurement: the resonance frequency, and the two half-power points above and below the resonance frequency. (The electrical impedance curve also has a characteristic rise at higher frequencies, due to the inductance of the voice coil.) Thiele's method requires both a free-air impedance measurement and a perturbation impedance measurement.

3.4.1 Linear Loudspeaker System Parameters

Measurement of certain moving-coil loudspeaker parameters (Thiele/Small parameters) is necessary for adequate representation of a linear driver system. These

include Bl, C_{MS}, L_{VC}, M_{MS}, R_{MS}, and R_{VC}, or alternatively f_s, L_{VC}, Q_{MS}, Q_{ES}, Q_{TS}, and V_{AS}, where Q_{MS}, Q_{ES}, and Q_{TS} are the mechanical, electrical and total quality factors, respectively. The first set of parameters are the same parameters that represent the linear driver system in the equivalent circuit model of Fig. 3.3. The second set of parameters, which contain the same information as the first set of parameters, are given by the relationships

$$f_S = \frac{1}{2\pi}\sqrt{\frac{1}{M_{MS}C_{MS}}}, \tag{3.2}$$

$$Q_{MS} = \frac{1}{2\pi f_S C_{MS} R_{MS}}, \tag{3.3}$$

$$Q_{ES} = \frac{2\pi f_S R_{VC} M_{MS}}{(Bl)^2}, \tag{3.4}$$

$$Q_{TS} = \frac{Q_{MS}Q_{ES}}{Q_{MS}+Q_{ES}}, \tag{3.5}$$

$$V_{AS} = \rho_0 c^2 C_{MS} S_D{}^2. \tag{3.6}$$

They are commonly used to describe a linear loudspeaker system [14, pp.9-36], [52, p.6-31b].

3.4.2 Free-Air Impedance Procedure

The electrical impedance magnitude is typically used for parameter estimation using the three-point method. The frequency where the electrical impedance magnitude is at a maximum (where mechanical impedance is at a minimum) is the resonance frequency. It is typically well below the inductance-controlled impedance magnitude rise. However, the resonance frequency may also be obtained from a negative-slope zero

crossing of the phase curve [15]. A typical numerical example of an electrical impedance curve is shown in Fig. 3.5.

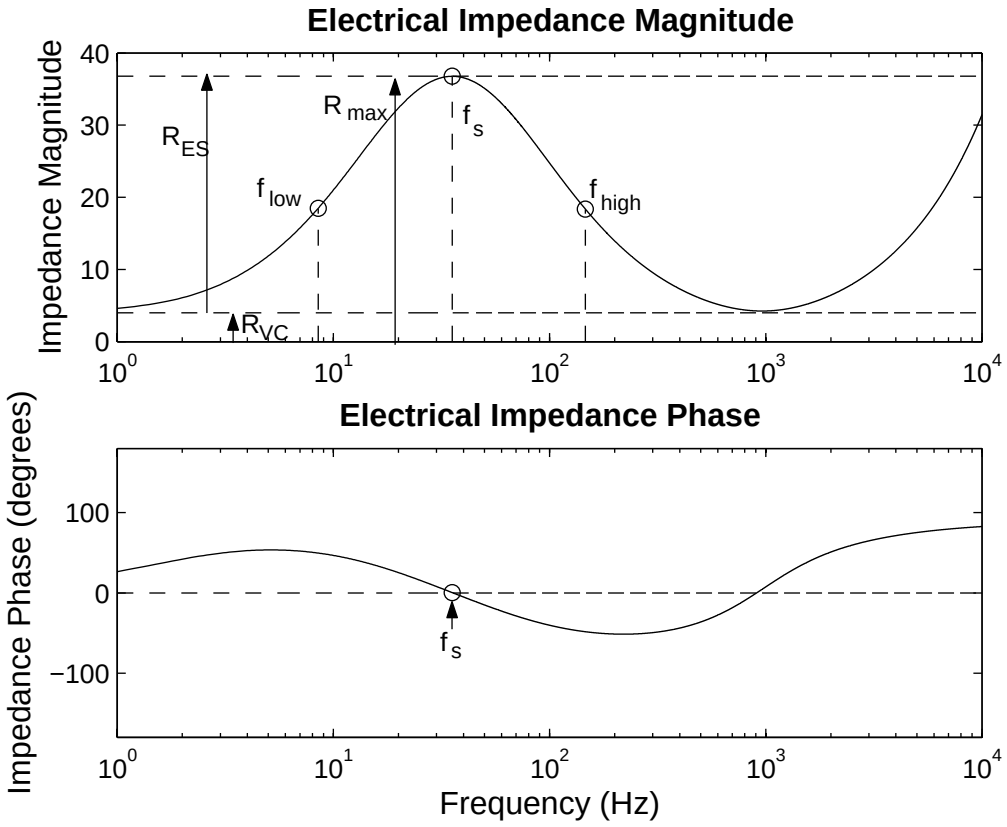

Fig 3.5. Numerically generated electrical impedance example. (Refer to the Glossary of Symbols.)

The derivation of parameters that follows closely follows the derivation given by D'Appolito [14, pp.9-36].

The DC resistance of the voice coil R_{VC} is usually measured separately using an ohmmeter. This value and the value at the impedance maximum $R_{\max}$ are used to determine the electrical parameter associated with the mechanical resistance

$$R_{ES} = R_{\max} - R_{VC} \tag{3.7}$$

where

$$R_{ES} = \frac{(Bl)^2}{R_{MS}}. \tag{3.8}$$

The value r_0 of the impedance magnitude at the half-power points is given by

$$r_0 = \frac{R_{\max}}{R_{VC}} = \frac{R_{ES} + R_{VC}}{R_{VC}} \tag{3.9}$$

Once these values are determined, the resonance quality factors (Q_{MS}, Q_{ES}, and Q_{TS}) may be obtained using the half-power frequencies f_{low} and f_{high}, and the half-power impedance magnitude:

$$Q_{MS} = \frac{f_S \sqrt{r_0}}{f_{high} - f_{low}}, \tag{3.10}$$

$$Q_{ES} = \frac{Q_{MS}}{r_0 - 1}, \tag{3.11}$$

$$Q_{TS} = \frac{Q_{MS} Q_{ES}}{Q_{MS} + Q_{ES}} = \frac{Q_{MS}}{r_0}. \tag{3.12}$$

3.4.3 The Added-Mass Technique

The added-mass technique requires that M_{MS} be determined first. The value of M_{MS} may be obtained through the measurement of the free-air impedance and the impedance with a known mass attached to the diaphragm of the driver under test (see Fig. 3.6):

$$M_{MS} = \frac{M_{ADD}}{\left(\frac{f_S}{f_S'}\right)^2 - 1} \tag{3.13}$$

where M_{ADD} is the added mass, and f_S' is the perturbed resonance frequency. The added mass causes a downward shift in the resonance frequency ($f_S' < f_S$).

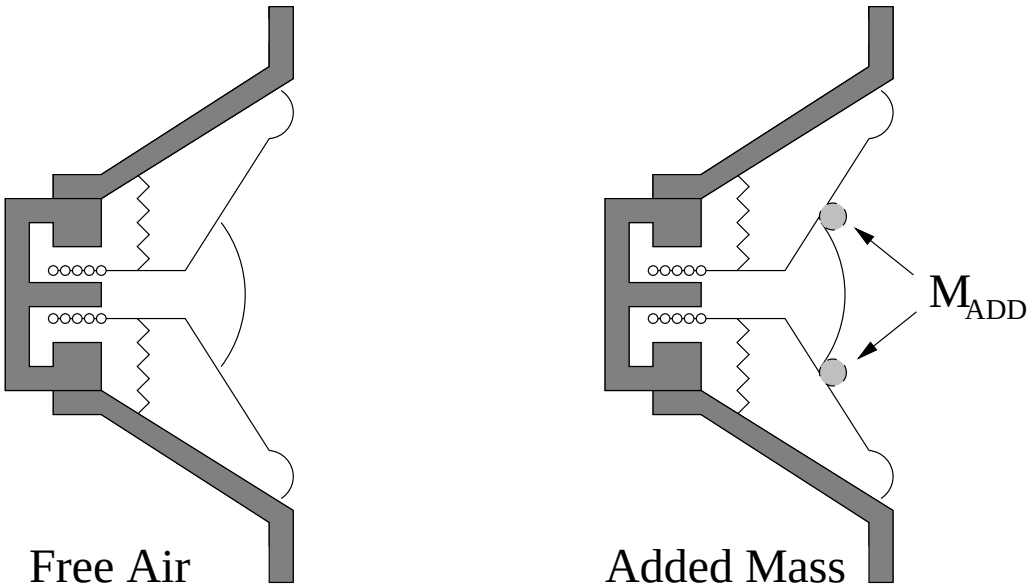

Fig. 3.6. Schematic drawing of the added-mass technique. The added mass in this example is mounted in a circle around the dust dome in an attempt to distribute the weight evenly. The added mass is represented by M_{ADD}.

Once M_{MS} is determined, the suspension compliance C_{MS} may be determined through the free-air resonance frequency:

$$C_{MS} = \frac{1}{(2\pi f_S)^2 M_{MS}}. \tag{3.14}$$

An estimation of S_D must be made in order to determine V_{AS}. It maybe predicted by measuring the diameter of the cone and including part of the surround to determine the effective cone diameter. By convention, some researchers include half of the surround [14, p.28] while others use only one third [27], [56]. The value of V_{AS} also depends on the ambient density of air and the speed of sound in air:

$$V_{AS} = \rho_0 c^2 C_{MS} S_D^2 . \tag{3.15}$$

The added mass should be chosen and mounted carefully so that the mass moves with the same velocity and phase as the driver cone and that any residue from the added mass material is limited (e.g., if one were using clay).

3.4.4 The Closed-Box Technique

If one is using the closed-box technique, the driver under test is mounted onto a test box of known volume V_B. The V_{AS} is then determined using the following equation:

$$V_{AS} = V_B \left[\frac{f_S' Q_{ES}'}{f_S Q_{ES}} - 1 \right], \tag{3.16}$$

where f_S' is the perturbed resonance frequency ($f_S' > f_S$), and Q_{ES}' is the electrical quality factor of the perturbed impedance curve. The closed-box technique allows V_{AS} to be determined directly, without requiring measurement of S_D. However, depending on how the driver is mounted, V_B will be altered (see Fig. 3.7). If the driver is mounted with its magnet facing out of the box, an additional volume created by the cone must be accounted for. If the driver is mounted with the magnet facing into the box, the volume displaced by the frame and magnet structure, along with the volume displaced by the presence of the cone, must be accounted for. The exact determination of V_B may therefore be somewhat challenging. The value for M_{MS} may be determined through the use of Eqns. (3.14) and (3.15).

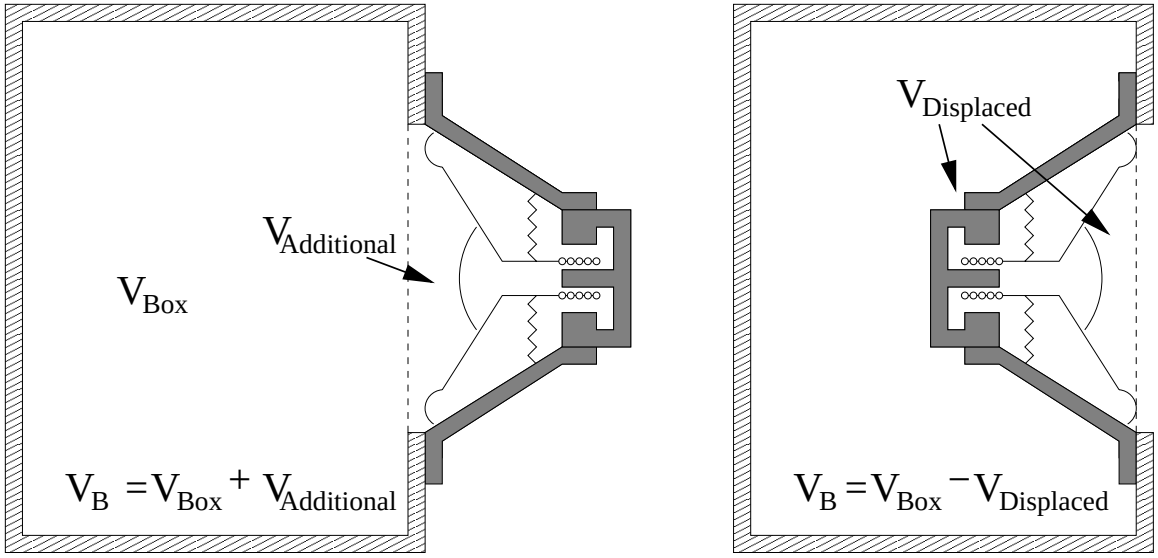

Fig. 3.7. Schematic drawing demonstrating how the box volume V_B must be modified according to how the driver under test has been mounted onto the box. The additional volume is represented by $V_{Additional}$ and the displaced volume is represented by $V_{Displaced}$.

3.5 Garrett Method (Incremental Mass Addition Method)

Because statically and dynamically measured stiffnesses differ, a dynamic measurement of compliance is necessary for driver characterization. While direct measurement of dynamic stiffness may be difficult to achieve, Garrett has developed an electrical test method that may serve as a useful basis for parameter comparisons [57]. The method is similar to that proposed earlier by Thiele and Small [7], [10]. It utilizes carefully measured shifts in driver resonance frequency (from an electrical impedance curve) as a function of the addition of known mass increments, which are mounted to a loudspeaker diaphragm. Linearizing the formula for the resonance frequency of a standard mass-spring system yields

$$f_S = \frac{1}{2\pi}\sqrt{\frac{k}{m_0}} \tag{3.17}$$

where m_0 is the effective moving mass of the diaphragm assembly, and k is the stiffness of the suspension system. A linear relationship exists between the square of the measured resonance periods, $T_i^2 = f_i^{-2}$ (where T_i represents the shifted resonance period, and f_i represents the shifted resonance frequency), and the added incremental masses m_i:

$$\frac{1}{f_i^2} = T_i^2 = \frac{4\pi^2}{k} m_i + \frac{4\pi^2}{k} m_0 . \tag{3.18}$$

A linear fit to this data then yields the desired compliance and moving mass parameters:

$$C_{MS} = \frac{1}{k} = \frac{\text{slope}}{4\pi^2}, \tag{3.19}$$

$$M_{MS} = m_0 = \frac{\text{intercept}}{\text{slope}}, \tag{3.20}$$

where M_{MS} equals m_0 under free-air loading conditions.

3.6 Other Electrical Methods Using Perturbation Techniques

There have been many modifications and improvements made to the original parameter derivation method proposed by Thiele [10], [12]-[24]. Some methods employ a curve fitting procedure to approximate the impedance magnitude, while other methods approximate the complex impedance. Methods have also been developed to utilize time domain measurements. Perturbation technique methods are commonly used in the audio industry by loudspeaker manufacturing companies and by hobbyists designing home loudspeaker systems. Some of the commercially available parameter derivation packages that employ perturbation techniques include DRA MLSSA, LinearX LMS, LinearX LEAP, CLIO, Goldline TEF, Ariel SYSid, and the Audio Precision System.

3.7 Electrical Methods that Do Not Require Perturbation Techniques

Perturbation technique methods are time consuming because they require two separate measurements of driver impedance. The accuracy of the derived loudspeaker parameters relies on accurate determination of added mass and S_D, or the volume of a closed box. The added-mass technique can potentially cause damage to a diaphragm assembly if one is not careful when attaching the added mass to the cone. If using the closed-box technique, one must ensure an airtight mounting seal between the driver and the test box. Due to these and other disadvantages, research has been conducted to develop parameter derivation methods that require only a single test run. In general, these methods fall under two categories: those requiring simultaneous measurement of cone velocity, and those utilizing optimization techniques.

3.7.1 Velocity Sensing Methods

While there are at least three types of velocity sensing parameter derivation methods, each method utilizes the same basic framework. They differ in the type of sensor employed. Sensors include accelerometers [25], laser velocity transducers [26]-[27], and microphones [28]. Each method utilizes combinations of transfer functions between cone velocity, voltage measured at the driver terminals, and current induced in the voice coil. The disadvantage of using an accelerometer is that the weight of the mounted accelerometer must be accounted for in the measurement. When using a microphone, the measurement has the potential to be corrupted by background noise. The laser velocity technique does not share these disadvantages. It has also been employed in the determination of non-linear parameters.

David Clark has developed a method for measuring loudspeaker driver parameters as a function of cone excursion [27]. He developed a setup wherein a driver may be rigidly mounted onto a pressure chamber. As the DC pressure is increased or decreased relative to atmospheric pressure, the cone is displaced. Parameters are derived through laser velocity sensing and electrical impedance techniques at various cone excursions. This allows one to determine the maximum excursion limitations of a given loudspeaker driver for linear operation.

3.7.2 Optimization Methods

Several different optimization methods have been developed that require only a single impedance measurement and do not require that diaphragm velocity be simultaneously measured [29]-[34]. Jain *et al* developed an optimization method for measurements in the time domain [29] as an extension of the work of Leach *et al* [13]. Jain *et al* also developed an optimization method using signal processing techniques [30]. Ureda developed an optimization method using nonlinear goal programming [31]. Nomura *et al* developed an optimization method using nonlinear least-squares optimization techniques [32]. Knudsen *et al* developed an optimization method using a system identification technique [33]. Finally, Waldman developed another optimization technique using nonlinear least squares estimation [34].

CHAPTER 4

ELECTRICAL IMPEDANCE MEASUREMENTS: EXPERIMENTAL RESULTS

This chapter briefly discusses the electrical impedance methods used in this study. The methods include those implemented in MLSSA, LMS, and LEAP, as well as the Garrett method and the three-point dual-channel FFT method. Photographs of some of the experimental setups will also be presented and discussed. Average parameter values will be presented for each driver under test.

4.1 Experimental Aspects of Electrical Methods

The various electrical methods were used to obtain parameter results for comparison with parameters derived later from plane wave tube measurements. The section describes various experimental aspects of each method.

4.1.1 MLSSA Parameter Measurements

The Maximum Length Sequence Signal Analyzer (MLSSA) is a PC-based hardware and software system developed by DRA Laboratories that incorporates a special Speaker Parameter Option (SPO). The SPO allows one to automate driver electrical impedance measurements, then derive loudspeaker parameters. As the name implies, MLSSA employs a maximum-length sequence signal in the measurement process. Its hardware is incorporated on an ISA PC card that contains a precision 1-Watt, 75.5 Ohm series resistor (accurate to 0.1%) in the connector interface. The precision resistor is used as a reference for the analyzer voltage divider setup. The user selects a

frequency range for the driver under test according to its estimated resonance frequency. To obtain reasonably accurate parameters, the frequency range should extend from DC up to approximately ten times the resonance frequency. The MLSSA system processes the complex driver impedance for the "unique set of driver parameters that result in the least squared error between the model and the measured driver impedance" [58, p.13].

4.1.2 LMS Parameter Measurements

The Loudspeaker Measurement System (LMS) is a PC-based analyzer developed by LinearX. It utilizes a 500 Ohm input impedance to create a voltage divider setup. According to the users manual, "The LMS software solves this voltage divider for the true load impedance of the speaker, automatically removing the effects of the LMS output impedance. This type of impedance measurement method is called *constant current*, since the driving impedance is relatively high. To enhance the accuracy of the measurement the shorted cable impedance can be measured first, and then subtracted from the speaker plus cable curve. . . ." [59, p.16-1]. The LMS user's manual also suggests that for precision parameter measurements, the 10 Hz to 40 kHz range should be used with 300 logarithmically spaced measurement points. Parameters are derived from the impedance magnitude using a numerical optimization procedure. The LMS system employs a stepped-sine signal in the measurement process.

4.1.3 LEAP Parameter Derivations

LinearX has also developed a software package known as the Loudspeaker Enclosure Analysis Program (LEAP). It incorporates a special utility to derive

loudspeaker parameters using complex-number curve fitting. Electrical impedance measurements from LMS may be imported directly into LEAP to use this utility. This step enables a comparison of parameters derived from different numerical techniques. However, before importing impedance data from LMS into LEAP, one must generate phase information for the data. An LMS software utility generates phase curves using a Hilbert transform method with some extrapolation, mirroring, and tail integration (i.e., to extrapolate from the 10 Hz to 40 kHz bandwidth to a 0 Hz to infinite frequency bandwidth required for the Hilbert transform). Once a complex impedance curve has been generated and imported into LEAP, the parameters are derived using "a very elaborate and complex curve fitting optimizer to obtain a *best fit model* to the *entire* impedance curve" [59, p.16-10].

4.1.4 Garrett Method (Incremental Mass Addition Method)

The method proposed by Garrett [57] was outlined in Section 3.5. It was carried out in this work to produce reference parameters for relative bias errors in suspension compliance and moving mass. Seven mass-increment measurements of the free-air resonance frequency were made for each of the nine drivers under test. The free-air resonance frequency was determined using the MLSSA analyzer.

4.1.5 Three-Point Dual-Channel FFT Method

The method outlined by Thiele [7] was implemented according to the procedure given by Struck [60]. Struck suggests the use of a voltage divider, with a 1000Ω resistor in parallel with the driver under test, to enable the measurement of the electrical

impedance. The three-point dual-channel FFT method was only carried out with the driver axes in the horizontal direction, using the added-mass technique.

4.2 Experimental Procedures

An anechoic chamber was employed as the measurement environment for the determination of loudspeaker driver parameters using the electrical measurement techniques. The chamber provided a quiet free-field environment to isolate the drivers from undesirable background noise and nonideal radiation conditions. Measurement runs consisted of ten standard parameter derivation procedures (following instructions given in each of the analyzer manuals) for each of the nine drivers. With the exceptions indicated above, the drivers were measured with their axes oriented vertically then horizontally. For each orientation, parameters were usually derived using both the added-mass technique and the closed-box technique.

The effective radiating surface area S_D was determined by using the cone diameter plus half the surround. The DC resistance of the voice coil R_{VC} was measured directly using the built-in ohmmeter function of the MLSSA system. As indicated above, the electrical measurement methods included the following: MLSSA, LMS, LEAP, the Garrett method (GM), and the dual-channel FFT method (FFT).

4.3 Electrical Impedance Technique Photographs

Figures 4.1 through 4.6 contain various photographs of the electrical impedance technique setups and the boxes used for the closed-box procedure. Figure 4.1 shows a sample driver with its axis vertical, in a free-air condition. Figure 4.2 shows a sample

driver with its axis vertical, in an added-mass condition. Figure 4.3 shows a sample driver with its axis horizontal in a free-air condition. Figure 4.4 shows a sample driver with its axis horizontal in an added-mass condition. Figure 4.5 shows two sample drivers with their axes vertical, placed on their respective test boxes for the closed-box technique. Figure 4.6 shows the various test boxes used in the closed-box technique.

Fig 4.1. Photograph of a driver in a free-field condition with its axis vertical.

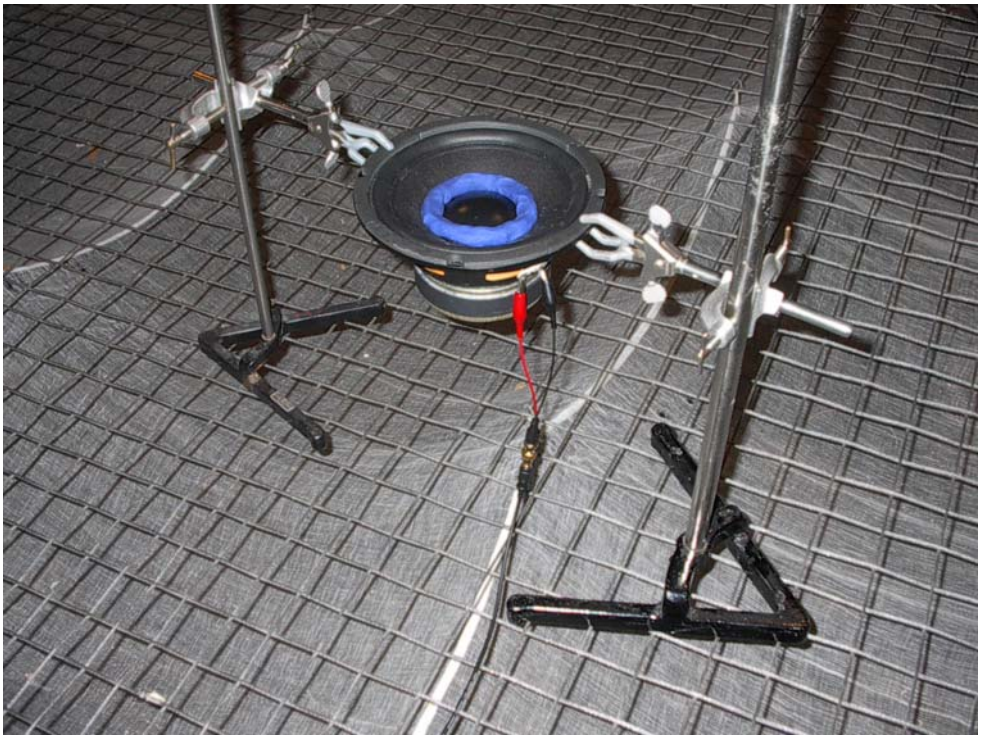

Fig. 4.2. Photograph of a driver in an added-mass configuration with its axis vertical.

Fig. 4.3. Photograph of a driver in a free-field configuration with its axis horizontal.

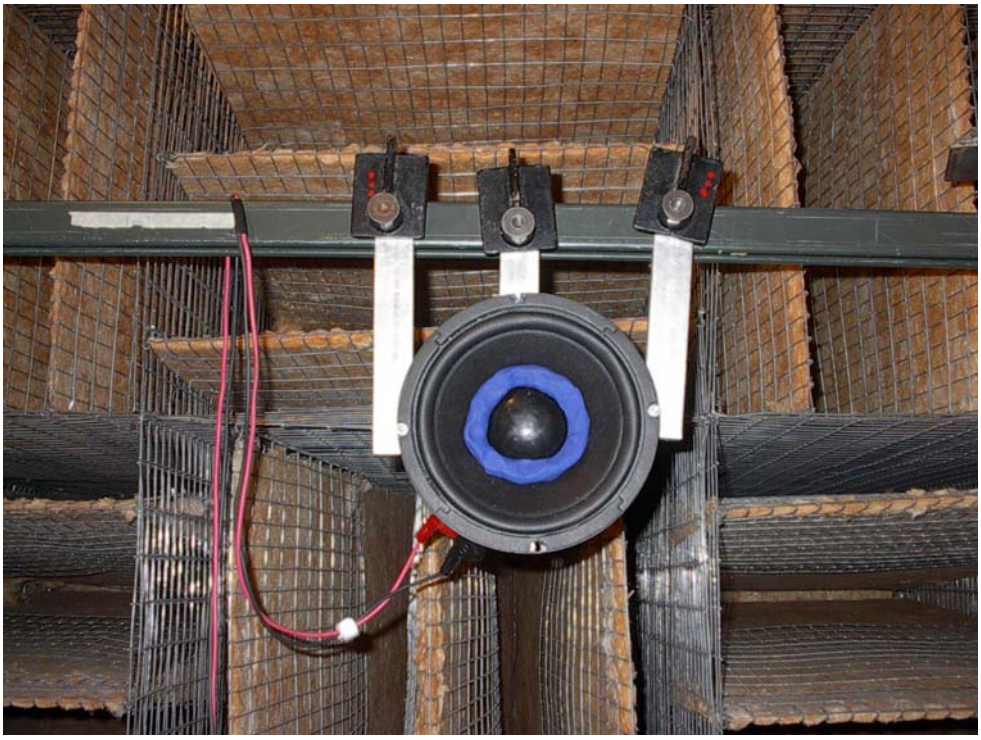

Fig. 4.4. Photograph of a driver in an added-mass configuration with its axis horizontal.

Fig. 4.5. Photograph of two sample drivers placed on test boxes with their axes vertical.

Fig. 4.6. Photograph of various test boxes used for closed box perturbation tests.

4.4 Experimental Results

This section discusses electrical measurement results for the parameters C_{MS}, M_{MS}, R_{MS}, Bl and L_{VC}. Tables 4.1 through 4.5 show the averages of ten measured values for each driver, from each technique and driver orientation used. The values in all five tables are listed with four significant figures. The acronyms for each of the analyzers have been used in the tables (see Section 4.1). The driver axis orientation is specified as H for the horizontal direction, and V for the vertical direction. The perturbation technique is specified as Mass for the added-mass technique and Box for the closed-box technique.

The average measured values for the mechanical suspension compliance C_{MS} are given in Table 4.1, in micrometers per Newton. The average measured values for the

mechanical moving mass (including free-air loading) M_{MS} are given in Table 4.2, in grams. The average measured values for the mechanical suspension resistance R_{MS} are given in Table 4.3, in kilograms per second. The average measured values for the electrical force factor or the Bl product are given in Table 4.4, in Tesla meters. The average measured values for the inductance of the voice coil L_{VC} are given in Table 4.5, in milihenries.

Cms	Driver Under Test								
	1	2	3	4	5	6	7	8	9
MLSSA H Mass	141.5	372.1	714.1	337.0	297.4	241.7	650.5	154.5	639.3
MLSSA V Mass	137.5	421.1	990.0	364.5	231.9	237.4	741.2	358.6	660.9
MLSSA H Box	124.6	312.4	648.0	329.2	252.4	239.2	659.2	340.9	605.6
MLSSA V Box	121.1	301.7	604.9	296.0	190.3	174.9	612.1	760.3	610.8
LMS H Mass	158.0	398.5	773.5	382.1	287.0	270.2	680.2	409.6	824.1
LMS V Mass	147.8	360.4	763.4	367.8	274.1	266.6	721.7	395.9	778.1
LMS H Box	130.1	321.4	591.2	309.1	211.6	212.3	710.3	289.9	617.5
LMS V Box	113.5	321.4	601.5	301.9	271.4	233.0	710.3	278.5	707.7
LEAP H Mass	164.6	403.4	774.1	389.3	287.5	275.1	695.2	412.4	839.0
LEAP V Mass	160.5	368.5	752.5	361.0	273.5	275.8	727.7	399.6	795.5
LEAP H Box	116.9	313.0	596.8	286.7	197.7	191.3	707.5	312.7	570.3
LEAP V Box	110.1	306.8	602.2	306.8	266.7	186.1	725.3	297.7	610.2
GM H Mass	143.7	369.2	750.3	353.4	268.9	246.8	656.1	353.5	682.8
GM V Mass	142.7	351.9	724.5	350.7	283.1	259.1	654.0	354.3	646.0
FFT V Mass	112.6	286.6	620.9	307.2	236.5	218.4	575.8	324.6	647.7

Table 4.1. Average values for C_{MS} ($\mu m / N$) for each of the nine drivers under test. Values determined from ten consecutive measurement runs using various electrical impedance techniques.

Mms	Driver Under Test								
	1	2	3	4	5	6	7	8	9
MLSSA H Mass	162.0	81.43	26.55	38.87	31.92	36.01	9.063	8.144	2.271
MLSSA V Mass	158.8	68.87	17.56	35.16	40.31	36.94	7.664	3.422	1.930
MLSSA H Box	187.0	98.77	28.96	40.75	37.25	36.04	9.052	3.834	2.221
MLSSA V Box	192.7	100.4	30.44	44.08	45.37	47.57	9.657	1.717	2.214
LMS H Mass	162.6	82.37	23.98	37.11	35.43	35.43	9.524	3.315	1.858
LMS V Mass	164.5	91.07	24.38	38.53	41.91	37.77	8.976	3.359	2.077
LMS H Box	197.5	102.1	31.42	46.88	48.05	45.10	9.120	4.684	2.480
LMS V Box	214.1	102.1	30.85	46.88	42.25	44.29	9.120	4.776	2.287
LEAP H Mass	151.2	79.73	24.38	35.55	34.32	33.67	9.172	3.389	1.769
LEAP V Mass	160.5	86.28	25.04	39.68	41.78	33.20	8.920	3.405	1.913
LEAP H Box	212.8	103.3	31.62	48.12	50.17	48.41	9.013	4.469	2.602
LEAP V Box	220.8	104.1	31.20	46.63	42.88	49.26	8.949	4.572	2.494
GM H Mass	157.0	82.10	24.49	37.06	31.18	34.86	9.046	3.785	1.960
GM V Mass	179.6	90.18	23.99	37.49	31.96	32.60	9.133	3.587	2.071
FFT V Mass	187.0	99.6	27.2	39.9	38.3	38.2	9.2	3.6	2.0

Table 4.2. Average values for M_{MS} (gm) for each of the nine drivers under test. Values determined from ten consecutive measurement runs using various electrical impedance techniques.

Rms	Driver Under Test								
	1	2	3	4	5	6	7	8	9
MLSSA H Mass	3.713	1.673	1.992	2.247	1.121	1.286	1.152	1.990	0.2924
MLSSA V Mass	4.926	1.624	1.544	2.056	1.470	1.309	1.056	0.8572	0.2539
MLSSA H Box	4.222	1.845	2.111	2.317	1.253	1.221	1.194	0.9105	0.2737
MLSSA V Box	4.335	1.969	2.230	2.488	1.530	1.550	1.223	0.4147	0.3122
LMS H Mass	4.875	1.961	2.097	2.179	1.775	1.561	1.382	0.8811	0.3435
LMS V Mass	4.479	2.428	2.051	2.376	0.8955	2.019	1.278	0.9199	0.4044
LMS H Box	5.930	2.599	2.772	3.049	2.377	1.988	1.323	1.245	0.4585
LMS V Box	5.831	2.720	2.597	2.893	0.9009	2.288	1.300	1.308	0.4400
LEAP H Mass	3.768	1.649	1.904	1.970	1.278	1.184	1.181	0.7917	0.2784
LEAP V Mass	4.044	1.760	1.929	2.315	1.039	1.430	1.134	0.8233	0.2963
LEAP H Box	5.307	2.141	2.470	2.795	1.873	1.703	1.161	1.044	0.4096
LEAP V Box	5.567	2.114	2.406	2.723	1.085	2.116	1.138	1.105	0.3862
FFT V Mass	5.427	2.804	2.502	2.606	1.637	1.622	0.2864	0.9772	0.2953

Table 4.3. Average values for R_{MS} (kg/s) for each of the nine drivers under test. Values determined from ten consecutive measurement runs using various electrical impedance techniques.

Bl	Driver Under Test								
	1	2	3	4	5	6	7	8	9
MLSSA H Mass	13.09	9.609	7.647	11.20	11.45	12.40	5.396	6.336	4.120
MLSSA V Mass	12.96	8.898	6.378	10.66	12.94	12.56	5.052	4.125	3.850
MLSSA H Box	14.04	10.37	8.006	11.46	12.31	12.32	5.408	4.357	4.112
MLSSA V Box	14.07	10.50	8.097	11.74	13.41	13.86	5.530	2.958	4.085
LMS H Mass	14.10	10.15	7.626	11.53	13.80	13.07	5.836	4.296	4.120
LMS V Mass	13.61	11.12	7.585	11.31	8.581	13.90	5.650	4.306	4.353
LMS H Box	15.55	11.30	8.767	12.88	16.08	14.75	5.711	5.107	4.760
LMS V Box	15.53	11.77	8.535	12.48	8.607	14.81	5.691	5.135	4.568
LEAP H Mass	12.53	9.339	7.234	10.62	11.91	11.83	5.372	4.113	3.710
LEAP V Mass	12.87	9.620	7.321	11.12	9.300	12.30	5.293	4.076	3.847
LEAP H Box	14.87	10.67	8.240	12.36	14.40	14.19	5.326	4.723	4.500
LEAP V Box	15.10	10.58	8.176	12.06	9.506	14.96	5.302	4.723	4.392
FFT V Mass	13.71	10.23	7.472	10.80	11.95	12.11	1.503	4.099	3.694

Table 4.4. Average values for Bl $(T \cdot m)$ for each of the nine drivers under test. Values determined from ten consecutive measurement runs using various electrical impedance techniques.

Lvc	Driver Under Test								
	1	2	3	4	5	6	7	8	9
MLSSA H Mass	0.9974	0.5877	0.4169	0.6654	0.5719	0.5773	0.3090	0.1719	0.2478
MLSSA V Mass	1.018	0.6103	0.4207	0.7050	0.6017	0.6018	0.3199	0.1810	0.2441
MLSSA H Box	1.001	0.5851	0.4168	0.6535	0.5719	0.5624	0.2954	0.1701	0.2175
MLSSA V Box	1.036	0.5901	0.4362	0.6871	0.5969	0.5956	0.3143	0.1785	0.2452
LMS H Mass	2.132	1.199	0.7386	1.469	1.245	1.193	0.5823	0.3425	0.3971
LMS V Mass	2.149	1.196	0.7483	1.468	1.168	1.176	0.5905	0.3406	0.4021
LMS H Box	2.132	1.199	0.7386	1.469	1.172	1.193	0.5819	0.3425	0.3971
LMS V Box	2.149	1.196	0.7483	1.468	1.681	1.176	0.5905	0.3406	0.4021
LEAP H Mass	2.195	1.252	0.8078	1.579	1.124	1.352	0.6520	0.4108	0.5202
LEAP V Mass	2.228	1.245	0.8206	1.592	1.303	1.294	0.6463	0.4089	0.5225
LEAP H Box	2.195	1.252	0.8078	1.579	1.124	1.352	0.6520	0.4108	0.5202
LEAP V Box	2.228	1.249	0.8206	1.592	1.303	1.294	0.6463	0.4089	0.5225

Table 4.5. Average values for L_{VC} (mH) for each of the nine drivers under test. Values determined from ten consecutive measurement runs using various electrical impedance techniques.

4.5 Discussion

A few conclusions may be drawn with regard to parameters derived from the various electrical methods. Parameters determined using the added-mass technique and those determined using the closed-box technique have relative bias errors (compare Reference [53]). Using average bias errors and the added-mass technique as a reference,

the relative bias errors are –18% for C_{MS}, +22% for M_{MS}, +21% for R_{MS}, and +11% for Bl. Parameters derived using different electrical measurement systems and methods show significant variation (compare References [27], [43], [46], and [53]). For some drivers, derived parameter values depend upon orientation of their axes, perhaps because of how their coils are hung (compare References [12], [14, p.22], [24, p.303], and [46]).

CHAPTER 5

PLANE WAVE TUBES: THEORY AND DESIGN

The theory and design of plane wave tubes will be presented in this chapter. The chapter begins with a discussion of one-dimensional wave propagation. The theory of the two-microphone plane wave tube technique will then be discussed along with acoustical quantities that may be determined using the technique. This will be followed by a practical discussion of issues involved in the design of a plane wave tube, with special attention to the tube used in this study. Finally, photographs of the constructed measurement system will be presented and discussed.

5.1 One-Dimensional Wave Propagation

A one-dimensional sound field may be established inside a plane wave tube below the cutoff frequency f_c of the first cross mode. For the purposes of this work, a plane wave tube includes a source driver operating below this frequency. It is positioned at one end of the tube to excite the field. (A sealed enclosure is typically constructed to enclose the back side of the source driver.) A plane wave tube should maintain a uniform cross-sectional area along its length. The plane wave tube section between the source driver and a material under test may be referred to as the source tube, or the upstream tube. A material to be tested typically terminates this section as a bounding surface. Transmission loss (TL) measurements require that a receiving tube also be used to produce a transmitted plane wave field. The receiving tube may be referred to as the downstream tube. For accurate transmission loss measurements, the receiving tube should be terminated by an anechoic termination.

One-dimensional sound field decomposition allows pressure fields to be separated into incident and reflected propagating components. Measurements of acoustic pressure at the walls of the duct assume that the pressure is uniform over the duct cross section. As the propagating pressure fields encounter a cross-sectional boundary, the sound field in the vicinity of the boundary may not be uniform over the cross section, particularly if the boundary is nonuniform. However, the pressure field becomes uniform over the cross section at a sufficient distance away from the boundary. In this work, one-dimensional sound field decomposition always assumes steady state conditions.

5.2 Two-Microphone Transfer Function Technique

Theory and experimental verification of the two-microphone technique for sound field decomposition has been developed by Chung and Blaser, and others [35]-[41]. A brief discussion of the two-microphone technique will be presented here.

A single microphone probing pressure a field measures the total pressure at that point; it may not distinguish between the incident and reflected propagating components. The signal at the microphone may be represented as the sum of the two components (see Fig. 5.1),

$$\hat{p} = \hat{p}_i + \hat{p}_r \tag{5.1}$$

where $\hat{p}$ is the total pressure at the microphone, $\hat{p}_i$ is the incident pressure, and $\hat{p}_r$ is the reflected pressure.

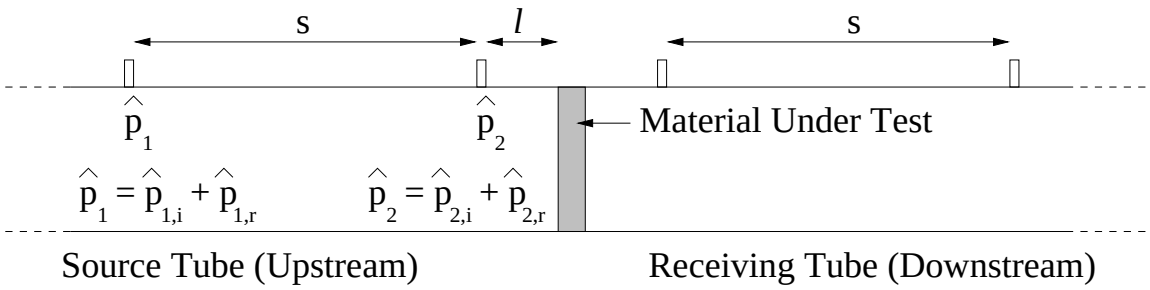

Fig. 5.1. Diagram of a plane wave tube configured for transmission loss measurements. The complex pressures represented in this figure are spatially dependent.

The signal at each of the microphones may be represented as the sum of the two propagating wave components. The transfer function H_{12} between the pressures at the two microphone positions may then be represented as

$$H_{12} = \frac{\hat{p}_2}{\hat{p}_1} = \frac{\hat{p}_{2,i} + \hat{p}_{2,r}}{\hat{p}_{1,i} + \hat{p}_{1,r}} \tag{5.2}$$

where $\hat{p}_1$ and $\hat{p}_2$ are the total pressures at microphones 1 and 2, respectively, $\hat{p}_{1,i}$ and $\hat{p}_{1,r}$ are the incident and reflected pressures at microphone 1, respectively, and $\hat{p}_{2,i}$ and $\hat{p}_{2,r}$ are the incident and reflected pressures at microphone 2, respectively.

Without calibration, the transfer function between the electrical outputs of two microphones would only be the same as H_{12} if their phase and amplitude responses matched. Without a matched pair, a calibration transfer function must be used to obtain the desired pressure transfer function. Chung and Blaser described a useful switching technique to obtain this calibration transfer function [36]. Two transfer functions are measured from the microphone output signals: one in an initial microphone configuration and another with switched microphone locations. The calibration function then results from the geometric mean of the two transfer functions:

$$H_{Cal,12} = \left[H_{12}^{o} H_{12}^{s}\right]^{1/2}, \tag{5.3}$$

where $H_{Cal,12}$ is the calibration function, H_{12}^{o} is the measured transfer function between microphones 1 and 2 in their original positions, and H_{12}^{s} is the measured transfer function between microphones 1 and 2 in their switched positions. The transfer function between pressures at the positions of microphones 1 and 2 can then be found by dividing the measured transfer function $H_{Measured,12}$ by the calibration function:

$$H_{12} = \frac{H_{Measured,12}}{H_{Cal,12}}. \tag{5.4}$$

5.3 Acoustic Quantities

Several acoustic quantities may be derived from the pressure transfer function. These include the reflection coefficient, acoustic impedance, and absorption coefficient of a material under test. The complex reflection coefficient R may be expressed in terms of the pressure transfer function as follows [39]:

$$R = |R| e^{j\phi_R} = \frac{\hat{p}_r}{\hat{p}_i} = \frac{H_{12} - e^{-jks}}{e^{jks} - H_{12}} e^{j2k(l+s)} \tag{5.5}$$

where ϕ_R is the phase of the complex reflection coefficient, j is the imaginary number ($\sqrt{-1}$), k is the wavenumber, l is the distance between the termination and the microphone closest to the termination, and s is the spacing between the microphone pair. The normal-incidence sound absorption coefficient may then be expressed in terms of the complex reflection coefficient [39]:

$$\alpha = 1 - |R|^2. \tag{5.6}$$

The mechanical impedance Z_M may also be expressed in terms of the complex reflection coefficient [39]:

$$Z_M = \rho_0 c S \frac{1+R}{1-R} = Z_A S^2, \tag{5.7}$$

where $\rho_0 c S$ is the characteristic mechanical impedance of air in the tube with a cross-sectional area S. Equation (5.7) also shows the relationship between mechanical impedance Z_M and acoustic impedance Z_A.

Decomposition of the complex downstream pressure field using the two-microphone transfer function technique can be important in the derivation of transmission properties for a material or device under test. While an ideal anechoic receiving tube has only a transmitted component of sound, an anechoic termination often provides insufficient absorption at the lowest frequencies of interest. In this case, the receiving space sound field should be decomposed. The normal-incidence power transmission coefficient τ may be defined in terms of the squared modulus of the ratio between the peak transmitted pressure (the pressure transmitted past the material into the receiving tube) and the peak incident pressure (incident upon the material) [36]:

$$\tau = \left|\frac{\hat{p}_t}{\hat{p}_i}\right|^2 = \frac{W_t}{W_i} = \frac{G_{dd} S_d}{G_{uu} S_u} \frac{\rho_u c_u}{\rho_d c_d} \left|\frac{1+R_u}{1+R_d}\right|^2. \tag{5.8}$$

In this equation, $\hat{p}_t$ is the transmitted pressure, W_i and W_t are the incident and transmitted sound powers, respectively, G_{dd} and G_{uu} are the downstream and upstream auto power spectra, respectively, S_d and S_u are the downstream and upstream cross-sectional areas of the respective tubes, $\rho_u c_u$ and $\rho_d c_d$ are the upstream and downstream characteristic fluid impedances, respectively, and R_u and R_d are the upstream and

downstream complex reflection coefficients, respectively. If the fluids and the cross-sectional areas of the upstream and downstream tubes are identical, Eq. (5.8) reduces to

$$\tau = \frac{G_{dd}}{G_{uu}} \left| \frac{1+R_u}{1+R_d} \right|^2 . \tag{5.9}$$

One plane wave tube measurement quantity of particular importance in this work is the transmission loss of the device under test [36]:

$$TL = 10\log_{10}\left(\frac{1}{\tau}\right) = 10\log_{10}\frac{G_{uu}}{G_{dd}} + 20\log_{10}\left|\frac{1+R_d}{1+R_u}\right| . \tag{5.10}$$

In order to obtain an accurate determination of these transmission quantities, a calibration transfer function between upstream microphones and downstream microphones must also be measured to compare relative values for the auto power spectra ratios.

5.4 Limitations

The dimensions of a plane wave tube must be chosen carefully because of inherent limitations in the assumption of plane wave propagation. Propagating components of the internal field consist of plane waves only below the cutoff frequency of the first cross mode. Another limitation that must be considered is how close a microphone may be placed to a tube termination (the excitation source or the device under test). Evanescent cross modes must decay sufficiently over distance if their contributions to measured sound pressures are to remain negligible. As a rule-of-thumb, microphones should be positioned no closer than one effective tube diameter from a termination [39]. There are also inherent requirements in the spacing of microphone pairs. If the spacing approaches half a wavelength (or integer multiples of half a wavelength), data derived from the two-microphone transfer function technique becomes

indeterminate [37]. Steps should be taken to ensure that the signal-to-noise ratio at each microphone is sufficiently high for accurate results. The duct should also be constructed in a manner that minimizes acoustic losses.

5.4.1 Cutoff Frequency

The cutoff frequency of the first cross mode for a rectangular duct is defined in terms of the largest cross-sectional dimension d and the speed of sound [39]:

$$f_c = 0.500\frac{c}{d}. \tag{5.11}$$

For circular ducts, the cutoff frequency is defined by the equation [39], [40]

$$f_c = 0.586\frac{c}{d}, \tag{5.12}$$

where d represents the diameter. As measurement frequencies approach these cutoff frequencies, data becomes corrupted due to cross mode contributions. However, if the microphone is placed at a nodal line for a given cross mode, the microphone detects much less of the modal energy. While for a rectangular duct, the microphone might be placed at one of the cross-mode nodal lines, as shown in Fig. 5.2, the microphone remains affected by the cross mode in the orthogonal direction.

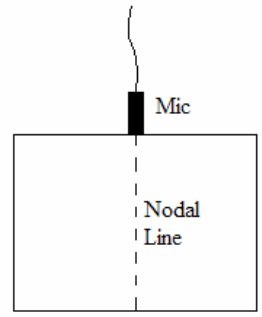

Fig 5.2. Cross-sectional diagram of a microphone positioned at the nodal line for a cross mode in a plane wave tube.

5.4.2 Microphone Spacing

Bodén and Åbom determined limits on microphone spacing for a maximum of 1% error in the determination of the transfer function [37]. They give the following equation:

$$0.1\pi < ks < 0.8\pi\,, \tag{5.13}$$

where s is the microphone spacing. Rearranging Eq. (5.13) to determine the upper and lower frequency limits f_U and f_L for a given microphone spacing, one finds that

$$f_U = \frac{2c}{5s}\,, \tag{5.14}$$

$$f_L = \frac{c}{20s}\,. \tag{5.15}$$

5.4.3 Attenuation of Evanescent Modes

As Kinsler *et al* have noted, "If the [plane wave tube] is excited with a frequency just below the cutoff frequency of some particular mode, then this and higher modes are evanescent and not important at appreciable distances form the source" [61, p.253]. While a standard rule-of-thumb is to place the closest microphone at least one effective duct diameter away from a tube boundary, attenuation of a higher-order mode depends upon frequency as well as distance. The attenuation $L_{Attenuation}$ of a higher-order evanescent mode between two points along the axis of a plane wave tube may be expressed as follows [52, p.8-3a]:

$$L_{Attenuation} = -20\log_{10}\left[e^{-kx\sqrt{\left(\frac{f_c}{f}\right)^2-1}}\right] \approx 0.16x\sqrt{f_c^{\,2}-f^2}\,, \tag{5.16}$$

where f_c is the cross-mode cutoff frequency, f is the excitation frequency below the cutoff frequency, and x is the distance between points. A high level of attenuation of higher modes is desired for all frequencies of interest so that data is not significantly corrupted.

5.4.4 Tube Losses

The duct should be rigid and limited in length, when possible, to limit losses caused by thermo-viscous effects. Quoting the ASTM standard, "The tube shall be straight and its inside surface shall be smooth and free of dust to maintain low attenuation. The tube walls shall be massive and sufficiently rigid so that sound energy transmission through them is negligible" [39].

5.5 Plane Wave Tube Design

The dimensions of the tube constructed for this research were chosen to accommodate several different sizes of loudspeaker drivers. It also needed to be long enough to allow accurate operation at sufficiently low frequencies—an important requirement in the determination of driver resonance frequencies and other driver properties. Medium density fiberboard (MDF) of 1.9 cm thickness was chosen for its construction because it is smooth, massive, non-porous, relatively rigid, and easy to use in fabrication. The tube walls were composed of two laminated layers of MDF.

5.5.1 Usable Frequency Range

The cross-sectional dimensions of the duct were chosen to be 30.5 cm by 30.5 cm to accommodate drivers up to 30.5 cm (12 in.) in diameter. The cutoff frequency for the first cross mode was then $f_c = 564Hz$. Accurate data could be measured up to approximately 500 Hz before corruption due to higher modes became significant.

Two microphone pairs (low and high frequency pairs) were chosen to increase the usable frequency range of the system. Setting 564 Hz as the upper usable frequency limit for the high-frequency pair of microphones gives a microphone spacing of 24.4 cm. This spacing also imposed a lower usable frequency limit of 70.5 Hz. The low-frequency microphone pair might have been spaced to allow an upper usable frequency limit of about 71 Hz. However, the required microphone spacing of 193 cm, would have pushed the microphones positions too close to the boundaries (inside the one duct diameter rule-of-thumb) of the 246 cm long tubes. Further analysis was required to determine a suitable low-frequency microphone spacing.

Figure 5.3 shows the level of attenuation of the first cross mode as a function of frequency and distance from the termination to the closest microphone [see Eq. (5.16)]. A 25 dB attenuation of the first cross mode can be achieved up to about 75 Hz if the microphones are placed 30.5 cm (one duct diameter) away from the boundary. Placement of the microphones 30.5 cm away from the nearest boundaries sets the low frequency microphone pair spacing to 185 cm, for 246 cm source and receiving tubes.

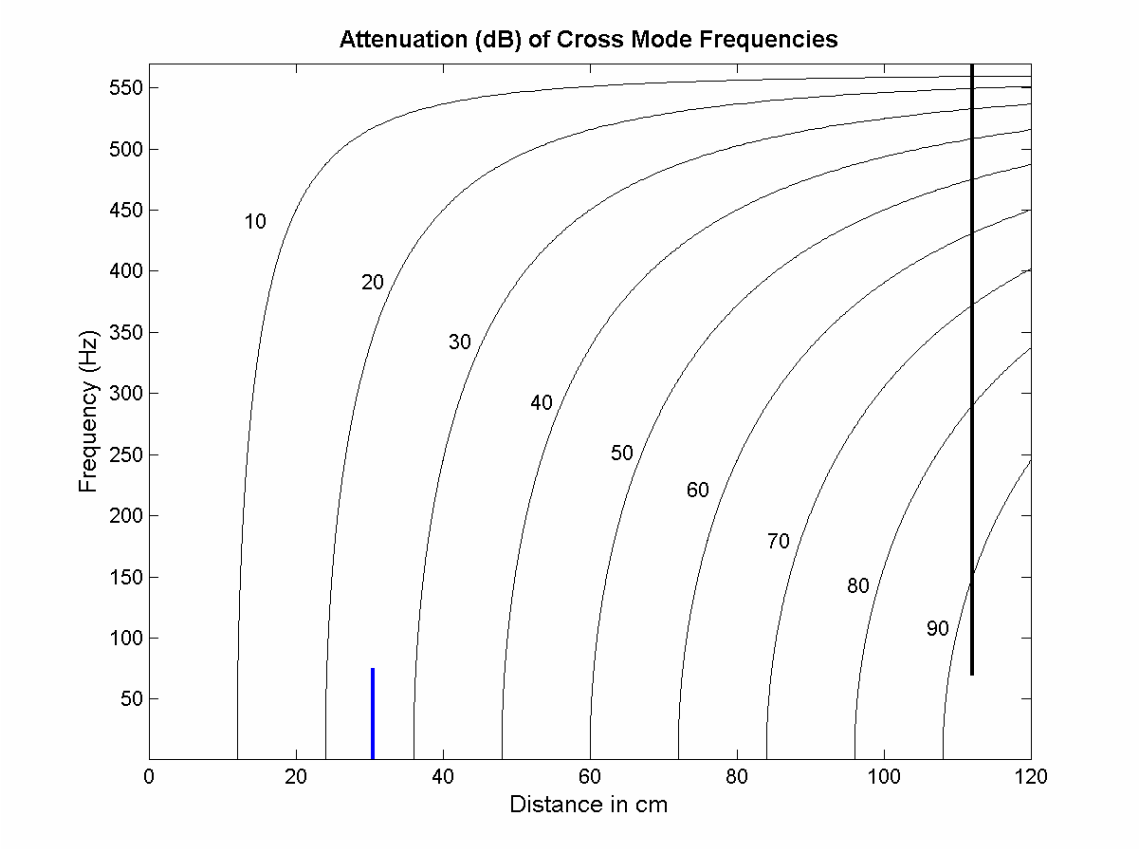

Fig. 5.3. Contour plot of the level of attenuation (dB) of higher modes as a function of distance from a given boundary and excitation frequency. Numbers on contours represent the level of attenuation in decibels. The vertical lines represent the distances from a tube termination to the closest microphone for the low (lower left) and high (upper right) frequency microphone pair.

The resulting upper usable frequency limit for the low-frequency microphone spacing is 74.2 Hz, with a lower usable frequency limit of 9.3 Hz. Since the low-frequency microphone spacing may only be used up to 74.2 Hz, the attenuation level of higher-order modes would be no less than 25 decibels at the microphone positions. Attenuation for the proposed high frequency microphone spacing would be at least 25 decibels below 540 Hz. To summarize, the plane wave tube would be able to accurately measure data from 9.3 Hz to 540 Hz, with a crossover frequency between microphone pairs at 72.0 Hz.

5.5.2 Baffle Design

The thickness of baffles used for measuring drivers under test should satisfy the assumption that the mechanical impedance of the baffles are very large compared to the mechanical impedances of the diaphragm assemblies in the drivers under test. Modeling the baffle as a simply supported finite plate allows ballpark design consideration for the desired large-impedance assumption [62, p.82]. The modal frequencies of the plate are given by

$$f_{pq} = \frac{1}{2\pi}\sqrt{\frac{D}{m}}\left[\left(\frac{p\pi}{L_x}\right)^2 + \left(\frac{q\pi}{L_y}\right)^2\right] \tag{5.17}$$

$$D = \frac{\mathrm{Y}h^3}{12\left(1-\sigma^2\right)} \tag{5.18}$$

where p and q are modal indicies, m is the mass of the plate per unit area, L_x and L_y are the dimensions of the plate, Y is Young's modulus, h is the plate thickness, and σ is Poisson's ratio. The first modal frequency for a given baffle as a function of thickness and material composition is given in Fig. 5.3 [based on Eq. (5.17)].

A double-thickness (3.8 cm thick) laminated MDF baffle should have a resonance frequency of approximately 960 Hz. Below this resonance frequency the impedance of the baffle is dominated by its stiffness. Various baffles were constructed with mounting holes to accommodate the various driver sizes to be studied. Care was taken to ensure that all driver components were either flush with or slightly past the upstream face of the baffle.

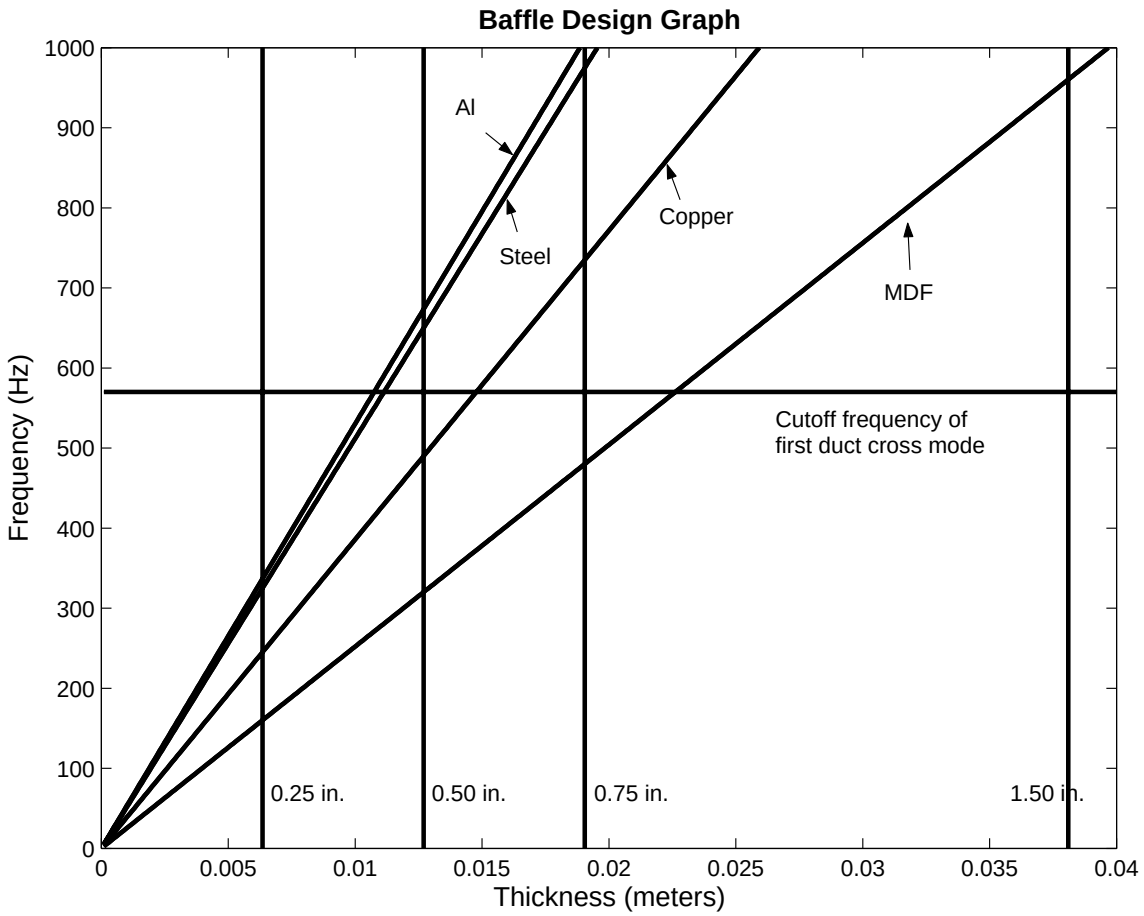

Fig. 5.4. The resonance frequency for a given baffle as a function of thickness and material composition: Al – Aluminum 6061-T6, Stainless Steel, Copper, MDF – Medium Density Fiberboard.

5.5.3 Termination Design

The principles used in the design of an anechoic tube termination are the same as those involved in the design of anechoic chamber wedges. Although considerable research has been done in the design of wedges [63]-[68], the empirical suggestions given by Beranek over 50 years ago are still widely used [63]. Figure 6 of Beranek's paper allows one to select the low frequency cutoff frequency of the wedge.

An anechoic termination that provides a purely resistive loading down to very low frequencies is desirable. However, the maximum practical length, based on the length of

a sheet of MDF used in the wedge enclosure, was 246 cm. Beranek's graphs must be linearly extrapolated in order to obtain the desired design information. A wedge measuring 246 cm in overall length gives an expected low frequency cutoff frequency of approximately 36 Hz.

5.6 Photographs of Constructed Plane Wave Tube Apparatus

Figure 5.5 shows the entire constructed plane wave tube assembly, with the source loudspeaker enclosure in the forefront. Figure 5.6 shows a photograph of the partition containing driver number 2, with the adjacent ends of the source and receiving tubes in view. Figure 5.7 shows a photograph of the partition positioned between the source and receiving tubes. Figure 5.8 shows an outside photograph of a sample microphone used in the plane wave tube measurements while Fig. 5.9 shows a view of the microphone from inside the tube.

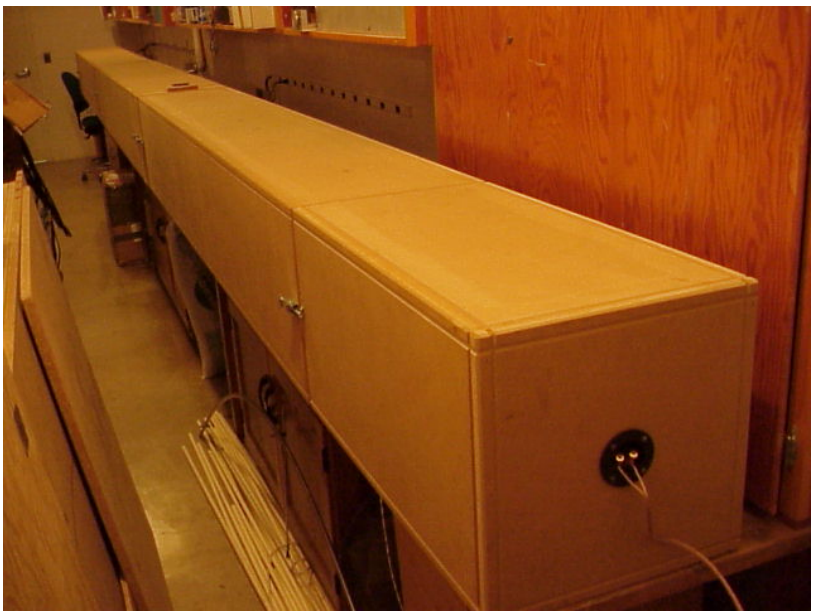

Fig. 5.5. Photograph of the entire constructed plane wave tube. View is arranged with the excitation source in the forefront and with the termination at the far end.

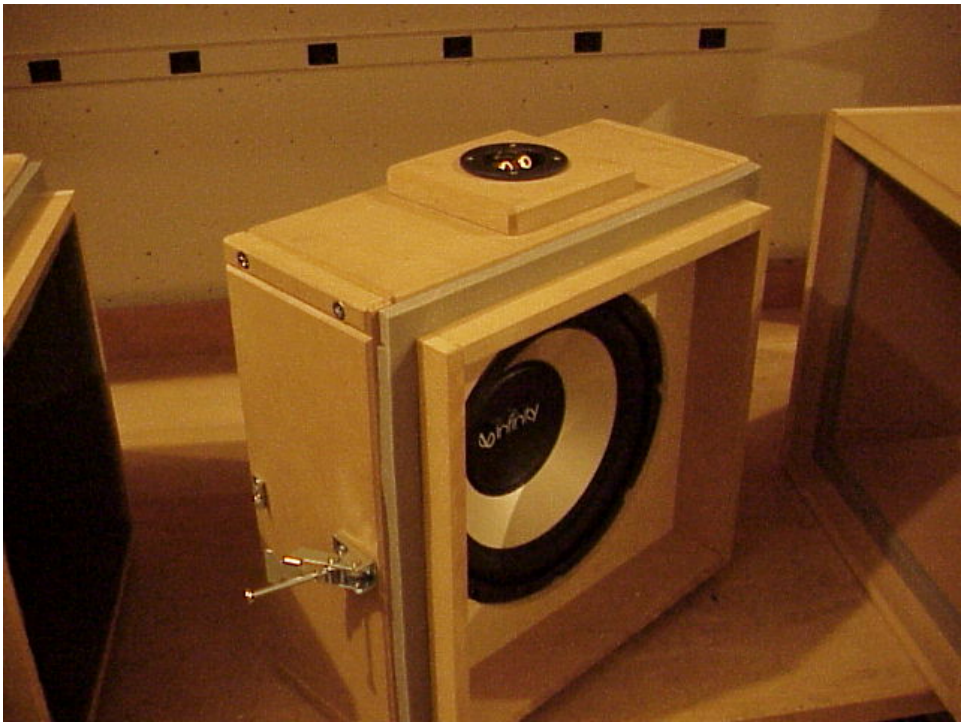

Fig. 5.6. Photograph of the partition containing mounted driver number 2 in a surrounding baffle.

Fig. 5.7. Photograph of the partition between the source and receiving tubes.

Fig. 5.8. Photograph of a microphone used in the plane wave tube measurements (outside view).

Fig. 5.9. Photograph of a microphone used in the plane wave tube measurements (inside view).

CHAPTER 6

LUMPED-PARAMETER CIRCUIT MODELING FOR A MOVING-COIL LOUDSPEAKER DRIVER IN A PLANE WAVE TUBE

In this chapter, a circuit model will be developed for a driver under test in the plane wave tube arrangement. It will be developed for a driver in either an open-circuit condition (no electrical portion included) or a closed-circuit condition (a wire connecting the terminals). The development will initially begin with a theoretical "black box" model. An equivalent circuit model for a damped single-leaf mass-spring partition, which fills the tube cross section, will then be presented. The circuit will subsequently be expanded to represent a damped mass-spring piston system mounted in a surrounding rectangular baffle of finite mechanical impedance. This circuit will finally be applied to a driver under test, with needed assumptions to simplify the analysis. Equivalent circuit models for the open-circuit and closed-circuit conditions will be given in a simplified form.

6.1 Black Box Circuit Model

For a composite system of a baffled driver mounted in a plane wave tube, the complex excitation signal and the characteristics of the source tube do not need to be known explicitly for all types of measurements, as long as the tube sound field can be decomposed into incident and reflected components. The excitation source and the source tube may be represented in an equivalent circuit as an arbitrary Thevenin equivalent source. The baffled driver under test may initially be represented as a black box, which

includes its unknown complex impedance $Z_{M,BB}$ (see Fig. 6.1, where $\langle\ \rangle_S$ represents a spatial average). Leishman used this approach to establish generalized formulas for normal-incidence transmission losses of arbitrary devices [69, pp.139-143]. The following discussion has been adapted from his work.

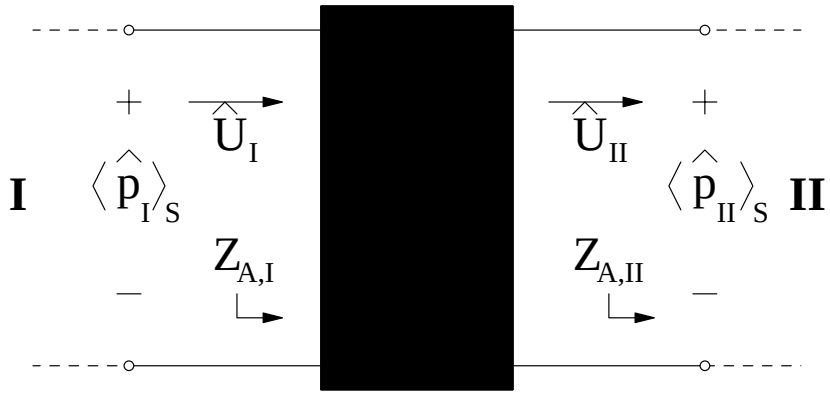

Fig. 6.1. Black-box schematic showing spatially averaged pressures, volume velocities, and acoustic impedances looking into and beyond a black box. The Roman numeral subscripts for the quantities used in this figure denote the upstream (I) or downstream (II) of the black box.

As suggested earlier, the receiving tube and termination should ideally provide an anechoic downstream impedance beyond the black box. However, because of the low-frequency limits inherent in passive anechoic terminations, the impedance is best represented as an unknown acoustic impedance Z_{AT}.

The normal-incidence transmission loss of a partition in a plane wave tube may be expressed in terms of its power transmission coefficient

$$TL = 10\log_{10}\left(\frac{1}{\tau}\right). \tag{6.1}$$

The transmission coefficient for the black box is the ratio of the time-averaged sound power transmitted through it to the time-averaged sound power incident upon it:

$$\tau = \frac{\langle W_t \rangle_T}{\langle W_i \rangle_T} = \frac{\rho_I c_I S_{II} \langle \hat{p}_t \rangle_T^2}{\rho_{II} c_{II} S_I \langle \hat{p}_i \rangle_T^2} = \frac{\rho_I c_I S_{II}}{\rho_{II} c_{II} S_I} \frac{|\hat{p}_t|^2}{|\hat{p}_i|^2}, \tag{6.2}$$

where the quantities $\rho_I c_I$ and $\rho_{II} c_{II}$ are the characteristic fluid impedances of the fluid upstream and downstream of the partition, respectively, and the angled brackets ($\langle \ \rangle_T$) denote a time average.

The incident pressure field may be expressed in terms of the volume velocity $\hat{U}_I$, the characteristic acoustic impedance of the fluid, and the impedance $Z_{A,I}$ looking into the partition:

$$\hat{p}_i = \frac{\hat{U}_I}{2} \left[Z_{A,I} + \frac{\rho_I c_I}{S_I} \right]. \tag{6.3}$$

The transmitted pressure field may be expressed similarly:

$$\hat{p}_t = \frac{\hat{U}_{II}}{2} \left[Z_{A,II} + \frac{\rho_{II} c_{II}}{S_{II}} \right]. \tag{6.4}$$

Substituting these expressions into Eq. (6.2) yields the following formula:

$$\tau = \frac{\rho_I c_I S_{II}}{\rho_{II} c_{II} S_1} \left| \frac{\hat{U}_{II}}{\hat{U}_I} \right|^2 \left| \frac{Z_{A,II} + \frac{\rho_{II} c_{II}}{S_{II}}}{Z_{A,I} + \frac{\rho_I c_I}{S_I}} \right|^2. \tag{6.5}$$

If one assumes both sides of the partition have identical characteristic acoustic impedances (i.e., the tube cross section is consistent and the medium is air), the expressions simplifies to

$$\tau = \left| \frac{\hat{U}_{II}}{\hat{U}_I} \right|^2 \left| \frac{Z_{A,II} + \frac{\rho_0 c}{S}}{Z_{A,I} + \frac{\rho_0 c}{S}} \right|^2. \tag{6.6}$$

If the volume velocity is identical on either side of the black box (as is often the case for single-leaf partition structures), the volume velocity ratio becomes unity. In addition, the impedance looking into the black box from the upstream side includes the downstream acoustic impedance $Z_{A,II}$ in series with the black box $Z_{M,BB}/S^2$. This means the reciprocal of the transmission coefficient reduces to the form

$$\frac{1}{\tau} = \left| \frac{\frac{Z_{M,BB}}{S^2} + \frac{Z_{M,II}}{S^2} + \frac{\rho_0 c}{S}}{\frac{Z_{M,II}}{S^2} + \frac{\rho_0 c}{S}} \right|^2 = \left| \frac{Z_{M,BB} + Z_{M,II} + \rho_0 c S}{Z_{M,II} + \rho_0 c S} \right|^2, \tag{6.7}$$

where S is the cross-sectional area of the plane wave tube and black box partition.

6.2 Damped Single-Leaf Mass-Spring Partition

In the development of an equivalent circuit model for a loudspeaker driver mounted in a plane wave tube, a natural starting point is to assume that the driver cone behaves an rigid piston spanning the entire cross section of the tube. This piston (with mass M_{MP}) has an associated suspension system with compliance C_{MP} and resistance R_{MP}. A mechanical schematic drawing for the partition is shown in Fig. 6.2. The dark walls of the plane wave tube in Fig. 6.2 are grounded to show that they are rigid. The equivalent circuit given in Fig. 6.3 provides a model for the system. The quantity r_{MP} in the circuit denotes the mechanical responsiveness of the suspension system, which is equivalent to the reciprocal of the mechanical resistance. The quantity Z_{AT} denotes the downstream impedance seen by the partition. The spatially averaged blocked pressure on the source side of the partition and the upstream acoustic radiation impedance are denoted by $\langle \hat{p}_B \rangle_S$ and Z_{AR}, respectively.

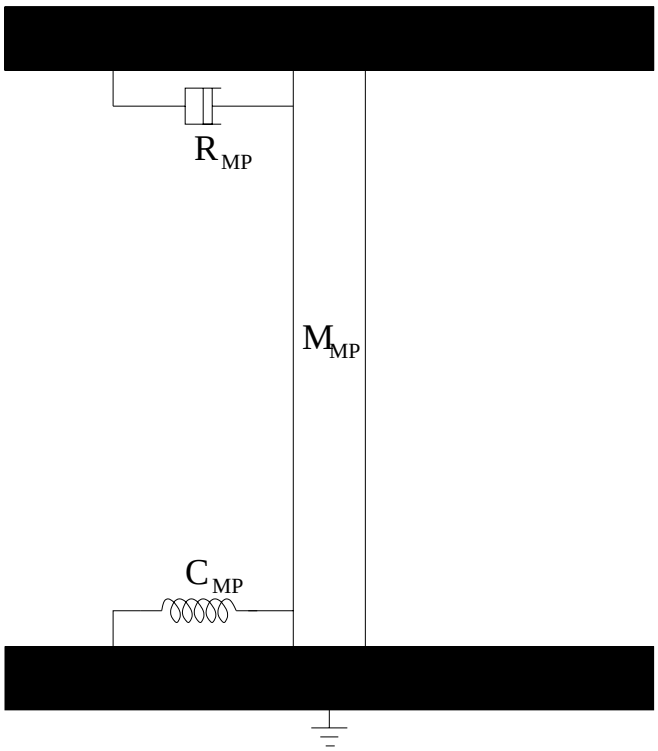

Fig. 6.2. Schematic drawing of a theoretical piston system with mass M_{MP}, compliance C_{MP}, and resistance R_{MP}. Its surface area is equivalent to the cross-sectional area of the plane wave tube.

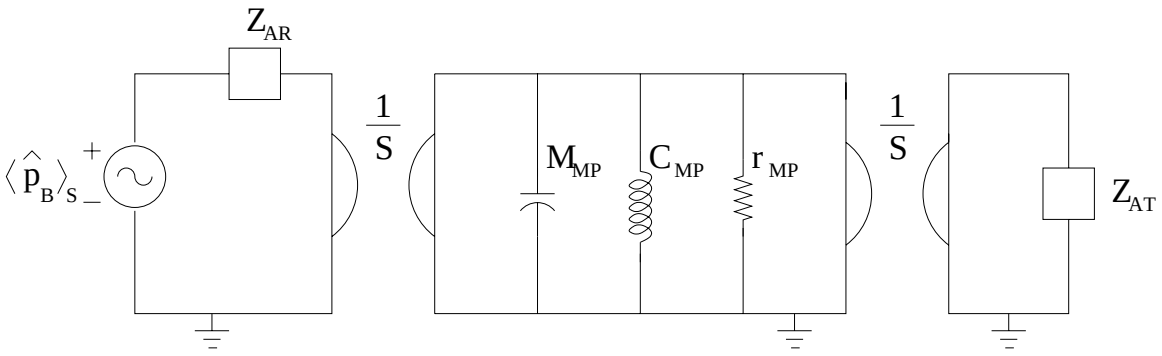

Fig. 6.3. Equivalent circuit for a damped mass-spring partition with a surface area equivalent to the cross-sectional area of a plane wave tube (see Fig. 6.2).

6.3 Damped Mass-Spring Piston in a Baffle of Finite Impedance

If a rigid piston were mounted in a finite impedance baffle within the tube, the modeling becomes more complicated [69, pp.144-146]. A mechanical schematic drawing of this arrangement is given in Fig. 6.4.

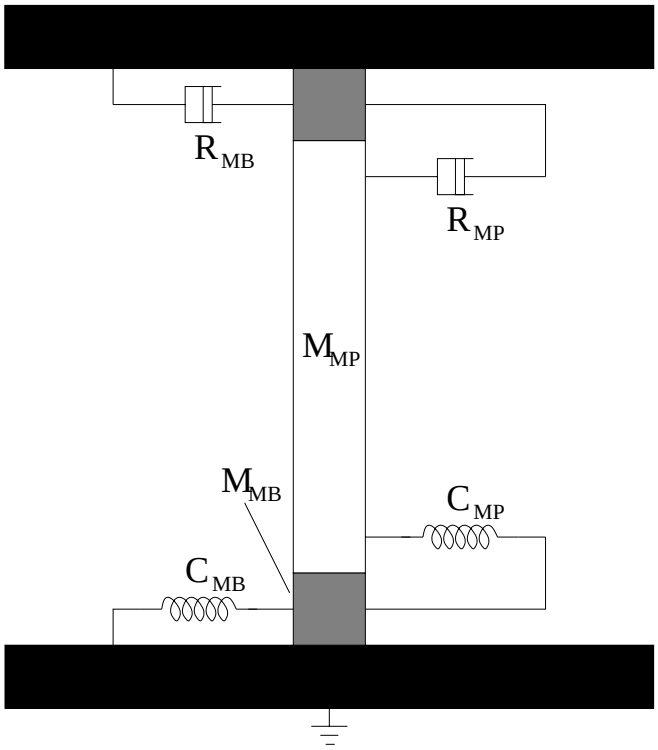

Fig. 6.4. Schematic drawing of a theoretical piston with mass M_{MP}, compliance C_{MP}, and resistance R_{MP}, mounted in a baffle of finite impedance inside a plane wave tube.

The finite impedance baffle is modeled as a lumped element system. The mechanical circuit elements of the inner piston system are not directly connected to mechanical ground. Instead, they are connected to the mechanical circuit elements of the baffle. The model requires dual area gyrators for the equivalent circuit, as the volume velocity through the composite partition has a "choice" of whether to go through the baffle or through the piston. The equivalent circuit for the arrangement is shown in Fig. 6.5.

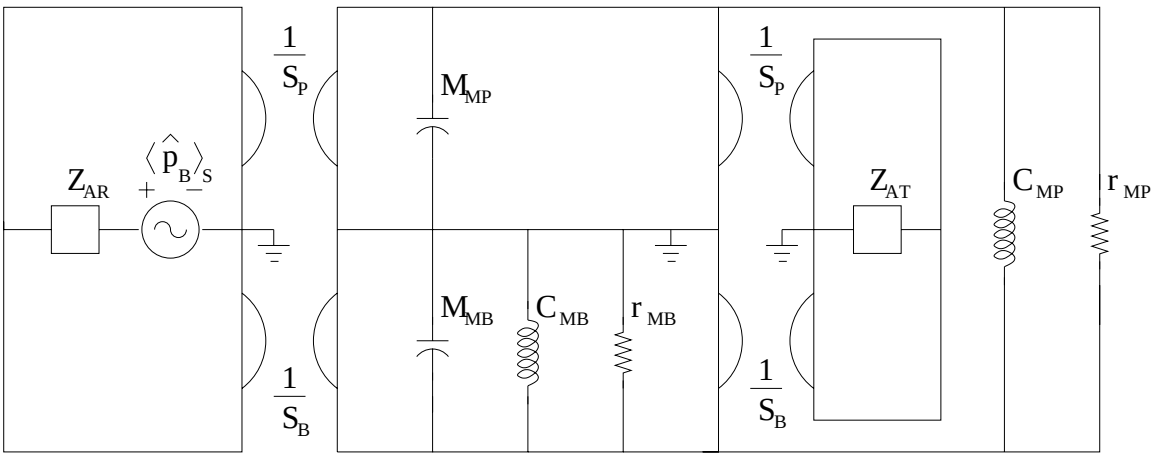

Fig. 6.5. Multiple-domain equivalent circuit for a rigid piston mounted in a baffle of finite impedance (see Fig. 6.4).

6.4 Moving-Coil Driver Mounted in a Rigid Baffle

A drawing of a loudspeaker driver mounted in a baffle of finite impedance is shown in Fig. 6.6. It should be noted that the mass of the driver frame and magnet structure will affect the impedance of the baffle; it must be included with the mass of the baffle. An equivalent circuit modeling the arrangement is shown in Fig. 6.7 [69, pp.203-210]. Two differences from the circuit given in Fig. 6.5 should be pointed out. First, the loudspeaker driver may contain an electrical impedance portion Z_E, which is shown in the mechanical mobility domain in Fig. 6.7. Second, the termination impedance Z_{AT} is now represented as Z'_{AT}, showing that Z_{AT} has been translated up to the downstream face of the driver cone through the acoustical filtering of the magnet structure and frame. The subscripts MS and MD denote the mechanical elements of the suspension and the diaphragm respectively.

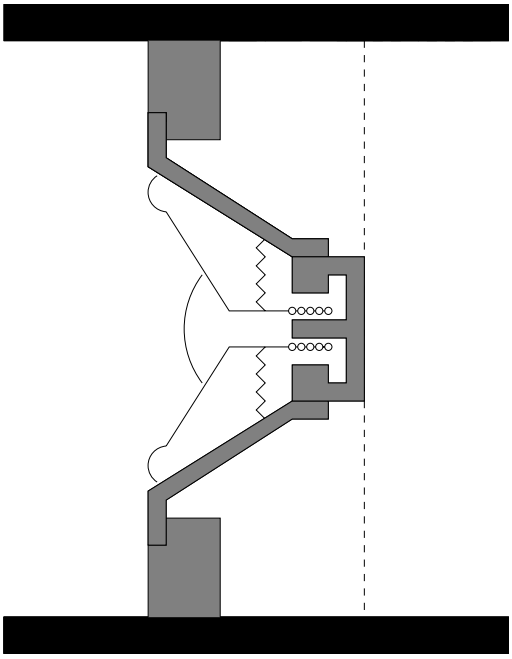

Fig. 6.6. Schematic drawing of a loudspeaker driver mounted in a baffle of finite impedance [69, Fig. 5.6]. The dashed line represents the point at which the previous termination impedance Z_{AT} began.

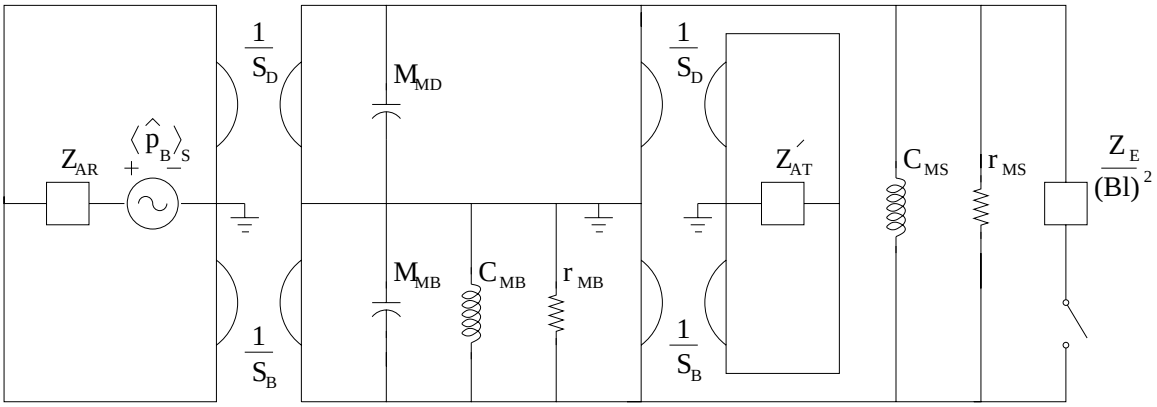

Fig. 6.7. Multiple-domain equivalent circuit for the setup displayed in Fig. 6.6. The switch in the circuit represents a wire that may be connected to include the electrical portion of the driver [69, Fig. 5.7].

A reasonable assumption may be made in order to simplify the circuit in Fig. 6.7: the impedance of the baffle is very large compared with the impedance of the driver diaphragm assembly. This assumption, along with the long-wavelength assumption,

allow the baffled driver under test to be represented by the simplified equivalent circuit shown in Fig. 6.8 [70]-[71].

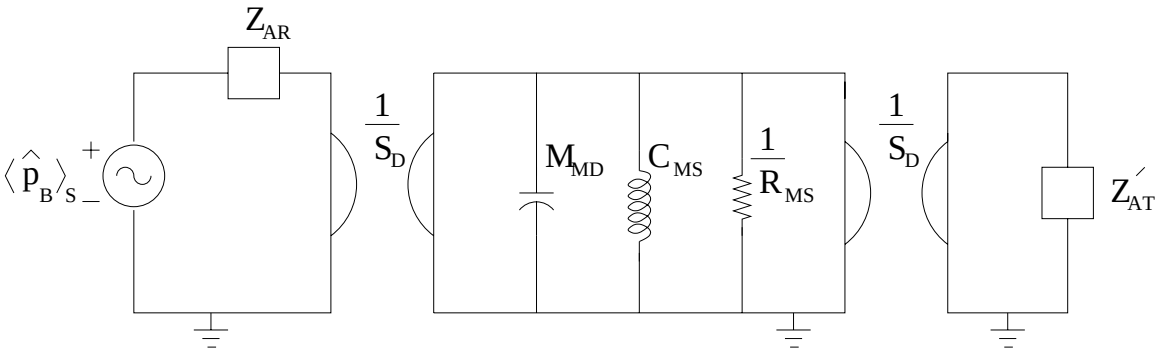

Fig. 6.8. Simplified multiple-domain equivalent circuit after some assumptions have been made. The loudspeaker driver modeled here is in an open-circuit condition (electrical portion not included).

The circuit given in Fig. 6.8 may be represented entirely in the acoustic impedance domain, as shown in Fig. 6.9 [70]-[71].

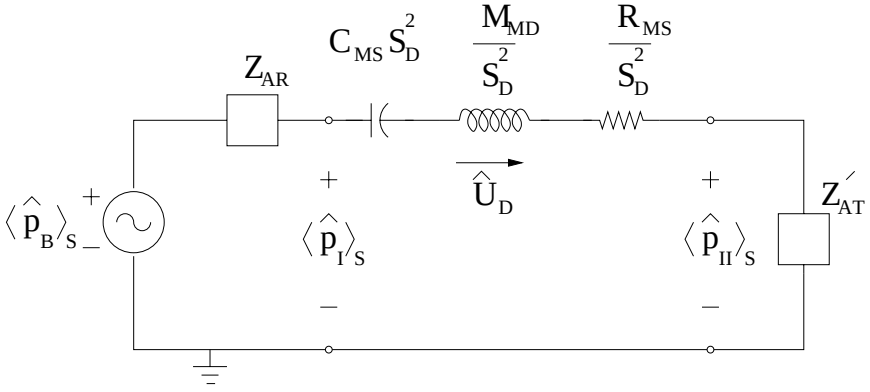

Fig. 6.9. Simplified acoustic impedance equivalent circuit for a driver under test in an open-circuit condition.

The loudspeaker driver may be configured in an open or closed-circuit condition. An open-circuit condition means that the electrical impedance portion of the driver is not included (see Figs. 6.7-6.9). The closed-circuit condition means that a wire has been

placed between the driver terminals to include the electrical impedance of the driver under test, as shown in Fig. 6.10.

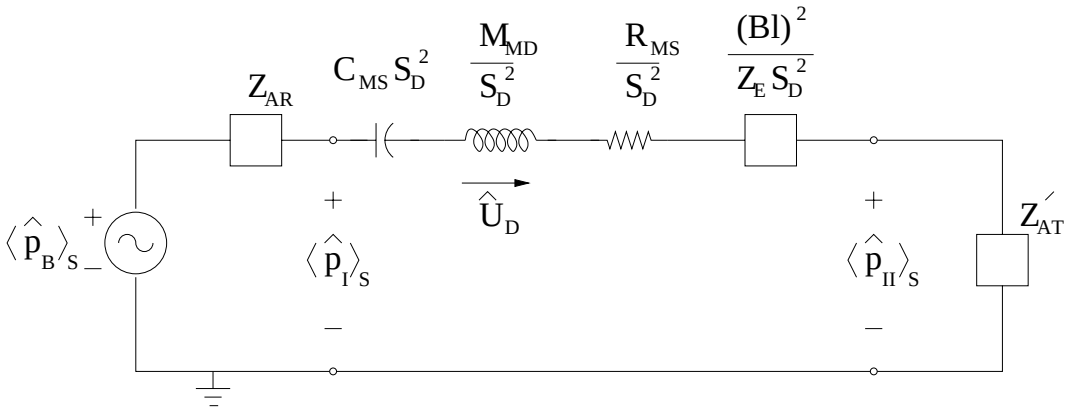

Fig. 6.10. Acoustic impedance equivalent circuit for a driver under test in the closed-circuit condition.

In experimental work, an initial measurement of the open-circuit condition is useful because the mechanical portion of the loudspeaker driver is separated entirely from the electrical portion. This means the mechanical parameters cannot be contaminated by an incorrect estimate of the force factor (Bl product). In addition, the inductance of the voice coil does not need to be neglected in the process. Once the mechanical parameters have been thus determined, an accurate determination of the electrical parameters should follow.

One potential limitation in the acoustical measurement of a driver mounted inside a plane wave tube is the frequent uncertainty of the exact acoustic one-dimensional center of the driver. Some acoustical quantities rely on an accurate determination of its location. Others, such as the transmission coefficient, reflection coefficient modulus, and absorption coefficient are not nearly as sensitive to its location (assuming a lossless tube).

CHAPTER 7

DRIVER PARAMETER MEASUREMENTS USING PLANE WAVE TUBES: THEORETICAL DEVELOPMENTS

In Chapter 5, expressions were developed for several acoustically determined quantities. As shown in Chapter 6, these expressions are functions of the impedance of the driver under test. The resonant nature of the open-circuit driver impedance and the predictable behavior of the closed-circuit condition lend themselves to straightforward parameter derivations. The following sections present the theory of the proposed parameter derivations, a discussion of parameters derived from experimental data, and a discussion of inherent limitations of the method.

7.1 Parameter Expressions Using Transmission Coefficients

At the open-circuit resonance frequency of a driver under test, the reactance of the impedance vanishes, allowing determination of mechanical resistance. Once mechanical resistance is known, the mechanical reactance can be determined as a function of frequency. When the circuit is closed, the electrical impedance portion is included. Since three unknowns result from the addition of the electrical impedance, some assumptions must be made to maximize the utility of this second condition and its resulting data. At lower frequencies, the impedance due to inductance is small compared to the DC resistance of the voice coil. Thus, if the DC resistance is already known (e.g., via an ohmmeter measurement) the force factor Bl may be determined in the low frequency limit. Once the force factor is determined in this fashion, the value may be

substituted back into a governing equation to allow determination of voice coil inductance as a function of frequency.

The expressions given for transmission loss, under both open and closed-circuit conditions, may be analyzed to yield desired parameters. They depend upon the baffled driver impedance and the downstream impedance of the receiving tube. Ideally, the receiving tube should be anechoically terminated so that its input impedance is the characteristic impedance of the medium. An important benefit of transmission loss measurements over other acoustical measurements is that they are relatively insensitive to the precise distance between a measurement microphone and the one-dimensional acoustic center of a driver under test. As indicated in Chapter 6, other acoustic quantities require knowledge of these distances to a high degree of accuracy [41]. Nevertheless, when using transmission loss measurements, the accuracy of derived parameters depends upon the accuracy of the resonance frequency measured at the minimum of the transmission loss curve. Unfortunately, the downstream loading seen by the driver can significantly influence this minimum.

A theoretical basis for deriving loudspeaker parameters from transmission loss measurements will be given in the following subsections. Formulas will be derived for both open-circuit and closed-circuit conditions.

7.1.1 Open-Circuit Determination of Mechanical Parameters

In Chapter 5, an expression was given for the transmission loss in terms of the transmission coefficient [see Eq. (5.10)]:

$$TL = 10\log_{10}\left(\frac{1}{\tau}\right). \tag{7.1}$$

Because of the form of the argument in this expression and for reasons of simplicity, the inverse of the transmission coefficient will be analyzed in the following developments. Referring to Fig. 6.9 and Eq. (6.7), the black box impedance $Z_{M,BB}$ is the mechanical impedance of the driver under test. The mechanical impedance $Z_{M,II}$ is the translated mechanical termination impedance Z_{MT} seen by the downstream driver face. (Here we assume $Z'_{AT} = Z_{AT} = Z_{MT}/S^2$.) These substitutions allow Eq. (6.7) to be expressed in the following form:

$$\frac{1}{\tau_{OC}} = \left| \frac{Z_M \left(\frac{S}{S_D} \right)^2 + Z_{MT} + \rho_0 c S}{Z_{MT} + \rho_0 c S} \right|^2, \tag{7.2}$$

where the mechanical impedance of the driver is

$$Z_M = R_{MS} + jX_M = R_{MS} + j\left(\omega M_{MD} - \frac{1}{\omega C_{MS}} \right). \tag{7.3}$$

In these expressions, X_M is the mechanical reactance of the open-circuit driver and Z_{MT} consists of resistive and reactive components R_{MT} and X_{MT}:

$$Z_{MT} = R_{MT} + jX_{MT}. \tag{7.4}$$

At the mechanical resonance frequency of the driver, the imaginary part of the open-circuit driver impedance vanishes so that

$$\frac{1}{\tau_{OC,0}} = \left| \frac{R_{MS} \left(\frac{S}{S_D} \right)^2 + Z_{MT,0} + \rho_0 c S}{Z_{MT,0} + \rho_0 c S} \right|^2, \tag{7.5}$$

where the subscript 0 denotes the respective values at the resonance frequency. The mechanical resistance R_{MS} may be solved directly from Eq. (7.5):

$$R_{MS} = \left(\frac{S_D}{S}\right)^2 \left(\pm \left[\left[(\rho_0 cS + R_{MT,0})^2 + X_{MT,0}^2 \right] \frac{1}{\tau_{OC,0}} - X_{MT,0}^2 \right]^{\frac{1}{2}} - (\rho_0 cS + R_{MT,0}) \right), \quad (7.6)$$

where the positive root is chosen for physical reasons because the negative root gives a negative resistance. Once the mechanical resistance is known, the reactance of the open-circuit impedance is determined from Eqs. (7.2) and (7.3):

$$X_M = \left(\frac{S_D}{S}\right)^2 \left(\pm \left[\left[(\rho_0 cS + R_{MT})^2 + X_{MT}^2 \right] \frac{1}{\tau_{OC}} - \left[\rho_0 cS + R_{MT} + R_{MS} \left(\frac{S}{S_D}\right)^2 \right]^2 \right]^{\frac{1}{2}} - X_{MT} \right), \quad (7.7)$$

where the appropriate root is chosen to maintain a physically valid solution over frequency. The expression for the reactance in Eq. (7.7) is frequency dependent due to τ_{OC}, R_{MT}, and X_{MT}.

7.1.2 Open-Circuit Anechoic Termination Simplification

As the termination impedance approaches an anechoic value, the expressions given above for resistance and reactance of the open-circuit driver impedance simplify to the following:

$$R_{MS} = \left(\frac{S_D}{S}\right)^2 (2\rho_0 cS) \left(\pm \left[\frac{1}{\tau_{OC,0}} \right]^{\frac{1}{2}} - 1 \right), \quad (7.8)$$

$$X_M = \pm\left(\frac{S_D}{S}\right)^2\left[(2\rho_0 cS)^2\frac{1}{\tau_{OC}} - \left[2\rho_0 cS + R_{MS}\left(\frac{S}{S_D}\right)^2\right]^2\right]^{\frac{1}{2}}. \tag{7.9}$$

7.1.3 Closed-Circuit Determination of Electrical Parameters

Referring to Fig. 6.10 and Eq. (6.7), the black box impedance $Z_{M,BB}$ for the closed-circuit condition includes the driver electrical elements. Equation (6.7) may then be expressed in the following form:

$$\frac{1}{\tau_{CC}} = \left|\frac{Z_M\left(\frac{S}{S_D}\right)^2 + \frac{(Bl)^2}{Z_E}\left(\frac{S}{S_D}\right)^2 + Z_{MT} + \rho_0 cS}{Z_{MT} + \rho_0 cS}\right|^2, \tag{7.10}$$

where τ_{CC} is the closed-circuit transmission coefficient and $Z_E = R_{VC} + j\omega L_{VC}$ is the electrical impedance of the isolated electrical portion of the driver.

In the derivation of parameters using electrical impedance measurements, it is common to ignore the effects of voice-coil inductance at low frequencies (see Section 3.1). Using this assumption, the isolated electrical impedance becomes purely real. In practice, it is common to measure DC resistance of the voice coil separately from other impedance measurements using a simple ohmmeter test. If the DC resistance is known from this type of measurement, it can be used along with the preceding results for the mechanical impedance, and the force factor can be determined from Eq. (7.10) in the low frequency limit:

$$Bl \approx \pm \left(\begin{array}{l} \pm R_{VC} \left(\frac{S_D}{S} \right)^2 \left[\left[(\rho_0 cS + R_{MT})^2 + X_{MT}^2 \right] \frac{1}{\tau_{CC}} - \left[\left(\frac{S}{S_D} \right)^2 X_M + X_{MT} \right]^2 \right]^{\frac{1}{2}} \ldots \\ \ldots - \left[\rho_0 cS + R_{MT} + \left(\frac{S}{S_D} \right)^2 R_{MS} \right] \end{array} \right)^{\frac{1}{2}}, \tag{7.11}$$

where the appropriate roots are chosen to maintain a physically valid solution over frequency.

Once the force factor is thus determined, the inductance of the voice coil may be characterized as a function of frequency. Solving Eq. (7.10) for the inductance yields

$$L_{VC} = \frac{-(Bl)^2 \left(\frac{S}{S_D} \right)^2 \left[X_M \left(\frac{S}{S_D} \right)^2 + X_{MT} \right] \pm \left[\begin{array}{l} -(R_{VC}\gamma)^2 \ldots \\ \ldots + \left[(Bl)^2 \left(\frac{S}{S_D} \right)^2 \right]^2 \left[\gamma + \left[X_M \left(\frac{S}{S_D} \right)^2 + X_{MT} \right]^2 \right] \ldots \\ \ldots + 2R_{VC} (Bl)^2 \gamma \left(\frac{S}{S_D} \right)^2 \left[R_{MT} + \rho_0 cS + R_{MS} \left(\frac{S}{S_D} \right)^2 \right] \end{array} \right]^{\frac{1}{2}}}{\omega\gamma}, \tag{7.12}$$

where

$$\gamma = \frac{1}{\tau_{CC}} \left[X_{MT}^2 + (R_{MT} + \rho_0 cS)^2 \right] - \left[\left[R_{MT} + \rho_o cS + R_{MS} \left(\frac{S}{S_D} \right)^2 \right]^2 + \left[X_M \left(\frac{S}{S_D} \right)^2 + X_{MT} \right]^2 \right] \tag{7.13}$$

and roots are again chosen to maintain physical validity.

7.1.4 Closed-Circuit Anechoic Termination Simplification

As the termination impedance approaches the impedance of an anechoic termination, the above expressions for the force factor and the inductance of the closed-circuit driver impedance simplify to the following:

$$Bl \approx \pm\left(R_{VC}\left(\frac{S_D}{S}\right)^2\left(\pm\left[\left[(2\rho_0 cS)^2\right]\frac{1}{\tau_{CC}} - \left[\left(\frac{S}{S_D}\right)^2 X_M\right]^2\right]\right)^{\frac{1}{2}} - \left[2\rho_0 cS + \left(\frac{S}{S_D}\right)^2 R_{MS}\right]\right)^{\frac{1}{2}} \quad (7.14)$$

$$L_{VC} = \frac{-(Bl)^2\left(\frac{S}{S_D}\right)^2\left[X_M\left(\frac{S}{S_D}\right)^2\right] \pm \left[\begin{array}{l} -(R_{VC}\gamma)^2 + \left[(Bl)^2\left(\frac{S}{S_D}\right)^2\right]^2\left[\gamma + \left[X_M\left(\frac{S}{S_D}\right)^2\right]^2\right]\ldots \\ \ldots + 2R_{VC}(Bl)^2\gamma\left(\frac{S}{S_D}\right)^2\left[2\rho_0 cS + R_{MS}\left(\frac{S}{S_D}\right)^2\right] \end{array}\right]^{\frac{1}{2}}}{\omega\gamma} \quad (7.15)$$

where

$$\gamma = \frac{1}{\tau_{CC}}\left[(2\rho_0 cS)^2\right] - \left[\left[2\rho_o cS + R_{MS}\left(\frac{S}{S_D}\right)^2\right]^2 + \left[X_M\left(\frac{S}{S_D}\right)^2\right]^2\right]. \quad (7.16)$$

7.2 Parameter Derivations from Experimental Data

When using plane wave tube measurement data, the derivation of parameter values from the equations in Section 7.1 requires special attention. The following subsections discuss several issues regarding experimentally determined parameters.

7.2.1 Mechanical Parameters from Open-Circuit Transmission Loss

Two types of parameter derivation procedures have been developed to derive loudspeaker parameters from the measured transmission loss of a baffled driver under test. One parameter derivation procedure involves frequency limit assumptions and the other involves a curve fit of the mechanical reactance [Eq. (7.7) or (7.9)]. Both involve the same effective radiating surface area, *in vacuo* resonance frequency, and mechanical resistance. They differ in the method used to obtain the reactance parameters of the mechanical system (M_{MD} and C_{MS}).

The effective radiating surface area of the diaphragm is determined by measuring the diameter of the cone and adding half the width of the surround [14, p.28]:

$$S_D = \pi\left(\frac{d}{2}\right)^2, \tag{7.17}$$

where d is the overall diameter. The *in vacuo* resonance frequency is estimated from the frequency at the minimum of the transmission loss curve. The mechanical resistance of the suspension system is determined using the transmission loss value at the resonance frequency, as indicated in Eq. (7.6) or Eq. (7.8).

The frequency-limit approach utilizes the fact that the impedance due to the moving mass dominates the high frequency mechanical impedance in the open-circuit condition; the contribution due to the suspension compliance is neglected. Equations (7.7) and (7.9) are then modified and solved for the moving mass M_{MD} directly. Once the value for M_{MD} is determined in the high frequency limit, the value for the suspension compliance is obtained through the *in vacuo* resonance frequency:

$$C_{MS} = \frac{1}{(2\pi f_0)^2 M_{MD}}. \tag{7.18}$$

The curve-fitting approach involves fitting the broadband reactance curve given in Eqs. (7.7) and (7.9). The curve fit searches for a least-squares weighted optimum fit to a transfer function containing two zeros and one pole:

$$X_{fit} = \frac{M_{MD}s^2 + \frac{1}{C_{MS}}}{s} = \frac{b_1 s^2 + b_2 s + b_3}{a_1 s + a_2}, \tag{7.19}$$

where X_{fit} is the transfer function form of the mechanical reactance X_M, $s = j\omega$, and the coefficients b_1, b_2, b_3, a_1, and a_2 refer to the coefficients of the transfer function form used in the complex curve fitting routines of MATLAB. (Even though the reactance is not complex, a complex curve fit algorithm was used.) Once the complex curve fit algorithm has found a least squares solution for the coefficients, determination of the values for the moving mass and the suspension compliance is straightforward:

$$M_{MD} = b_1, \tag{7.20}$$

$$C_{MS} = \frac{1}{b_3}. \tag{7.21}$$

If the curve fit is successful, the other coefficients should satisfy the following relationships:

$$b_2 = a_2 = 0, \tag{7.22}$$

$$a_1 = 1. \tag{7.25}$$

7.2.2 Electrical Parameters from Closed-Circuit Transmission Loss

As indicated in Eqs. (7.11) and (7.14) above, the force factor Bl may be determined in the low-frequency limit of the transmission loss data if the DC voice-coil resistance is given and the impedance due to the voice-coil inductance is neglected. However, because of inherent low-frequency limitations in the two-microphone transfer function technique, the accurate low-frequency portion of the curve must be fitted with a least-square linear approximation then extrapolated to lower frequencies. The force factor equals the extrapolated y-intercept value of the linear fit.

Using the experimentally determined force factor, the voice-coil inductance follows from Eqs. (7.12) and (7.13) or from Eqs. (7.15) and (7.16). If the inductance is constant over frequency, these complicated equations should produce a flat broadband estimate. However, D'Appolito suggests that the voice-coil inductance tends to decrease with increasing frequency [14, p.32]. The acoustical testing method provides a convenient means to verify this prediction.

7.3 Accuracy of Parameter Derivation Methods

Numerically generated transmission loss data can provide a means of investigating the accuracy of the parameter derivation methods described above. The data is generated from the following hypothetical driver parameters: $C_{MS} = 400\mu m/N$,

$M_{MD} = 80g$, $R_{MS} = 4kg/s$, $S_D = 0.030m^2$, $Bl = 8T \cdot m$, $R_{VC} = 5\Omega$, and $L_{VC} = 1mH$. Figures. 7.1 and 7.2 show the theoretical transmission loss curves for open and closed-circuit conditions, and the offset effect that a measured termination impedance may have on transmission loss data at low frequencies (also see Fig. 7.3).

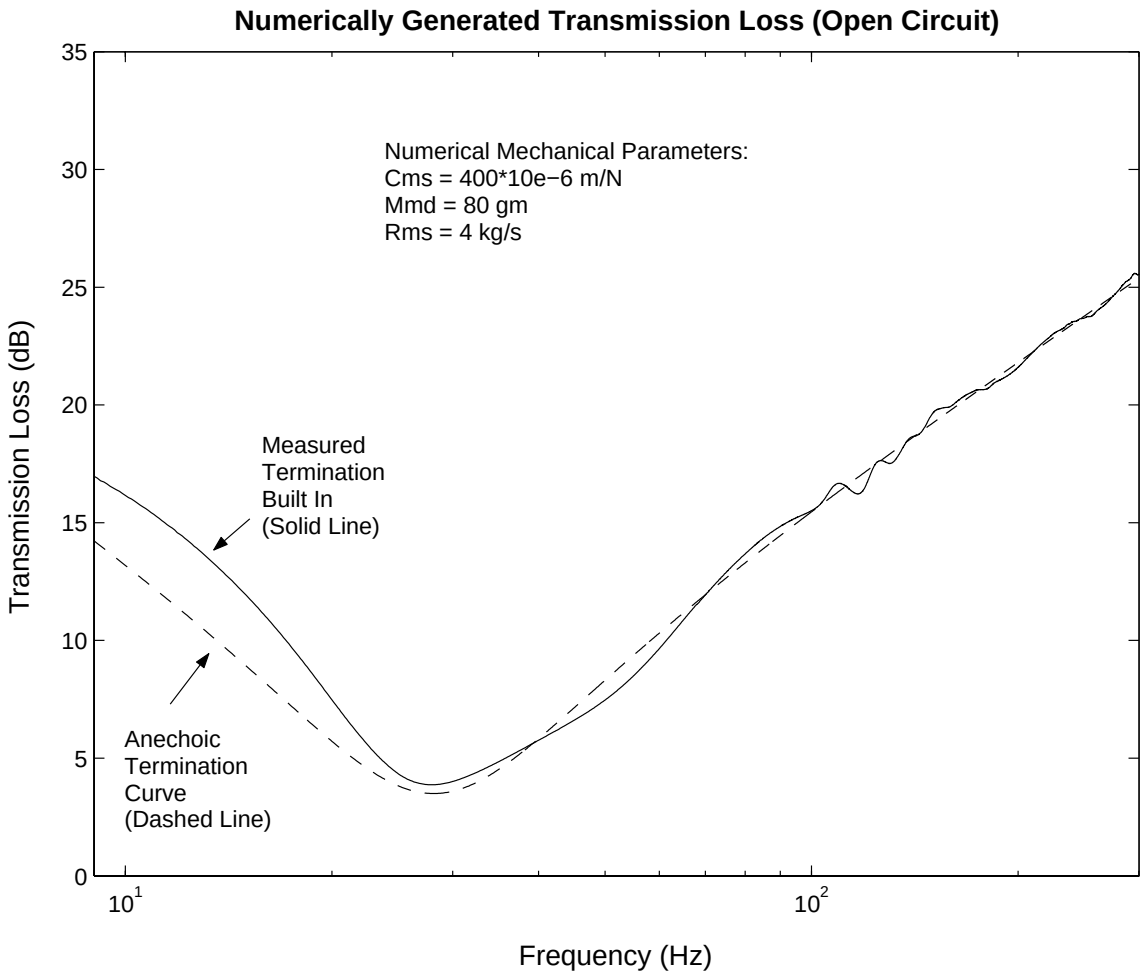

Fig. 7.1. Numerically generated transmission loss for an open-circuit driver with a presumed anechoic termination (dashed line) and an experimentally measured termination impedance (solid line).

The curves show that nonanechoic behavior of the measured termination causes the transmission loss curve to deviate from the anechoic termination curve at lower frequencies and oscillate about the anechoic termination curve at higher frequencies.

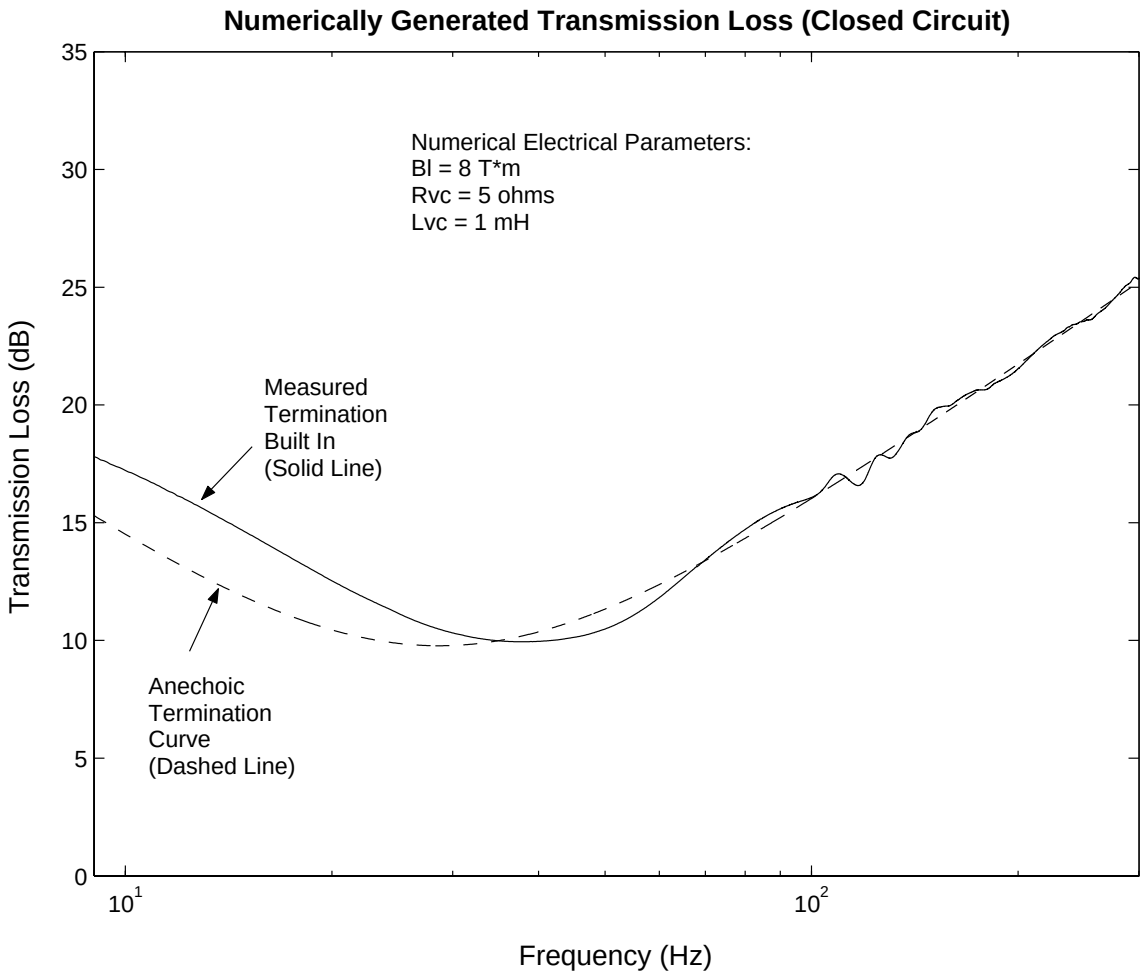

Fig. 7.2. Numerically generated transmission loss for a closed-circuit driver with a presumed anechoic termination (dashed line) and an experimentally measured termination impedance (solid line).

The measured reflection coefficient magnitude of the experimental termination is shown in Fig. 7.3. It reveals the increasingly non-anechoic behavior of the termination with decreasing frequency. Typically, a termination is considered anechoic if its reflection coefficient magnitude is less than 0.1. (This means that the termination absorbs at least 99% of sound energy incident upon it [72].) For ideal anechoic conditions, the reflection coefficient magnitude should be identically equal to zero. The

low-frequency rise in the reflection coefficient magnitude explains why there is an offset in the transmission loss curves in Figs. 7.1 and 7.2. One may also notice that bumps in the reflection coefficient curve correlate to undulations in the transmission loss curve involving the measured termination impedance.

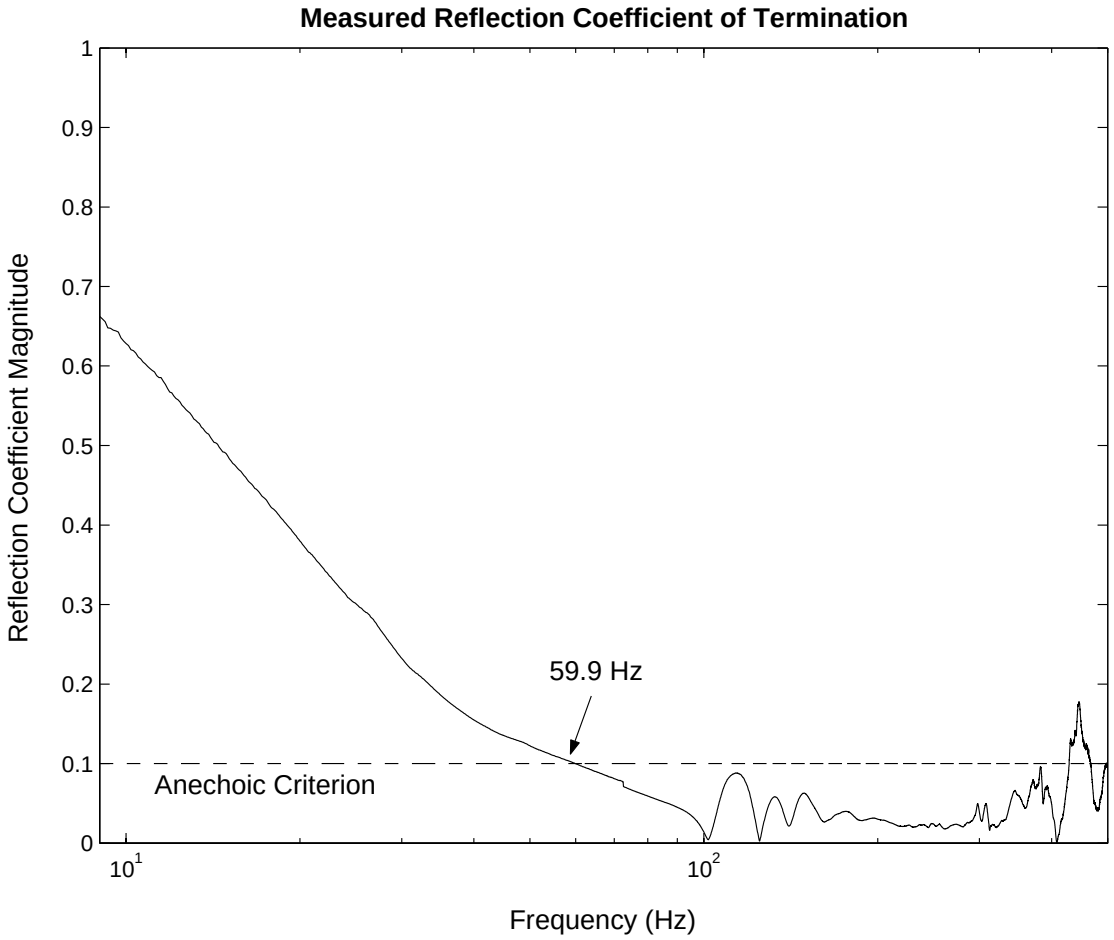

Fig. 7.3. Measured reflection coefficient magnitude of the termination. The dashed line represents the anechoic qualification limit (measured termination data below this line is considered to provide an anechoic loading).

The measured termination transmission loss curves may be processed using the proposed parameter derivation methods to generate a set of parameters that are compared with the original theoretical parameters. Table 7.1 displays the values obtained through the use of the methods described in Section 7.2. Table 7.2 shows the bias errors resulting from the measured termination behavior and the assumptions made in Section 7.2 (such as the assumption that the high frequency data is not affected by the impedance due to the compliance of the suspension for the driver under test). The abbreviations in Tables 7.1 and 7.2 indicate the following: TL (transmission loss), P (high-frequency portion fit method), R (reactance curve fit method), A (assumed anechoic termination impedance), and MT (measured termination impedance).

Parameters	Numerical	TL P A	TL P MT	TL R A	TL R MT
Cms	400.0	419.4	417.1	379.8	420.6
Mmd	80.00	79.42	79.84	83.06	82.88
Rms	4.000	4.525	3.996		
Bl	8.000	8.478	8.664		

Table 7.1. Derived parameter values for C_{MS} $(\mu m/N)$, M_{MD} (g), R_{MS} (kg/s), and Bl $(T \cdot m)$, from the numerically generated transmission loss curve. The data either assumes an anechoic termination or includes the measured termination impedance.

Bias Errors	Numerical	TL P A	TL P MT	TL R A	TL R MT
Cms (mu m/N)	0.00	4.85	4.28	-5.05	5.15
Mmd (gm)	0.00	-0.72	-0.20	3.83	3.60
Rms (m. ohms)	0.00	13.13	-0.10		
Bl (T*m)	0.00	5.98	8.30		

Table 7.2. Percent bias errors of derived parameter values using the original set of theoretical parameter values as the reference values.

Some interesting conclusions may be drawn from the results in Table 7.2. The moving mass estimate result contains a small bias error, while the suspension compliance estimate result contains a much larger bias error. This may be attributed to the estimate of the *in vacuo* resonance frequency from the minimum of the transmission loss curve. The estimate of the *in vacuo* resonance frequency assumes an anechoic termination loading, which is not exactly the case in Fig. 7.1. Therefore, compliance estimates will largely depend upon the assumption that the termination loading is anechoic. It may also be noted that the accuracy of the force factor estimate is inherently limited.

CHAPTER 8

DRIVER PARAMETER MEASUREMENTS USING PLANE WAVE TUBES: EXPERIMENTAL RESULTS

Chapter 7 outlined equations and procedures for the determination of loudspeaker parameters using the plane wave tube method. This chapter presents experimental results of the method using the constructed plane wave tube system and the nine drivers previously tested using electrical techniques. Sample measurements will be discussed for one of the drivers. Average parameter results will then be presented for all nine drivers.

8.1 Measurement System

An advantage of the two-microphone transfer function technique is that it enables one to decompose one-dimensional sound fields using inexpensive microphones. The chief requirement for the microphones is that they remain stable throughout calibration and measurement runs. Nevertheless, eight type 1 precision microphones were used in the measurements of this work: the Larson Davis model 2551, 1/2" ICP microphones with The Modal Shop (a division of PCB) TMS426C01 preamps. A Hewlett Packard E1432A Dynamic Signal Analyzer card was used to power the microphones and process the microphone signals. The VXI analyzer was controlled using the Data Physics SignalCalc 620 software package. The multiple-input, multiple-output (MIMO) option was used to obtain the necessary measurement transfer functions. Calibration runs were performed using the basic transfer function option. As suggested earlier, the various calibration runs between each microphone pair consisted of a measurement of the transfer

function in an original position, and a measurement of the transfer function with microphone positions switched. Measurement of the auto-power spectrum also had to be performed for one microphone in each pair of microphones (microphones 4, 6, 7, and 9, in Fig. 8.1). The auto-power spectrum measurement allows comparison of upstream and downstream sound pressure levels, which is essential to establish the fraction of sound power transmitted through the driver under test.

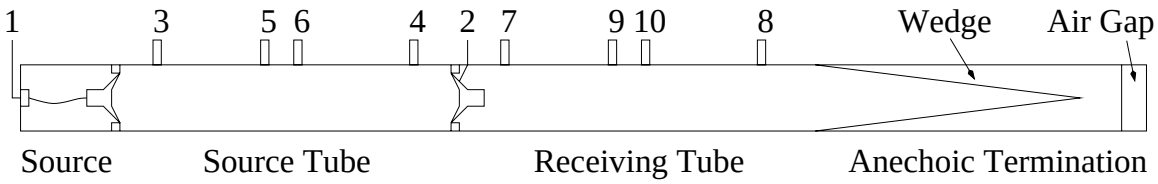

Fig. 8.1. Diagram of channel numbering and tube layout for the constructed plane wave tube.

A total of ten channels were used in the measurement procedure. A random noise signal generated by the analyzer was amplified and used to drive the tube excitation loudspeaker. This signal was also monitored by the analyzer input channel 1. Channel 2 was used to monitor the open-circuit voltage signal generated at the terminals of the driver under test. Channels 3 through 6 were used for the upstream pairs of microphones, with 3 and 4 used in the low-frequency spacing and 5 and 6 used in the high-frequency spacing. Channels 7 though 10 were used for the downstream pairs of microphones, with 7 and 8 used in the low-frequency spacing and 9 and 10 used in the high-frequency spacing. The MIMO analyzer option requires that a reference channel be specified for each pair of microphones. The lower channel number in each microphone pair was used as the reference microphone; it was consistently the upstream microphone relative to the other microphone.

8.2 Signal Processing

The SignalCalc 620 software allows measured transfer functions to be exported in an ASCII file format. This output data was then imported into MATLAB to calibrate the measured transfer functions and compute desired acoustical quantities. The required processing for each microphone pair is identical. The raw data imported into MATLAB for each pair is made up of the following quantities: the original position and switched position calibration transfer functions H_{mn}^{o} and H_{mn}^{s}, the auto-power spectrum G_{mm} for the signals of microphones closest to the driver under test (both upstream and downstream of the driver partition), and the measured transfer function $H_{Measured,mn}$ from the microphone signals.

Here is an example of the calibration processing, used in the computation of transmission loss at low frequencies (L) (refer to Fig. 8.1 and Chapter 5). The upstream (U) calibration transfer function $H_{Cal,34}^{U,L}$ is computed using the following equation:

$$H_{Cal,34}^{U,L} = \sqrt{H_{34}^{U,O} H_{34}^{U,S}} \,. \tag{8.1}$$

The downstream (D) calibration transfer function $H_{Cal,78}^{D,L}$ is computed similarly:

$$H_{Cal,78}^{D,L} = \sqrt{H_{78}^{D,O} H_{78}^{D,S}} \,. \tag{8.2}$$

A transmission (T) calibration transfer function, $H_{Cal,47}^{T,L}$, must also be computed to calibrate the microphones used for the auto-power spectrum measurements (microphones 4 and 7)

$$H_{Cal,47}^{T,L} = \sqrt{H_{47}^{T,O} H_{47}^{T,S}} \,. \tag{8.3}$$

Once these calibration transfer functions have been computed, the measured transfer functions H_{34}^{U} and H_{78}^{D} may be calibrated as follows:

$$H_{34}^{U} = \frac{H_{Data,34}^{U,L}}{H_{Cal,34}^{U,L}}, \tag{8.4}$$

$$H_{78}^{D} = \frac{H_{Data,78}^{D,L}}{H_{Cal,78}^{D,L}}. \tag{8.5}$$

Computation of transmission quantities, such as the power transmission coefficient and the transmission loss of the driver under test, requires that the upstream and downstream reflection coefficients be computed:

$$R_{34}^{U} = \frac{H_{34}^{U} - e^{-jks_1}}{e^{jks_1} - H_{34}^{U}} e^{j2ks_1}, \tag{8.6}$$

$$R_{78}^{D} = \frac{H_{78}^{D} - e^{-jks_1}}{e^{jks_1} - H_{78}^{D}}, \tag{8.7}$$

where s_1 is the spacing between microphones 3 and 4, and microphones 7 and 8. It should be noted that the upstream reflection coefficient must be evaluated at microphone position 4 where the auto-power spectrum measurement is made. Thus, the e^{j2ks_1} term translates the complex reflection coefficient from microphone position 3 to microphone position 4. The downstream auto-power spectrum measurement is made at microphone position 7; no translation is necessary.

If the upstream and downstream reflection coefficients are desired at the position of the driver under test, both coefficients must be translated from the microphone positions. The complex acoustic impedance of the driver depends upon the complex reflection coefficient evaluated at the one-dimensional acoustic center of the driver. Unfortunately, this acoustic center is difficult to ascertain. While the acoustic impedance

would be an ideal quantity for use in the driver analysis, its sensitivity to the precise acoustic center renders it an impractical quantity for the methods described in this work. However, if the magnitude of the reflection coefficient is desired, translation to the acoustic center of the driver is unnecessary. If one assumes that the tube is lossless over the distance between a microphones and the acoustic center, the magnitude of the reflection coefficient remains constant over that distance.

The transmission coefficient, as shown in Eq. (5.9), must be modified to include the calibration transfer function for transmission quantities:

$$\tau = \frac{G_{77}}{G_{44}} \left| \frac{1}{H^{T}_{Cal,47}} \right|^2 \left| \frac{1+R^{U}_{34}}{1+R^{D}_{78}} \right|^2 , \tag{8.8}$$

where G_{77} and G_{44} are the auto power spectra from the signals of microphones 4 and 7, respectively. The transmission loss may also be computed using the form of Eq. (5.10), with the calibration transfer function included:

$$TL = 10\log_{10}\left(\frac{1}{\tau}\right) = 10\log_{10}\left(\frac{G_{44}}{G_{77}}\right) + 20\log_{10}\left|H^{T}_{Cal,47}\right| + 20\log_{10}\left|\frac{1+R^{D}_{78}}{1+R^{U}_{34}}\right| . \tag{8.9}$$

8.3 Experimental Example

An experimental example of the parameter determination process will now be presented. The upstream and downstream microphones are used to determine reflection coefficients in the source tube and receiving tube, respectively. The downstream reflection coefficient yields the dimensionless termination impedance $\frac{Z'_{AT}}{\rho_0 c/S}$, shown in Fig. 8.2.

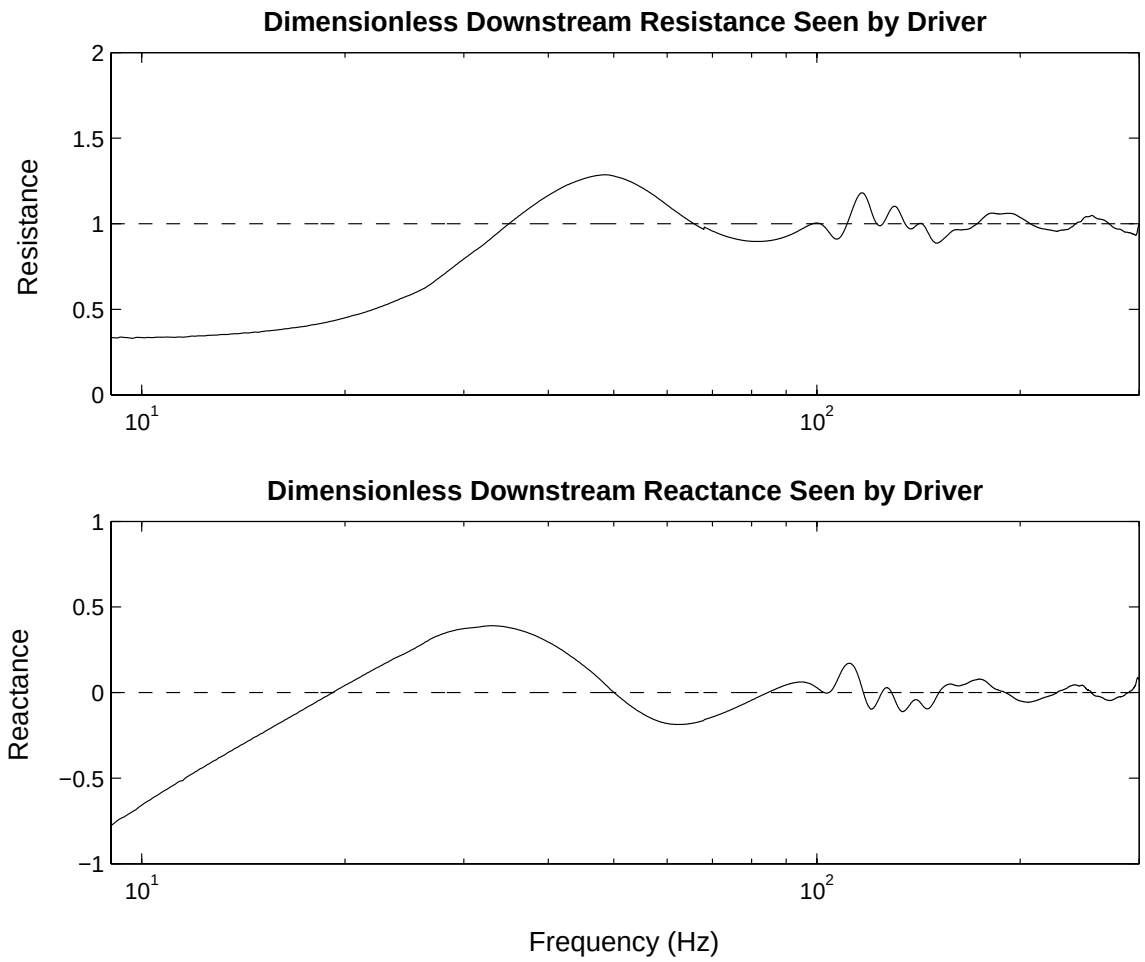

Fig. 8.2. Measured dimensionless termination impedance.

The measured upstream reflection coefficient moduli of the driver under both open and closed-circuit conditions are shown in Fig. 8.3.

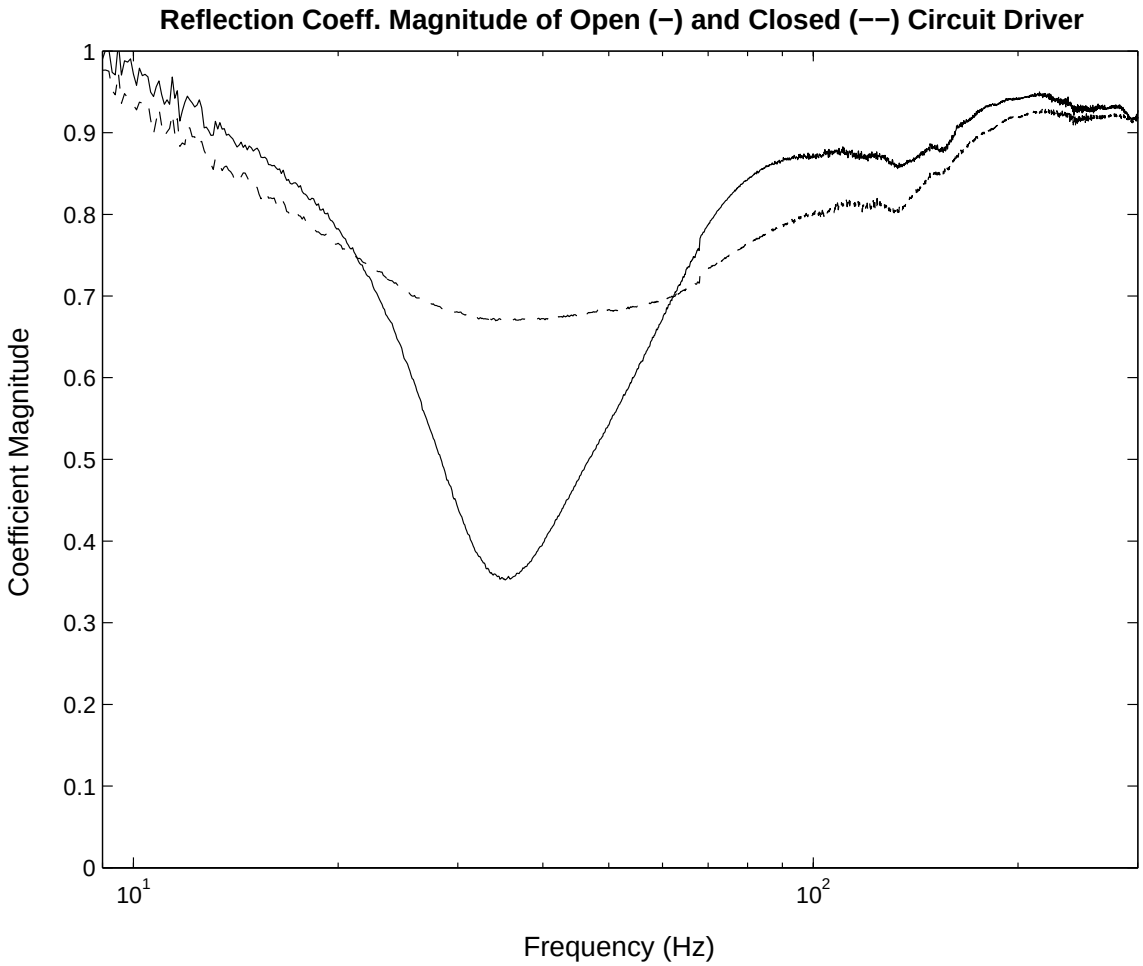

Fig. 8.3. Measured upstream reflection coefficient moduli of a sample driver under test [open circuit (solid line) and closed circuit (dashed line)].

Using both the upstream and downstream reflection coefficients, along with the auto-power spectra, the transmission loss is determined for the driver under test, as shown in Fig. 8.4.

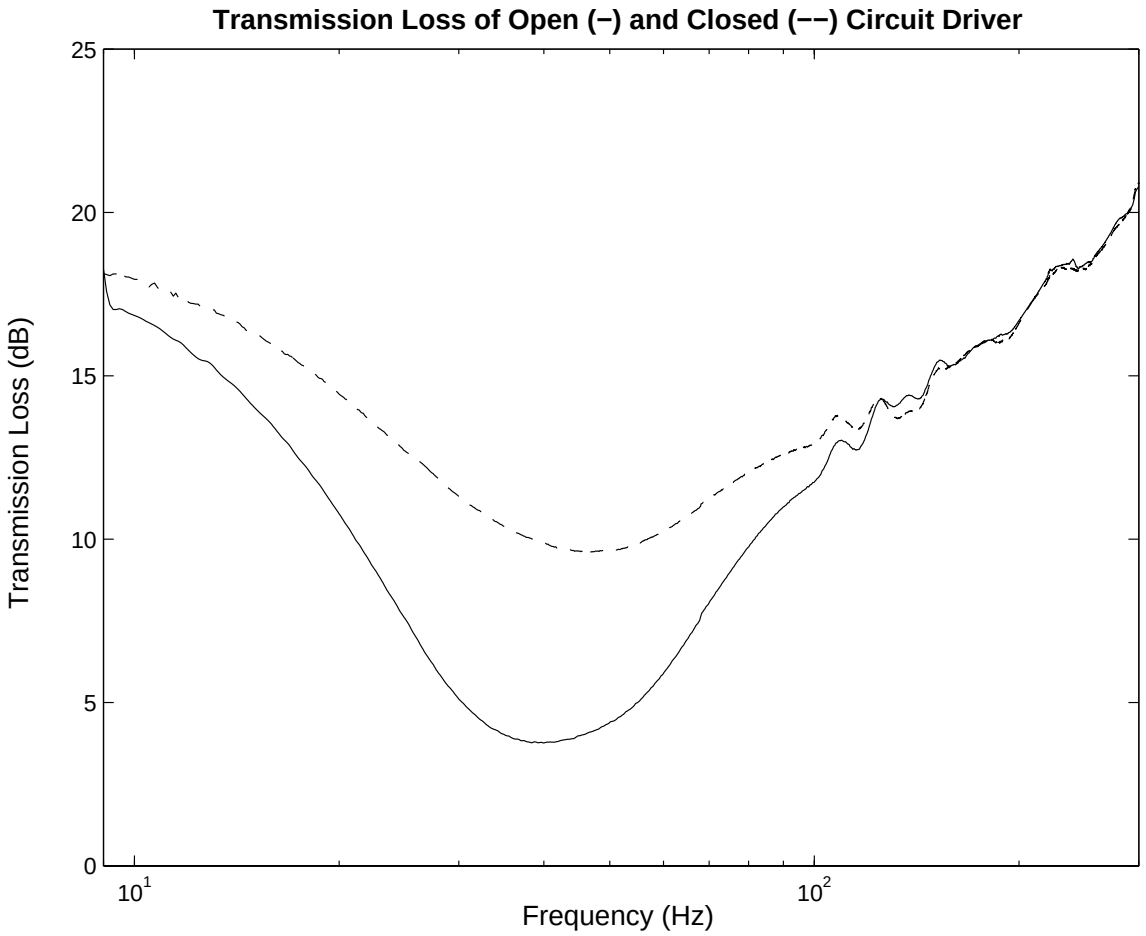

Fig. 8.4. Measured transmission loss of a sample driver under test [open circuit (solid line) and closed circuit (dashed line)].

As explained in Section 7.1, f_0 and R_{MS} are estimated from the minimum of the open-circuit transmission loss curve. In this example, $f_0 = 40.0\,Hz$ and $R_{MS} = 2.62\ kg/s$. Once R_{MS} is known, the value for M_{MD} may be determined from the high-frequency mechanical reactance divided by ω, as suggested in Fig. 8.5.

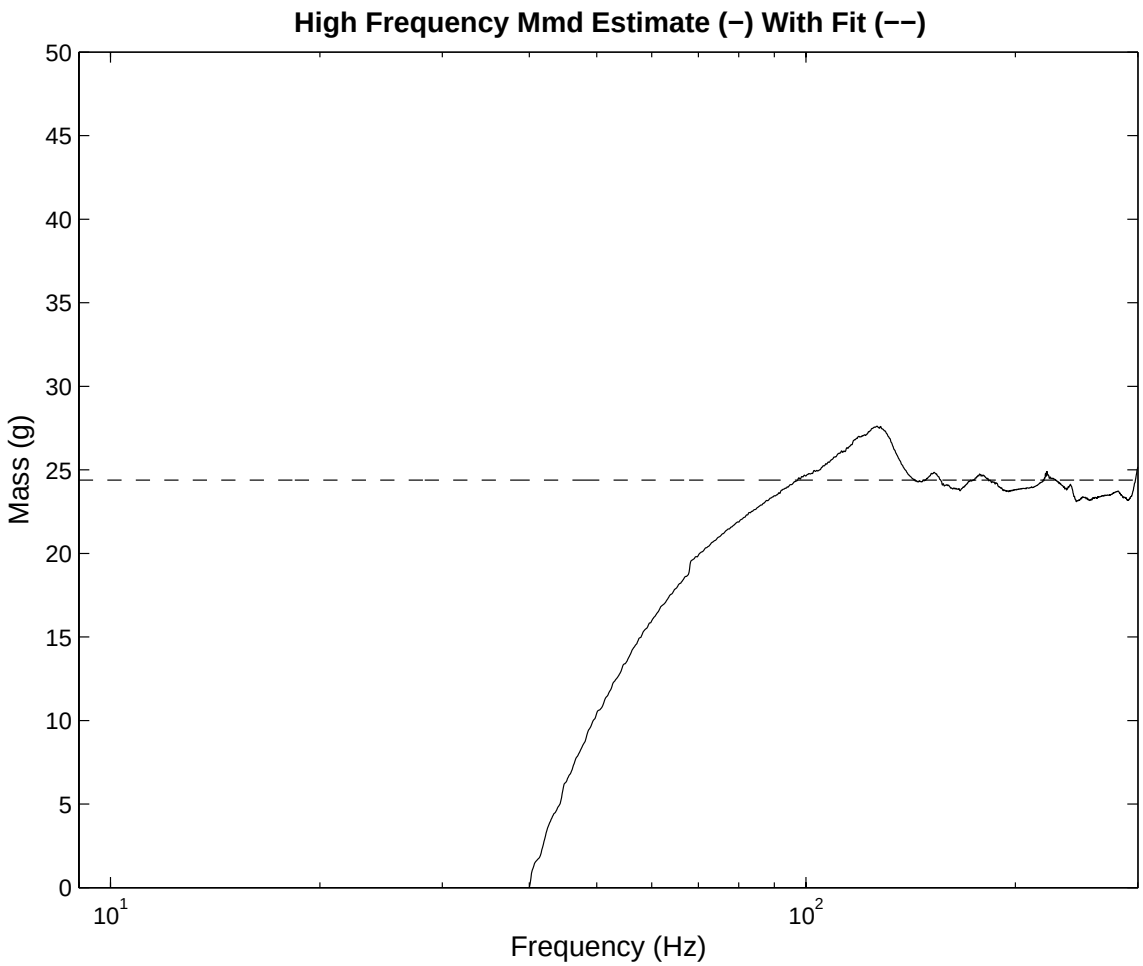

Fig. 8.5. Frequency-dependent M_{MD} estimate (solid line) and chosen value (dashed) for sample driver under test.

This technique yields a value of $M_{MD} = 24.4\ g$. Using this value and Eq. (7.18), $C_{MS} = 649 \mu m/N$. Finally, M_{MS} is determined by using Eq. (3.1) and f_s is determined from a modified version of Eq. (7.18) (by replacing f_0 with f_s and replacing M_{MD} with M_{MS}): $M_{MS} = 26.3\ g$ and $f_s = 38.5\ Hz$.

Using these open-circuit measurement results and the derived mechanical parameters, the electrical parameters are determined from the closed-circuit transmission loss curve. As shown in Fig. 8.6, the Bl product is determined in the low-frequency

limit using a linear curve fit (on a logarithmic frequency scale). After neglecting the impedance due to L_{VC}, $Bl = 7.29\ T \cdot m$.

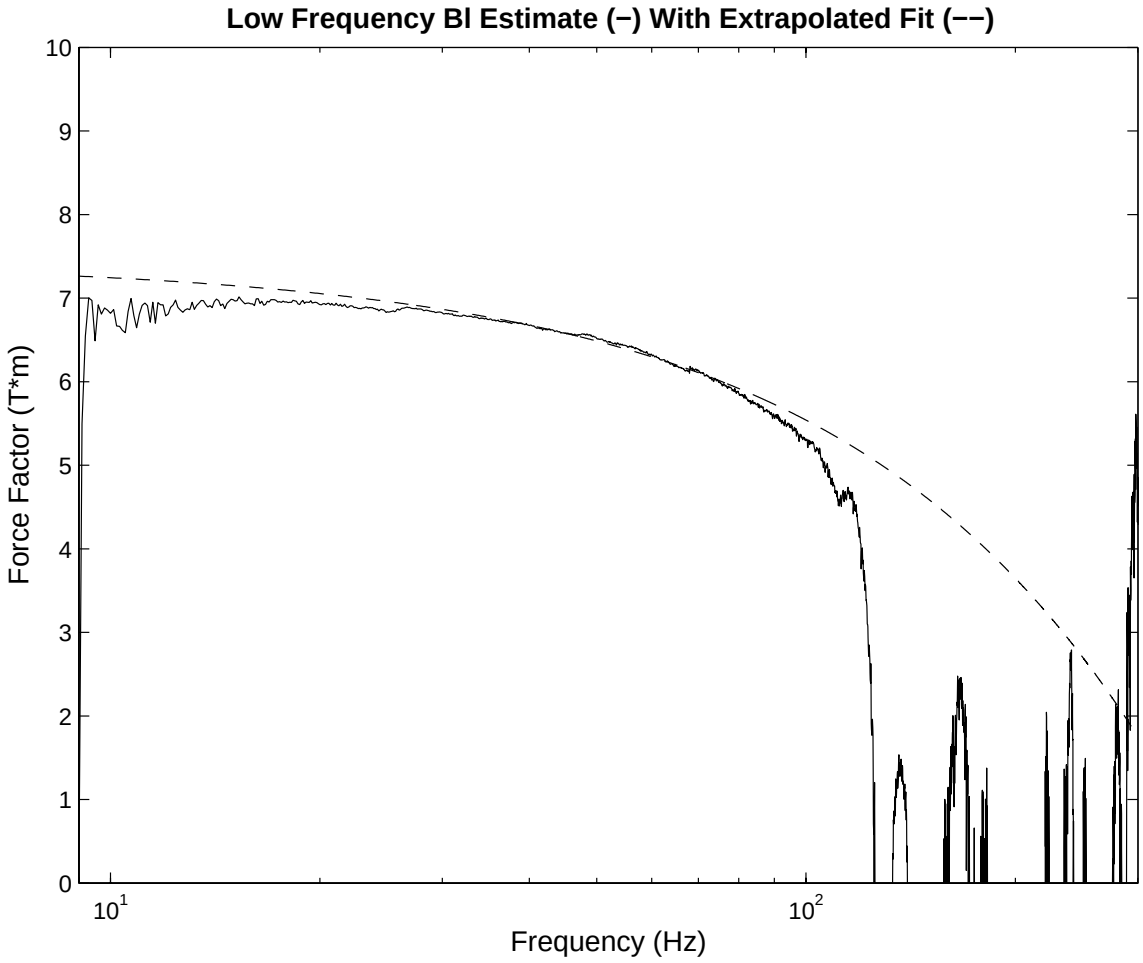

Fig. 8.6. Low frequency Bl estimate (solid line) and linear curve fit (dashed line) for sample driver under test.

Using this value as a constant Bl, a frequency-dependent curve of L_{VC} is obtained as shown in Fig. 8.7.

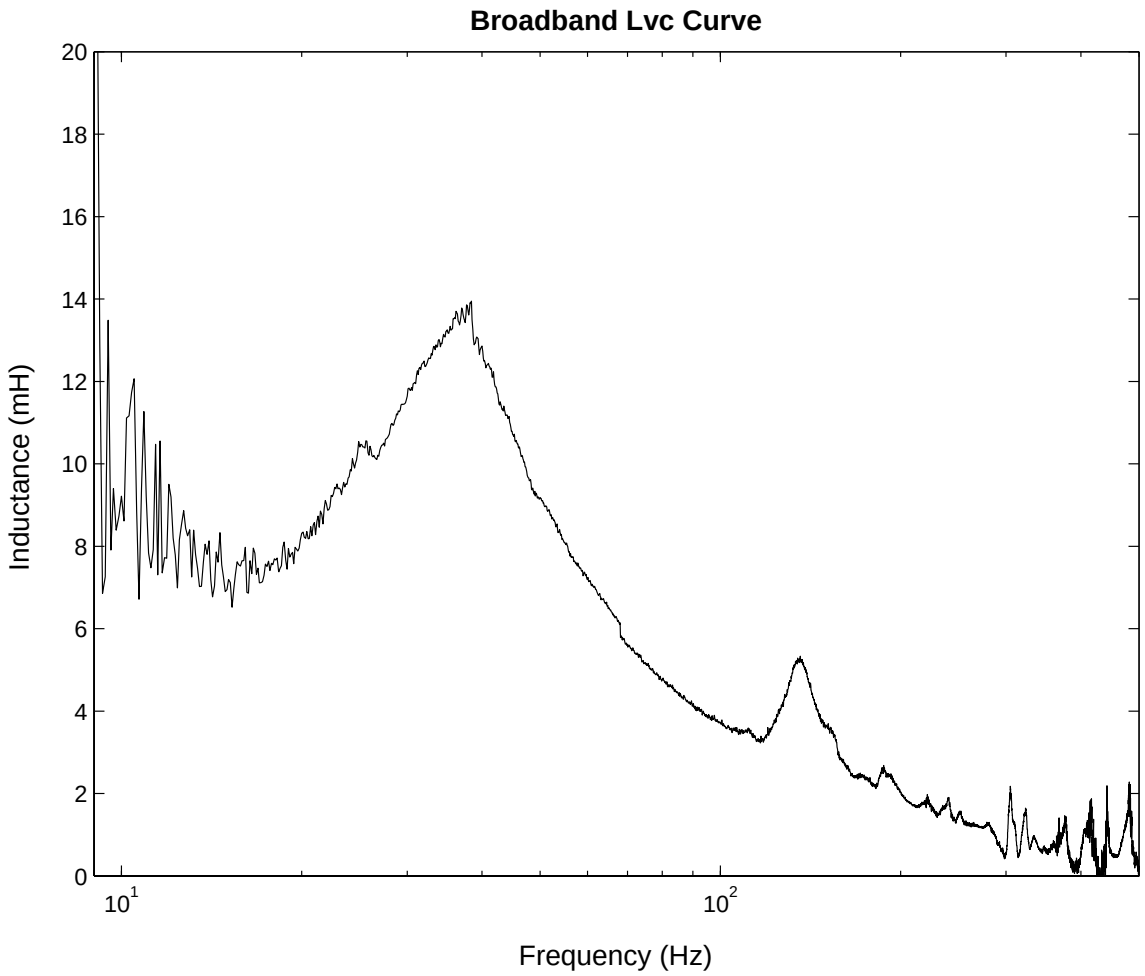

Figure 8.7. Frequency-dependent L_{VC} curve for sample driver under test.

Although the figure shows that the inductance is frequency dependent (as suggested in [14, p.32]), further investigation is required to clarify its behavior.

8.4 Plane Wave Tube Results

This section discusses the measurement results for the parameters C_{MS}, M_{MS}, R_{MS}, and Bl for all drivers tested. The names for each of the two derivation techniques have been used to identify them. "Portion Fit" refers to the high frequency method for

determining M_{MD} (Section 7.2.1). "Curve Fit" refers to the curve fit method for determining both C_{MS} and M_{MD} from the mechanical reactance (Section 7.2.1). Tables 8.1 through 8.4 show the averages of ten measured values for each driver and for each technique used. The two assumed termination loading conditions are A (anechoic) and MT (measured termination).

The average measured values for the mechanical suspension compliance C_{MS} are given in Table 8.1, in micrometers per Newton. The average measured values for the mechanical moving mass M_{MS} (including estimated free-air loading) are given in Table 8.2, in grams. The average measured values for the mechanical suspension resistance R_{MS} are given in Table 8.3, in kilograms per second. The average measured values for the electrical force factor Bl are given in Table 8.4, in Tesla meters. A typical example of the difficultly in assessing a constant voice-coil inductance L_{VC} was shown in Fig. 8.7. Due to the apparent frequency dependant behavior, fixed values for inductance are not specified in this study.

Cms	Numbers Correspond to the Driver Under Test								
	1	2	3	4	5	6	7	8	9
Portion Fit A	221.3	441.3	644.8	296.5	323.7	295.8	720.6	815.3	3195
Portion Fit MT	225.2	439.3	644.0	297.6	324.4	296.4	724.7	824.9	3244
Curve Fit A	210.7	437.7	632.5	282.7	317.6	282.7	691.7	598.3	3235
Curve Fit MT	214.9	453.1	693.3	281.6	317.9	281.6	650.5	657.8	4045

Table 8.1. Average values for C_{MS} ($\mu m/N$). Values result from ten consecutive measurement runs for each of the nine drivers under test.

Mms	Numbers Correspond to the Driver Under Test								
	1	2	3	4	5	6	7	8	9
Portion Fit A	112.8	75.15	26.88	30.58	30.34	30.65	9.208	2.161	0.7032
Portion Fit MT	110.9	75.47	26.91	30.47	30.27	30.58	9.161	2.139	0.6939
Curve Fit A	117.0	75.97	27.35	32.89	31.14	32.89	9.750	2.896	0.8106
Curve Fit MT	117.0	75.83	27.08	32.77	30.99	32.77	9.787	2.740	0.7455

Table 8.2. Average values for M_{MS} (g). Values result from ten consecutive measurement runs for each of the nine drivers under test.

Rms	Numbers Correspond to the Driver Under Test								
	1	2	3	4	5	6	7	8	9
Portion Fit A	4.529	2.572	2.388	1.453	1.407	1.453	1.516	0.7537	0.2270
Portion Fit MT	4.464	2.291	2.616	1.626	1.587	1.626	1.527	0.7882	0.2476

Table 8.3. Average values for R_{MS} (kg/s). Values result from ten consecutive measurement runs for each of the nine drivers under test.

Bl	Numbers Correspond to the Driver Under Test								
	1	2	3	4	5	6	7	8	9
Portion Fit A	15.05	12.10	8.669	9.740	11.76	9.740	4.528	3.043	1.772
Portion Fit MT	13.35	10.58	7.264	11.86	10.54	11.86	5.548	4.027	2.160

Table 8.4. Average values for Bl $(T \cdot m)$. Values result from ten consecutive measurement runs for each of the nine drivers under test.

8.5 Discussion

Several conclusions may be drawn about the parameters derived from the proposed plane wave tube technique. The two smallest drivers, 8 and 9, cause problems for the measurement system. Their C_{MS} values are unreasonably high, relative to the values derived from electrical impedance techniques. This suggests that the plane wave

system is only reliable for measurement of drivers with S_D values that are at least a seventh of the tube cross-sectional area.

By comparing the results to those found in Chapter 4, the parameters derived from the plane wave tube technique are seen to compare better with those derived using the added-mass electrical technique than those derived using the closed-box electrical technique. Electrical impedance techniques allow direct determination of M_{MS}, while plane wave tube techniques allow direct determination of M_{MD}. In order to obtain an estimate for M_{MS} from plane wave tube data, one must add the estimated free-air loading, which depends directly on the atmospheric density of air ρ_0 [see Eq. (3.1)]. However, a 5.7% error in the value for ρ_0 results in an average bias error of only 0.37% for three drivers under test (drivers 1, 4, and 7). The resulting estimate for M_{MS} is not significantly altered.

Although not presented as part of this thesis, research has been conducted to show that the determination of loudspeaker parameters through the measurement of reflection coefficient moduli in the source tube alone does not lend itself to accurate results. It is believed that the problem results from tube losses, which are not as significant in parameter measurements based on transmission losses.

CHAPTER 9

COMPARISON OF RESULTS

This chapter presents a comparison of parameters determined using the proposed acoustical method and those determined using electrical methods. Relative bias errors were investigated to establish their level of agreement. Random errors (in terms of standard deviation divided by mean values) were also investigated to determine the consistency of each method.

The error analysis will be given for the following parameters: mechanical suspension compliance C_{MS}, the mechanical moving mass M_{MD}, mechanical suspension resistance R_{MS}, and the electrical force factor Bl. The final two parameters, R_{VC} and L_{VC}, were not included in the error analysis. The voice-coil resistance R_{VC} was not analyzed because it was consistently determined using an ohmmeter approach (no variation among methods). The voice-coil inductance L_{VC} was not analyzed because of the difficulty in obtaining fixed values from plane wave tube data and because of large variations in the values produced by electrical measurement techniques. Because of the problems encountered in the measurement of very small diameter drivers, parameter comparisons are only given for drivers 1 through 7. Following the presentation of results, a discussion will be provided to highlight pertinent findings.

9.1 Comparison of Mechanical Suspension Compliance Values

Previous research has shown that the value for the static compliance of a suspension system is different than a value obtained using dynamic methods through the

resonance frequency (see Section 2.2). Research concerning electrical parameter derivation techniques suggests that determination of the suspension compliance is not always accurate or repeatable [43], [45]-[46]. Electrically determined suspension compliance values have been shown to vary by as much as 10%, depending upon the perturbation technique employed [53].

A comparison of relative bias errors for average suspension compliance values is given in Table 9.1. The values were determined using static methods, electrical impedance methods, and plane wave tube methods.

Cms Bias Error	Driver Under Test							
	1	2	3	4	5	6	7	Average Error
Static Values	55.7	180.5	12.9	43.9	94.2	104.7	21.0	73.3
Electrical								
MLSSA H Mass	-1.5	0.8	-4.8	-4.7	10.6	-2.1	-0.9	-0.4
MLSSA V Mass	-4.3	14.1	31.9	3.1	-13.8	-3.8	13.0	5.8
MLSSA H Box	-13.3	-15.4	-13.6	-6.9	-6.1	-3.1	0.5	-8.3
MLSSA V Box	-15.7	-18.3	-19.4	-16.2	-29.2	-29.1	-6.7	-19.2
LMS H Mass	10.0	7.9	3.1	8.1	6.7	9.5	3.7	7.0
LMS V Mass	2.9	-2.4	1.7	4.1	1.9	8.0	10.0	3.7
LMS H Box	-9.5	-12.9	-21.2	-12.5	-21.3	-14.0	8.3	-11.9
LMS V Box	-21.0	-12.9	-19.8	-14.6	0.9	-5.6	8.3	-9.3
LEAP H Mass	14.5	9.3	3.2	10.2	6.9	11.5	6.0	8.8
LEAP V Mass	11.7	-0.2	0.3	2.2	1.7	11.8	10.9	5.5
LEAP H Box	-18.6	-15.2	-20.5	-18.9	-26.5	-22.5	7.8	-16.3
LEAP V Box	-23.4	-16.9	-19.7	-13.2	-0.8	-24.6	10.5	-12.6
GM H Mass	0.0	0.0	0.0	0.0	0.0	0.0	0.0	0.0
GM V Mass	-0.7	-4.7	-3.4	-0.8	5.3	5.0	-0.3	0.1
FFT V Mass	-21.6	-22.4	-17.2	-13.1	-12.0	-11.5	-12.2	-15.7
Plane Wave Tube								
Portion Fit A	54.0	19.5	-14.1	-16.1	20.4	19.8	9.8	13.3
Portion Fit MT	56.7	19.0	-14.2	-15.8	20.6	20.1	10.5	13.9
Curve Fit A	46.6	18.6	-15.7	-20.0	18.1	14.5	5.4	9.6
Curve Fit MT	49.5	22.7	-7.6	-20.3	18.2	14.1	-0.9	10.8

Table 9.1. Relative bias errors (%) for measured C_{MS} values obtained from static methods, electrical impedance methods, and plane wave tube methods. The reference technique used in the bias error determination is the Garrett method, using added masses with horizontal driver axes.

For purposes of comparison, the reference technique used in this table is the Garrett method, using added masses and horizontal driver axes. The abbreviations given in this table and the remainder of the tables in the chapter refer to the method used. The acronyms MLSSA, LMS, LEAP, GM, and FFT refer to the methods discussed in Section 4.1. "Portion Fit" and "Curve Fit" refer to the methods discussed in Section 7.2. The other abbreviations refer to other specifics of the method employed: H and V refer to the orientation of the driver axis for electrical impedance methods (horizontal or vertical), "Mass" and "Box" refer to the use of either the added-mass or the closed-box perturbations techniques, and A and MT refer to the type of termination assumed in each plane wave tube technique (anechoic or measured). A comparison of random errors for consecutive suspension compliance measurement runs, determined using electrical impedance techniques and plane wave tube techniques, is given in Table 9.2.

Cms Random Error	Driver Under Test							
	1	2	3	4	5	6	7	Average Error
Electrical								
MLSSA H Mass	9.7	0.9	18.1	2.1	13	1.7	4.7	7.2
MLSSA V Mass	5.8	11.6	10.7	3.8	1.7	3.3	2.4	5.6
MLSSA H Box	5.7	5	1.6	4.5	7.7	5.2	2.2	4.6
MLSSA V Box	3	3	4.9	1.8	1.6	5.5	1.7	3.1
LMS H Mass	2.4	0	0	4.8	0	0	0	1
LMS V Mass	0	0	6.3	3.9	4.6	5.1	0	2.8
LMS H Box	4.5	0	4.2	0	0	0	0	1.2
LMS V Box	0	0	2.7	0	0	26.6	0	4.2
LEAP H Mass	0.7	0.2	2.9	5.9	0.3	0.1	0.6	1.5
LEAP V Mass	0.3	0.2	5.8	3.8	5.8	2.1	0.4	2.6
LEAP H Box	1.5	0.7	3.7	0.3	1.3	0.3	2.1	1.4
LEAP V Box	0.6	0.4	3.7	1.2	8.6	5.1	1.5	3
FFT V Mass	3.1	2.2	3.1	1.6	1.1	1.3	0.9	1.9
Plane Wave Tube								
Portion Fit A	1.9	1	3	1	1.5	1	1.8	1.6
Portion Fit MT	1.9	1	3	1	1.5	1	1.8	1.6
Curve Fit A	0.6	0.3	0.5	0.3	0.5	0.3	0.5	0.4
Curve Fit MT	0.9	0.5	0.7	0.4	0.4	0.4	0.3	0.5

Table 9.2. Random errors (% relative standard deviation) for consecutive C_{MS} values from electrical impedance and plane wave tube measurement runs.

9.2 Comparison of Mechanical Moving Mass Values

A comparison of relative bias errors for average moving mass values is given in Table 9.3. The values were determined using electrical and plane wave tube methods with the Garrett method again used as the reference. The values given for the plane wave tube measurements include the estimated fluid loading from Eq. (3.1).

Mms Bias Error	Driver Under Test							
	1	2	3	4	5	6	7	Average Error
Electrical								
MLSSA H Mass	-3.2	0.8	-8.4	-4.9	-2.4	-3.3	-0.2	-3.1
MLSSA V Mass	-1.1	16.1	28.3	5.1	-29.3	-6.0	15.3	4.1
MLSSA H Box	-19.1	-20.3	-18.3	-10.0	-19.5	-3.4	-0.1	-12.9
MLSSA V Box	-22.7	-22.3	-24.3	-18.9	-45.5	-36.5	-6.8	-25.3
LMS H Mass	-3.6	-0.3	2.1	-0.1	-13.6	-1.6	-5.3	-3.2
LMS V Mass	-4.8	-10.9	0.4	-4.0	-34.4	-8.3	0.8	-8.7
LMS H Box	-25.8	-24.4	-28.3	-26.5	-54.1	-29.4	-0.8	-27.0
LMS V Box	-36.4	-24.4	-26.0	-26.5	-35.5	-27.1	-0.8	-25.2
LEAP H Mass	3.7	2.9	0.4	4.1	-10.1	3.4	-1.4	0.4
LEAP V Mass	-2.2	-5.1	-2.2	-7.1	-34.0	4.8	1.4	-6.4
LEAP H Box	-35.5	-25.8	-29.1	-29.8	-60.9	-38.9	0.4	-31.4
LEAP V Box	-40.6	-26.8	-27.4	-25.8	-37.5	-41.3	1.1	-28.3
GM H Mass	0.0	0.0	0.0	0.0	0.0	0.0	0.0	0.0
GM V Mass	-14.4	-9.8	2.0	-1.2	-2.5	6.5	-1.0	-2.9
FFT V Mass	-19.1	-21.3	-10.9	-7.6	-22.7	-9.6	-1.4	-13.2
Plane Wave Tube								
Portion Fit A	28.2	8.5	-9.7	17.5	2.7	12.1	-1.8	8.2
Portion Fit MT	29.4	8.1	-9.9	17.8	2.9	12.3	-1.3	8.5
Curve Fit A	25.5	7.5	-11.7	11.3	0.1	5.7	-7.8	4.4
Curve Fit MT	25.5	7.6	-10.6	11.6	0.6	6.0	-8.2	4.6

Table 9.3. Relative bias errors (%) for measured M_{MS} values obtained from electrical impedance methods and plane wave tube methods. The reference technique used in the bias error determination is the Garrett method, using added masses with horizontal driver axes.

A useful bias error analysis also arises through the use of destructively obtained moving mass values. As indicated in Section 2.3, it is possible to determine the fraction of the suspension system and wire leads in each moving mass estimate. Table 9.4 gives the fraction for three drivers, in decimal form. The fractional mass values $M_{MD,Fraction}$

represent the fraction of the suspension that each average value would imply. It is determined

Mmd fraction	Driver Under Test			
	1	3	7	Average Fraction
Reference				
Lower Limit	0.0	0.0	0.0	0.0
1/3 of Suspension	0.3	0.3	0.3	0.3
1/2 of Suspension	0.5	0.5	0.5	0.5
Upper Limit	1.0	1.0	1.0	1.0
Electrical				
MLSSA H Mass	0.7	0.87	0.694	0.8
MLSSA V Mass	0.7	-0.25	0.256	0.2
MLSSA H Box	1.2	1.18	0.691	1.0
MLSSA V Box	1.4	1.36	0.880	1.2
LMS H Mass	0.8	0.55	0.839	0.7
LMS V Mass	0.8	0.60	0.667	0.7
LMS H Box	1.5	1.48	0.712	1.2
LMS V Box	1.8	1.41	0.712	1.3
LEAP H Mass	0.5	0.60	0.728	0.6
LEAP V Mass	0.7	0.68	0.649	0.7
LEAP H Box	1.8	1.51	0.678	1.3
LEAP V Box	1.9	1.46	0.658	1.3
GM H Mass	0.6	0.61	0.689	0.6
GM V Mass	1.1	0.55	0.716	0.8
FFT V Mass	1.2	0.95	0.728	1.0
Plane Wave Tube				
Portion Fit A	-0.2	0.91	0.740	0.5
Portion Fit MT	-0.3	0.92	0.725	0.5
Curve Fit A	-0.2	0.97	0.910	0.6
Curve Fit MT	-0.2	0.94	0.921	0.6

Table 9.4. Suspension system fraction comparison of average measured M_{MD} values, for drivers 1, 3, and 7, determined using destructively obtained reference moving mass values, electrical impedance measured values, and plane wave tube measured values. The fractional values represent what fraction of the suspension system each estimate would imply.

from the following equation:

$$M_{MD,Fraction} = \frac{M_{MD,Measured} - M_{MD,LowerLimit}}{M_{Suspension}}, \tag{9.1}$$

where $M_{MD,Measured}$ is the measured estimate of M_{MD} in question, $M_{MD,LowerLimit}$ is the mass of the measured lower limit in Table 2.2, and $M_{Suspension}$ is the mass of the suspension in Table 2.2.

According to Eq. (9.1), a negative value for $M_{MD,Fraction}$ indicates that the measured estimate of M_{MD} is smaller than would be physically possible. A value greater than 1 indicates that the measured estimate of M_{MD} is larger than would be physically possible. From the table, it is then clear that several M_{MD} estimates are physically unrealizable. The values given for driver number 1 cast doubt upon the average fraction values for the plane wave tube system. A possible reason for the negative values is that its resonance frequency lies in the nonanechoic region of the termination impedance, resulting in an incorrect determination of the resonance frequency. The spread in the fractional values derived from plane wave tube data requires more investigation.

A comparison of random errors for consecutive moving mass measurement runs, determined using electrical impedance techniques and plane wave tube techniques, is given in Table 9.5.

9.3 Comparison of Mechanical Suspension Resistance Values

A comparison of relative bias errors for average suspension resistance values, determined using both electrical impedance techniques and plane wave tube techniques, is given in Table 9.6. The reference method for the table is that of the MLSSA measurement system, using added mass perturbation and horizontal driver axes. A comparison of random errors for consecutive suspension resistance measurement runs is given in Table 9.7.

Mms Random Error	Driver Under Test							
	1	2	3	4	5	6	7	Average Error
Electrical								
MLSSA H Mass	11.0	0.9	28.9	1.6	11.8	1.9	4.8	8.7
MLSSA V Mass	5.7	10.9	10.5	3.6	2.1	3.5	2.5	5.5
MLSSA H Box	5.1	4.9	1.8	4.3	7.7	5.2	3.3	4.6
MLSSA V Box	3.1	3.1	6.2	1.7	1.4	6.7	1.7	3.4
LMS H Mass	4.0	0.0	0.0	4.8	0.0	0.0	0.0	1.3
LMS V Mass	0.0	0.0	6.2	3.7	4.4	17.5	0.0	4.5
LMS H Box	3.0	0.0	4.3	0.0	0.0	0.0	0.0	1.0
LMS V Box	0.0	0.0	2.9	0.0	0.0	13.0	0.0	2.3
LEAP H Mass	1.3	0.6	4.1	6.0	0.8	0.2	2.1	2.2
LEAP V Mass	0.5	0.5	7	3.6	7.8	2.9	1.5	3.4
LEAP H Box	0.9	0.2	3.4	0.1	0.7	0.2	0.6	0.9
LEAP V Box	0.4	0.2	2.5	0.6	5.4	2.9	0.4	1.8
FFT V Mass	3.7	2.5	3.2	2.1	1.6	2.6	1.7	2.5
Plane Wave Tube								
Portion Fit A	0.0	0.0	0.1	0.1	0.0	0.1	0.0	0.1
Portion Fit MT	0.1	0.0	0.1	0.1	0.0	0.1	0.0	0.1
Curve Fit A	0.1	0.1	0.1	0.0	0.1	0.0	0.2	0.1
Curve Fit MT	0.1	0.1	0.1	0.1	0.1	0.1	0.2	0.1

Table 9.5. Random errors (% relative standard deviation) for consecutive M_{MS} values from electrical impedance and plane wave tube measurement runs.

Rms Bias Error	Driver Under Test							
	1	2	3	4	5	6	7	Average Error
Electrical								
MLSSA H Mass	0.0	0.0	0.0	0.0	0.0	0.0	0.0	0.0
MLSSA V Mass	-32.7	2.9	22.5	8.5	-31.1	-1.8	8.3	-3.3
MLSSA H Box	-13.7	-10.3	-5.9	-3.1	-11.8	5.0	-3.7	-6.2
MLSSA V Box	-16.7	-17.7	-11.9	-10.7	-36.5	-20.6	-6.1	-17.2
LMS H Mass	-31.3	-17.2	-5.3	3.0	-58.4	-21.4	-20.0	-21.5
LMS V Mass	-20.6	-45.1	-3.0	-5.8	20.1	-57.0	-11.0	-17.5
LMS H Box	-59.7	-55.4	-39.2	-35.7	-112.0	-54.6	-14.9	-53.1
LMS V Box	-57.0	-62.6	-30.4	-28.8	19.6	-77.9	-12.8	-35.7
LEAP H Mass	-1.5	1.4	4.4	12.3	-14.0	8.0	-2.5	1.2
LEAP V Mass	-8.9	-5.2	3.2	-3.0	7.3	-11.2	1.6	-2.3
LEAP H Box	-42.9	-27.9	-24.0	-24.4	-67.1	-32.4	-0.8	-31.4
LEAP V Box	-49.9	-26.3	-20.8	-21.2	3.2	-64.5	1.3	-25.5
FFT V Mass	-46.2	-67.6	-25.6	-16.0	-46.0	-26.1	75.1	-21.8
Plane Wave Tube								
Value at fo A	-22.0	-53.8	-19.9	35.4	-25.5	-13.0	-31.6	-18.6
Value at fo MT	-20.2	-36.9	-31.3	27.7	-41.5	-26.4	-32.6	-23.0

Table 9.6. Relative bias errors (%) for measured R_{MS} values obtained from electrical impedance methods and plane wave tube methods. The reference comparison method is that of the MLSSA measurement system, using added mass with horizontal driver axes.

Rms Random Error	Driver Under Test							
	1	2	3	4	5	6	7	Average Error
Electrical								
MLSSA H Mass	11.0	0.9	28.0	1.6	11.9	1.9	4.7	8.6
MLSSA V Mass	6.1	10.9	10.0	3.5	2.4	3.6	2.6	5.6
MLSSA H Box	5.9	10.0	1.3	3.9	7.8	5.2	17.5	7.4
MLSSA V Box	3.0	2.9	2.7	1.5	1.5	0.7	1.7	2.0
LMS H Mass	4.0	0.0	0.5	4.8	4.8	0.0	1.1	2.2
LMS V Mass	0.0	0.0	6.2	5.0	81.3	66.8	0.0	22.8
LMS H Box	3.1	0.0	4.1	0.0	4.8	0.0	1.1	1.9
LMS V Box	0.0	0.0	2.9	2.9	78.9	37.4	0.0	17.4
LEAP H Mass	2.7	1.6	3.3	5.8	3.5	1.6	2.0	2.9
LEAP V Mass	0.8	1.7	6.5	3.2	19.1	18.9	1.8	7.4
LEAP H Box	1.7	1.5	3.4	0.5	1.7	1.3	1.0	1.6
LEAP V Box	0.5	0.9	2.5	1.2	36.3	13.7	1.4	8.1
FFT V Mass	6.3	5.2	4.6	2.2	3.2	4.7	198.3	32.1
Plane Wave Tube								
Value at fo A	0.3	0.5	0.3	0.6	0.3	0.6	0.8	0.5
Value at fo MT	0.8	0.5	0.6	0.6	0.4	0.6	1.0	0.6

Table 9.7. Random errors (% relative standard deviation) for consecutive R_{MS} values from electrical impedance and plane wave tube measurement runs.

9.4 Comparison of Electrical Force Factor Values

A comparison of relative bias errors for average force factor values, determined using both electrical impedance techniques and plane wave tube techniques, is given in Table 9.8. A comparison of random errors for consecutive force factor measurements is given in Table 9.9.

9.5 Discussion

Using static measurement techniques, the values determined for the mechanical suspension compliances vary on average by 73.3%, relative to the dynamically measured values (see Table 9.1). These static values have also been shown to be driver dependent (possibly due to materials used in the construction of the suspension systems). This large variation is attributed to suspension creep effects (Compare References [15], [27], [33], and [43]-[46]).

Bl Bias Error	Driver Under Test							
	1	2	3	4	5	6	7	Average Error
Electrical								
MLSSA H Mass	0.0	0.0	0.0	0.0	0.0	0.0	0.0	0.0
MLSSA V Mass	1.0	7.4	16.6	4.8	-13.0	-1.3	6.4	3.1
MLSSA H Box	-7.3	-7.9	-4.7	-2.3	-7.5	0.6	-0.2	-4.2
MLSSA V Box	-7.5	-9.3	-5.9	-4.8	-17.1	-11.8	-2.5	-8.4
LMS H Mass	-7.7	-5.6	0.3	-2.9	-20.5	-5.4	-8.2	-7.2
LMS V Mass	-4.0	-15.7	0.8	-1.0	25.1	-12.1	-4.7	-1.7
LMS H Box	-18.8	-17.6	-14.6	-15.0	-40.4	-19.0	-5.8	-18.8
LMS V Box	-18.6	-22.5	-11.6	-11.4	24.8	-19.4	-5.5	-9.2
LEAP H Mass	4.3	2.8	5.4	5.2	-4.0	4.6	0.4	2.7
LEAP V Mass	1.7	-0.1	4.3	0.7	18.8	0.8	1.9	4.0
LEAP H Box	-13.6	-11.0	-7.8	-10.4	-25.8	-14.4	1.3	-11.7
LEAP V Box	-15.4	-10.1	-6.9	-7.7	17.0	-20.6	1.7	-6.0
FFT V Mass	-4.7	-6.5	2.3	3.6	-4.4	2.3	72.1	9.3
Plane Wave Tube								
Low freq. A	-15.0	-26.0	-13.4	13.0	-2.7	21.5	16.1	-0.9
Low freq. MT	-2.0	-10.1	5.0	-5.9	8.0	4.4	-2.8	-0.5

Table 9.8. Relative bias errors (%) for measured Bl values obtained from electrical impedance methods and plane wave tube methods. The reference comparison method used is that of the MLSSA measurement system, using added mass with horizontal driver axes.

Bl Random Error	Driver Under Test							
	1	2	3	4	5	6	7	Average Error
Electrical								
MLSSA H Mass	5.3	0.5	12.9	0.8	6.1	1.0	2.4	4.1
MLSSA V Mass	3.0	5.6	5.3	1.8	1.1	1.7	1.3	2.8
MLSSA H Box	2.6	1.3	0.4	2.0	3.9	2.6	0.9	2.0
MLSSA V Box	1.1	1.4	0.8	0.8	0.7	1.9	0.8	1.1
LMS H Mass	2.1	0.3	1.4	2.4	2.2	0.3	0.5	1.3
LMS V Mass	0.2	0.3	3.2	2.5	28.1	18.0	0.1	7.5
LMS H Box	1.5	0.3	2.1	0.1	2.2	0.3	0.5	1.0
LMS V Box	0.2	0.3	1.5	1.4	27.2	2.5	0.3	4.8
LEAP H Mass	0.5	0.4	1.7	3.0	0.8	0.2	0.9	1.1
LEAP V Mass	0.3	0.5	3.3	1.7	13.4	5.5	1.1	3.7
LEAP H Box	0.7	0.4	1.6	0.2	0.2	0.1	0.5	0.5
LEAP V Box	0.3	0.2	1.3	0.6	20.8	3.0	0.9	3.9
FFT V Mass	1.8	1.4	1.6	1.0	0.7	1.2	136.9	20.7
Plane Wave Tube								
Low freq. A	1.3	0.0	0.1	0.9	0.2	0.9	3.4	1.0
Low freq. MT	1.3	0.0	0.2	0.9	0.3	0.9	2.8	0.9

Table 9.9. Random errors (% relative standard deviation) for consecutive Bl values from electrical impedance and plane wave tube measurement runs.

A few conclusions may also be drawn with regard to parameters derived from the various electrical methods. Parameters determined using the added-mass technique and those determined using the closed-box technique have different bias errors (compare Reference [53]). Using the added-mass technique as a reference, the average relative bias errors are –18% for C_{MS}, +22% for M_{MS}, +21% for R_{MS}, and +11% for Bl. Parameters derived using different electrical measurement systems and methods show significant variation (compare References [27], [43], [46], and [53]). For some drivers, derived parameter values depend upon orientation of their axes (perhaps because of how their coils are hung [12], [14, p.22], [24, p.303], [46]). When using the closed-box technique, values derived for mechanical moving mass are often higher than the sum of the destructively measured cone assemblies, complete suspension systems and lead wires.

From analysis of Table 9.1 through Table 9.9, several conclusions may be drawn about the parameters derived from the proposed plane wave tube technique. The two smallest drivers, 8 and 9, caused problems for the plane wave tube measurement system (large C_{MS} values compared to electrically determined values). This suggests that the plane wave system is only useful for measurement of drivers with S_D values at least a seventh of the tube cross-sectional area. Parameters derived from the plane wave tube technique compare better with those derived using the added-mass electrical technique than those derived using the closed-box electrical technique. On the average, the C_{MS} values derived using the plane wave tube system are 6.8% higher than those derived from the added-mass technique. On the average, the M_{MS} values derived using the plane wave tube system are 9.2% lower than those derived from the added-mass technique. The R_{MS}

and Bl values derived using the plane wave tube system are comparable to those derived using the added-mass technique.

Random errors associated with the plane wave tube method are consistently lower than those associated with many of the electrical methods. Random errors with a zero value for the LMS analyzer may be deceiving in that the lack of deviation results in part from its limited resolution. The average error values in Tables 9.7 and 9.9 include measurements that resulted in unreasonable mechanical resistance and force factor estimates. However, these values were included in the analysis to show the true random nature of derived parameter values, as commonly encountered in electrical impedance techniques.

CHAPTER 10

CONCLUSIONS AND RECOMMENDATIONS

A plane wave tube transmission loss measurement system has been shown to derive moving-coil loudspeaker driver parameters comparable to those derived using common electrical measurement techniques. The plane wave tube method can thus be used as a new means to validate the results of other methods. The technique also provides a convenient means of assessing the frequency-dependant behavior of voice-coil inductance. The parameter values obtained from plane wave tube measurements compare better with those of added-mass perturbation techniques than with those of closed-box perturbation techniques. Random errors in derived parameter values were consistently lower than those encountered using electrical techniques.

As the surface area of a driver under test becomes small compared to the tube cross-sectional area, compliance estimates become unreasonably large, suggesting that only drivers with a surface area of at least one seventh of the tube cross-sectional area should be tested using the technique. Estimates for driver resonance frequency and compliance have been shown to depend upon the assumption that the downstream termination loading is anechoic. Drivers with low resonance frequencies may be difficult to accurately characterize if the downstream impedance becomes insufficiently anechoic.

Parameter values derived from electrical impedance techniques have been shown to vary significantly according to the technique or measurement system employed. Values obtained using the added-mass technique have been shown to vary by as much as 22% from values obtained using the closed-box technique (compare Reference [53]).

Moving mass estimates obtained from the closed-box perturbation technique have been shown to frequently yield physically unrealizable results, regardless of the measurement system employed. This result casts doubt upon the accuracy of the closed-box perturbation technique (contrary to the assertions of other authors [46] and [53]). Random errors encountered for consecutively derived parameter values have also been shown to be large for mechanical parameters (C_{MS}, M_{MS}, and R_{MS}).

10.1 Recommendations

Throughout the course of the investigation, many pertinent research topics have been identified. Through additional investigation, some of these topics may prove to significantly extend or enhance the plane wave tube techniques. These ideas include improvements to the procedures discussed in this work and the derivation of additional information about drivers under test. The following list may be used as a basis for further efforts:

- The inclusion of tube losses into equivalent circuit models might allow driver parameter determinations through upstream reflection coefficients alone.
- Filtering effects due to the presence of loudspeaker frames and magnet structures may be accounted for in the model in order to clean up higher frequency data (e.g., above 300 Hz).
- The reciprocal nature of loudspeakers may be used to measure open-circuit voltage or closed-circuit current responses at driver terminals at the same time as two-microphone transfer functions are being measured. Such combinations of measurements could allow determination of several useful quantities: DC voice-

coil resistance, position of the one-dimensional acoustic center of the driver, effective radiating surface area, and downstream impedance (including filtering due to the loudspeaker frame and magnet structure).

- The upstream sound power may be compared to the downstream sound power to obtain the power dissipated by the driver under test. In an ideal condition, the open-circuit dissipated power should depend solely upon the mechanical resistance of the suspension, allowing a broadband characterization. Once the broadband mechanical suspension resistance has been determined, the closed-circuit dissipated sound power may then be determined. The closed-circuit dissipated power should depend upon the DC voice coil resistance and the force factor (Bl product).
- The extended frequency range of a tube with a smaller cross section should allow study of additional driver effects. These include surround resonances and cone break up.
- For larger diameter drivers, the frequency range for plane wave data may be extended by placing microphones in the middle of the tube, at the nulls of the first cross modes. However, cross modes would still be excited and would emanate from the driver under test.
- The frequency-dependent behavior of the voice coil inductance assumes a constant force factor and may depend on the displacement of the driver diaphragm. Investigation of the excitation amplitude on the determination of voice coil inductance may be studied.

- The frequency-dependent behavior of the inductance could be further verified through other means such as simultaneous open-circuit voltage response or the closed-circuit current response measurements.
- A modified added-mass technique could be implemented with a plane wave system to obtain suspension compliance and moving mass from upstream reflection coefficient data only (through resonance frequency shifts). This would also reduce the number of required microphones since determination of the resonance frequency may be obtained from a single microphone spacing. There would no longer be a need for the receiving tube.
- A DC current may be applied to the terminals of a driver under test to vary the diaphragm equilibrium position. Because small-signal parameters may be measured as a function of equilibrium position, large-signal parameters such as the positional range for linear operation might be easily ascertained. The method proposed by Clark [27] may be appropriately applied to the plane wave tube system.
- The addition of known resistances or known electrical impedances across the terminals of the driver under test would add additional equations for analysis without the addition of unknowns.
- Further study may be carried out to better characterize the effects of fluid loading on driver cones.

REFERENCES

[1] E. W. Kellogg and C. W. Rice, "Notes on the Development of a New Type of Hornless Loud Speaker," J. American Institute of Electrical Engineers, vol. 44, pp. 982-991, (1925).

[2] N. W. McLachlan, *Loudspeaker, Theory, Performance, Testing and Design*, Dover Publications, Inc., 1960.

[3] H. F. Olson, *Elements of Acoustical Engineering*, D. Van Nostrand Company, Inc., 1940 and 1947.

[4] H. F. Olson, *Dynamical Analogies*, D. Van Nostrand Company, Inc., 1943.

[5] L. L. Beranek, *Acoustics*, McGraw-Hill, 1954 and Acoustical Society of America, 1986.

[6] J. F. Novak, "Performance of Enclosures for Low-Resonance High-Compliance Loudspeakers," IRE Transactions on Audio, January/February 1959.

[7] A. N. Thiele, "Loudspeakers in Vented Boxes: Parts I and II," Proceedings of the IRE, Australia, vol. 22, pp. 487-508, (1961, Aug.), reprinted in J. Audio Eng. Soc., May/June, 1971.

[8] J. E. Benson, "Theory and Design of Loudspeaker Enclosures, Parts 1,2, and 3," AWA Technical Review, vol. 14, no. 1, 1968, vol. 14, no. 3, 1971, 14, no. 4, 1972.

[9] R. H. Small, "Direct-Radiator Loudspeaker System Analysis," IEEE Transactions on Audio and Electroacoustics, AU-19, pp. 269-281, 1971.

[10] R. H. Small, "Closed-Box Loudspeaker Systems Parts I and II," J. Audio Eng. Soc., vol. 20, pp. 798-808, (1972 Sept.), vol. 21, pp. 11-18, (1973 Jan./Feb.).

[11] R. H. Small, "Vented-Box Loudspeaker Systems Parts I, II, III, and IV" J. Audio Eng. Soc., vol. 21, pp. 363-372, (1973 Jun.), vol. 21, pp. 438-444, (1973 Jul./Aug.), vol. 21, pp. 549-554, (1973 Sept.), vol. 21, (1973 Oct.).

[12] W. J. J. Hoge, "The Measurement of Loudspeaker Driver Parameters," presented at the 58th Convention of the Audio Eng. Soc., (1977 Nov.), New York, preprint 1287.

[13] W. M. Leach Jr., R.W. Schafer and T.P. Barnwell III, "Time-Domain Measurement of Loudspeaker Driver Parameters," IEEE Transactions on Acoustics, Speech, and Signal Processing, ASSP-27, (1979 no. 6).

[14] J. D'Appolito, *Testing Loudspeakers*, (Audio Amateur Press, New Hampshire 1998).

[15] J. R. Ashley and M.D. Swan, "Improved Measurement of Loudspeaker Parameters," presented at the 40th Convention of the Audio Eng. Soc., (1971 Apr.), preprint 803.

[16] R. C. Cabot, "Automated Measurements of Loudspeaker Small Signal Parameters," presented at the 81st Convention of the Audio Eng. Soc., (1986 Nov.), Los Angeles, preprint 2402.

[17] A. N. Thiele, "Measurement of the Thiele/Small Parameters of Tweeters," J. Electrical and Electronics Eng., Australia, vol. 9, pp. 186-199, (1989 no. 4).

[18] R. Gomez-Meda, "Measurement of the Thiele-Small Parameters for a Given Loudspeaker Without Using a Box," presented at the 91st Convention of the Audio Eng. Soc., (1991 Nov.), New York, preprint 3162.

[19] J. R. Ashley, "Home Computer Aided Measurement of Loudspeaker Driver Parameters," Proceedings – IMTC '85, IEEE, Instrumentation and Measurement Technology Conference, pp. 269-273, 1985.

[20] A. P. Berkhoff, "Impedance Analysis of Subwoofer Systems," J. Audio Eng. Soc., vol. 42, pp. 4-13, (1994 Jan./Feb.).

[21] J. R. Ashley, "Simple Measurements For Home Loudspeaker Systems," Proceedings – IMTC '88, IEEE Instrumentation and Measurement Technology Conference, pp. 341-344, 1988.

[22] E. Geddes and A. Phillips, "Efficient Loudspeaker Linear and Nonlinear Parameter Estimation," presented at the 91st Convention of the Audio Eng. Soc., (1991 Oct.), New York, preprint 3164.

[23] H. Blind, A. Phillips and E. Geddes, "Efficient Loudspeaker Parameter Estimation-An Extension," presented at the 93rd Convention of the Audio Eng. Soc., (1992 Oct.), preprint 3430.

[24] W. M. Leach, *Introduction to Electroacoustics and Audio Amplifier Design Second Edition*, (Kendall/Hunt Publishing Company, Iowa, 2001).

[25] J. Christophorou, "Low-Frequency Loudspeaker Measurements with an Accelerometer," J. Audio Eng. Soc., vol. 28, pp. 809-816, (1980 Nov.).

[26] J. N. Moreno, "Measurement of Loudspeaker Parameters Using a Laser Velocity Transducer and Two-Channel FFT Analysis," J. Audio Eng. Soc., vol. 39, pp. 243-249, (1991 Apr.).

[27] D. Clark, "Precision Measurement of Loudspeaker Parameters," J. Audio Eng. Soc., vol. 45, pp. 129-141, (1997 Mar.).

[28] E. R. Geddes, "Method for Determining Transducer Liner Operational Parameters," U.S. Patent 6,269,318, 2001.

[29] V. K. Jain, W. M. Leach and R. W. Schafer, "Time-Domain Measurement of Vented-Box Loudspeaker System Parameters," IEEE Transactions on Acoustics, Speech, and Signal Processing, ASSP-31, pp. 1-8, (1983 no. 1).

[30] V. K. Jain, W. M. Leach and R. W. Schafer, "Signal Processing Technique For Measurement of Vented-Box Loudspeaker System Parameters," Proceedings – ICASSP '82, IEEE, Acoustics, Speech, and Signal Processing Conference, pp. 1428-1431, 1982.

[31] M. Ureda, "Determination of Thiele-Small Parameters of a Loudspeaker Using Nonlinear Goal Programming," proceedings of the 72nd Convention of the Audio Eng. Soc., (1982 Oct.), preprint 1953.

[32] Y. Nomura, T. Ai, and K. Fukuda, "Estimation Method of Direct-Radiator Loudspeaker System Parameters in Low-Frequency Range by Nonlinear Optimization Technique," Electronics and Communications in Japan, Part 1, vol. 69, (1986 no. 7), Translated from Denshi Tsushin Gakkai Ronbunshi, vol. 68-A, pp. 504-511, (1985 May).

[33] M. H. Knudsen, J. G. Jensen, V. Julskjaer, and P. Rubak, "Determination of Loudspeaker Driver Parameters Using a System Identification Technique," J. Audio Eng. Soc., vol. 37, pp. 700-708, (1989, Sept.).

[34] W. Waldman, "Non-Linear Least Squares Estimation of Thiele-Small Parameters from Impedance Measurements," proceedings of the 94th Convention of the Audio Eng. Soc., (1993 Mar.), Berlin, Germany, preprint 3511.

[35] A. F. Seybert and D. F. Ross, "Experimental determination of acoustic properties using a two microphone random-excitation technique," J. Acoust. Soc. Am., vol. 61, pp. 1362-1370, (1977 no. 5).

[36] J. Y. Chung and D. A. Blaser, "Transfer function method of measuring in-duct acoustic properties. Parts I and II," J. Acoust. Soc. Am., vol. 68, pp. 907-921, (1980 no. 3).

[37] H. Bodén and M. Åbom, "Influence of errors on the two-microphone method for measuring acoustic properties in ducts," J. Acoust. Soc. Am., vol. 79, pp. 541-549, (1986 no. 2).

[38] S. Riggs and E. Geddes, "A Two Microphone Technique for the Measurement of Acoustic Waveguide Impedance," presented at the 87th Convention of the Audio Eng. Soc., (1989 Oct.), New York, preprint 2878.

[39] ASTM E 1050-90, "Standard Test Method for Impedance and Absorption of Acoustical Materials Using a Tube, Two Microphones, and a Digital Frequency Analysis System," American Society for Testing and Materials, Pennsylvania, 1990.

[40] AES 1id-1991, "AES Information Document – Plane-Wave Tubes: Design and Practice," Audio Engineering Society, Inc, New York, 1991.

[41] B. F. G. Katz, "Method to resolve microphone and sample location errors in the two-microphone duct measurement method," J. Acoust. Soc. Am., vol. 108, pp. 2231-2237, (2000 no. 5).

[42] R. L. Mason, R. F. Gunst, and J. L. Hess, *Statistical Design and Analysis of Experiments with Applications to Engineering and Science*, (John Wiley and Sons, Inc., New Jersey, 2003).

[43] M. H. Knudsen and J. G. Jensen, "Low-Frequency Loudspeaker Models That Include Suspension Creep," J. Audio Eng. Soc., vol. 41, pp. 3-18, (1993 Jan./Feb.).

[44] W. Klippel, "Dynamic Measurement and Interpretation of the Nonlinear Parameters of Electrodynamic Loudspeakers," J. Audio Eng. Soc., vol. 38, pp. 944-955, (1990 Dec.).

[45] A. J. M. Kaizer, "Modeling of the Nonlinear Response of an Electrodynamic Loudspeaker by a Volterra Series Expansion," J. Audio Eng. Soc., vol. 35, pp. 421-433, (1987 Jun.).

[46] B. J. Elliot, "On the Measurement of the Low-Frequency Parameters of Moving-Coil Piston Transducers," presented at the 58th Convention of the Audio Eng. Soc., (1977 Nov.), New York, preprint 1299.

[47] V. Dickason, *The Loudspeaker Design Cookbook Sixth Edition*, (Audio Amateur Press, New Hampshire, 2000).

[48] J. R. Ashley and M. D. Swan, "Experimental Determination of Low-Frequency Loudspeaker Parameters," J. Audio Eng. Soc., vol. 17, pp. 525-531, (1969 May).

[49] P. Moreland, "Improving Precision and Accuracy in the *g* Lab," The Physics Teacher, vol. 38, pp. 367-369, (2000 Sept.).

[50] J. Higbie, "Uncertainty in the linear regression slope," Am. J. Phys., vol. 59, (1991 Feb.).

[51] S. L. Garrett and J. F. Heake, "Hey kid! Wanna build a loudspeaker? The first one's free." presented at the 115th Convention of the Audio Eng. Soc., (2003 Oct.), New York.

[52] R. W. Buntenbach, "A Comprehensive Circuit Model for the Electromechanical/Acoustic Transducer," IEEE Transactions on Audio and Electroacoustics, AU-19, pp. 249-252, (1971 no. 3).

[53] T. W. Leishman, *Physics 562 Class Notes*, Department of Physics and Astronomy, 2002.

[54] D. B. Keele Jr., "Sensitivity of Thiele's Vented Loudspeaker Enclosure Alignments to Parameter Variations," J. Audio Eng. Soc., vol. 21, pp. 246-255, (1973 Apr.).

[55] J. N. White, "Loudspeaker Athletics," J. Audio Eng. Soc., vol. 27, pp. 891-897, (1979 Nov.).

[56] J. C. Cox, "A Comparison of Loudspeaker Driver Parameter Measurement Techniques," Proceedings – IMTC '85, IEEE Instrumentation and Measurement Technology Conference, Tampa, pp. 254-258, 1985.

[57] B. J. Elliot, "Accurate Methods for Determining the Low-Frequency Parameters of Electro-Mechanical-Acoustic Transducers with *Bli* Excitation," presented at the 61st Convention of the Audio Eng. Soc., (1978 Nov.), New York, preprint 1432.

[58] D. D. Rife, *Maximum Length Sequence Signal Analyzer, Speaker Parameter Option, Reference Manual V 4WA*, DRA Laboratories, copyright 1987-2001.

[59] C. Strahm, *LMS Operational Manual Rev. 3.50*, Audio Teknology, Inc., copyright Feb. 1993.

[60] C. J. Struck, "Determination of the Thiele-Small Parameters Using Two-Channel FFT Analysis," presented at the 82nd Convention of the Audio Eng. Soc., (1987 Mar.), preprint 2446.

[61] L. E. Kinsler, A. R. Frey, A. B. Coppens, and J. V. Sanders, *Fundamentals of Acoustics 4th Edition*, (John Wiley and Sons, Inc., New York, 1982).

[62] F. Fahy, *Sound and Structural Vibration, Radiation, Transmission and Resonpose 5th Edition*, (Academic Press Limited, Great Britain, 1985).

[63] L. L. Beranek, "The Design and Construction of Anechoic Sound Chambers," J. Acoust. Soc. Am., vol. 18, pp. 140-150, (1946 no. 7).

[64] W. A. Davern and J. A. E. Hutchinson, "Polyurethane Ether Foam Wedges for Anechoic Chamber," Applied Acoustics, vol. 4, pp. 287-302, (1971).

[65] W. Koidan, G. R. Hruska and M. A. Pickett, "Wedge Design for National Bureau of Standards Anechoic Chamber," J. Acoust. Soc. Am., vol. 52, pp. 1071-1076, (1972 no. 4).

[66] G. E. Warnaka, "A different look at the anechoic wedge," J. Acoust. Soc. Am., vol. 75, pp. 855-858, (1984, no. 3).

[67] Y. J. Kang and J. S. Bolton, "Optimal Design of Acoustical Foam Treatments," J. Vib. and Acoust., Transactions of the ASME, vol. 118, pp. 498-504, (1996 Jul.).

[68] C. N. Wang and M. K. Tang, "Boundary element evaluation on the performance of sound absorbing wedges for anechoic chambers," Eng. Analysis with Boundary Elements, vol. 18, pp. 103-110, (1996 no. 2).

[69] T. W. Leishman, "Active Control of Sound Transmission Through Partitions Composed of Discretely Controlled Modules," Ph.D. thesis, The Pennsylvania State University, 2000.

[70] T. W. Leishman and B. E. Anderson, "Derivation of Moving-Coil Loudspeaker Driver Parameters Using Acoustical Testing Techniques, Part 1: Theoretical Developments," J. Acoust. Soc. Am., vol. 113, p. 2201A, (2003, no. 4).

[71] B. E. Anderson and T. W. Leishman, "An Acoustical Measurement Method For the Derivation of Loudspeaker Parameters," presented at the 115th Convention of the Audio Eng. Soc., (2003 Oct.), New York.

[72] ISO 10534-1:1996 and 2:1998, "Acoustics – Determination of Sound Absorption Coefficient and Impedance in Impedance Tubes – Parts 1 & 2," International Organization for Standardization, Switzerland, 1996 and 1998.

APPENDIX A

MATLAB CODES

The following pages contain all the MATLAB code developed for processing data measured in the plane wave tube.

GetParameters.m

```
%Function Get Parameters
warning off MATLAB:divideByZero

freq=0;
tau=0;
TLNA=0;
TLCC=0;
TLparametersp=zeros(10,10); %2*[fs Cms Mms Rms Bl]
TLparametersi=zeros(10,10); %2*[fs Cms Mms Rms Bl]
Rparametersp=zeros(10,10); %2*[fs Cms Mms Rms Bl]
Rparametersi=zeros(10,10); %2*[fs Cms Mms Rms Bl]

global S Sd rho c freq TLNA TLparametersp TLparametersi Rparametersp Rparametersi
global fmax fcrs S34 S56 S78 S910 Zmt Re TLCC tt ii b a iii BlarrayE

deltatau=.1;
tt=1/deltatau;
fmax=640*tt+1;   %640Hz  maximum frequency for analysis
fcrs=68*tt+1; %72.5Hz  crossover frequency between mic pairs
c=344;  %speed of sound
rho=1.21;  %density of air

S=.0929;

Rearray=[4.666 3.2194 5.8692 6.585 6.151 6.204 6.3455 5.8407 6.872...
      4.666 3.2194 5.8692 6.3455 5.8407 6.872];

iii=input('Enter in Speaker number (1-9) - ');

Re=Rearray(iii);

darray=[23.7 20.9 16.8 16.5 16.5 16.5 13 8.7 6.2...
```

```
        23.7 20.9 16.8 13 8.7 6.2];

Sdarray(iii)=pi*(darray(iii)/200).^2;

Sd=Sdarray(iii);
parameters(:,1)=Sd;
for ii=1:10
graphdata;
close all
end

%Calculate Average Values
m(1,1)=mean(TLparametersp(:,2));
m(2,1)=mean(TLparametersp(:,7));
m(3,1)=mean(TLparametersi(:,2));
m(4,1)=mean(TLparametersi(:,7));

m(5,1)=mean(TLparametersp(:,3));
m(6,1)=mean(TLparametersp(:,8));
m(7,1)=mean(TLparametersi(:,3));
m(8,1)=mean(TLparametersi(:,8));

m(9,1)=mean(TLparametersp(:,4));
m(10,1)=mean(TLparametersp(:,9));

m(11,1)=mean(TLparametersp(:,1));
m(12,1)=mean(TLparametersp(:,6));
m(13,1)=mean(TLparametersi(:,1));
m(14,1)=mean(TLparametersi(:,6));

m(15,1)=mean(TLparametersp(:,5));
m(16,1)=mean(TLparametersp(:,10));

%Compute Random Errors
m(1,2)=std(TLparametersp(:,2))/m(1,1)*100;
m(2,2)=std(TLparametersp(:,7))/m(2,1)*100;
m(3,2)=std(TLparametersi(:,2))/m(3,1)*100;
m(4,2)=std(TLparametersi(:,7))/m(4,1)*100;

m(5,2)=std(TLparametersp(:,3))/m(5,1)*100;
m(6,2)=std(TLparametersp(:,8))/m(6,1)*100;
m(7,2)=std(TLparametersi(:,3))/m(7,1)*100;
m(8,2)=std(TLparametersi(:,8))/m(8,1)*100;

m(9,2)=std(TLparametersp(:,4))/m(9,1)*100;
m(10,2)=std(TLparametersp(:,9))/m(10,1)*100;
```

```
m(11,2)=std(TLparametersp(:,1))/m(11,1)*100;
m(12,2)=std(TLparametersp(:,6))/m(12,1)*100;
m(13,2)=std(TLparametersi(:,1))/m(13,1)*100;
m(14,2)=std(TLparametersi(:,6))/m(14,1)*100;

m(15,2)=std(TLparametersp(:,5))/m(15,1)*100;
m(16,2)=std(TLparametersp(:,10))/m(16,1)*100;

m
dlmwrite('pwtdataG.txt',m,'\t')
```

GraphData.m

```
function graphdata;

global freq rho c S Sd tau TLNA TLCC fmax fcrs Zmt ii iii hcalu hcald
global hcalt cc Rmag TLparametersp TLparametersi fo Rmagcc

if ii==1
[hcalu,hcald,hcalt]=Calibration;  %run the calibration m-file
end

cd U:\MastersResearch

for cc=1:2 %1 - open circuit;  2 - closed circuit

[H1,H2,su,sd]=getfiles;

cd U:\MastersResearch

ud=1; %means upstream
ru=reflectioncoeff(H1,hcalu,ud,cc);
if cc==1
   Rmag=abs(ru);
end
if cc==2
   Rmagcc=abs(ru);
end
%ru is the complex upstream reflection coefficient

ud=2; %means downstream
rd=reflectioncoeff(H2,hcald,ud,cc);
%rd is the complex downstream reflection coefficient
```

```
d1=-36.45-[-1 -1 1.5 1 .7 1 2 2.4 2.4 -1 -1 1.5 2 2.4 2.4];
d2=-116.95-[-1 -1 1.5 1 .7 1 2 2.4 2.4 -1 -1 1.5 2 2.4 2.4];

d1=d1/100;
d2=d2/100;

k=2*pi*freq/c;

%propagate the downstream reflection coeff to the driver
%face to compute the termination impedance
if cc==1
   rd1(1:fcrs)=rd(1:fcrs).*exp(2*j*k(1:fcrs)*(d1(iii)));
   rd1(fcrs+1:fmax)=rd(fcrs+1:fmax).*exp(2*j*k(fcrs+1:fmax)*(d2(iii)));
end
if cc==2
   rd2(1:fcrs)=rd(1:fcrs).*exp(2*j*k(1:fcrs)*(d1(iii)));
   rd2(fcrs+1:fmax)=rd(fcrs+1:fmax).*exp(2*j*k(fcrs+1:fmax)*(d2(iii)));
end

if (iii>9 & iii~=11)
   d1(iii)=d1(iii)+.402+.0381;
   d2(iii)=d2(iii)+1.207+.0381;
   if cc==1
      ru1(1:fcrs)=ru(1:fcrs).*exp(2*j*k(1:fcrs)*(d1(iii)));
      ru1(fcrs+1:fmax)=ru(fcrs+1:fmax).*exp(2*j*k(fcrs+1:fmax)*(d2(iii)));
   end
   if cc==2
      ru2(1:fcrs)=ru(1:fcrs).*exp(2*j*k(1:fcrs)*(d1(iii)));
      ru2(fcrs+1:fmax)=ru(fcrs+1:fmax).*exp(2*j*k(fcrs+1:fmax)*(d2(iii)));
   end
end


transmissionloss(ru,rd,su,sd,hcalt,cc);

TLNA=smooth(TLNA,10,'loess')';

end

rda=(rd1+rd2)/2;
Zmt=rho*c*S*(1+rda)./(1-rda);

figure
subplot(211)
semilogx(freq,real(Zmt/(rho*c*S)),'b-',freq,ones(size(freq)),'b--')
```

```
axis([9 300 0 2])
ylabel('Resistance Ratio')
title('Dimensionless Resistance Ratio of Termination as Seen by DUT')
subplot(212)
semilogx(freq,imag(Zmt/(rho*c*S)),'b-',freq,zeros(size(freq)),'b--')
axis([9 300 -1 1])
xlabel('Frequency (Hz)')
ylabel('Reactance Ratio')
title('Dimensionless Reactance Ratio of Termination as Seen by DUT')

if (iii>9 & iii~=11)
   rua=(ru1+ru2)/2;
   Zmtp=rho*c*S*(1+rua)./(1-rua);
   figure
   semilogx(freq,abs(rua))
   axis([9 300 0 1])
   figure
   subplot(211)
   semilogx(freq,real(Zmt),'b-',freq,real(Zmtp),'r-')
   axis([9 300 0 100])
   subplot(212)
   semilogx(freq,imag(Zmt),'b-',freq,imag(Zmtp),'r-')
   axis([9 500 -40 40])
   pause
end

figure
semilogx(freq,Rmag,'b-',freq,Rmagcc,'b--')
axis([9 300 0 1])
xlabel('Frequency (Hz)')
ylabel('Coefficient Magnitude')
title('Reflection Coefficient Magnitude of Open (-) and Closed (--) Circuit DUT')
figure
semilogx(freq,TLNA,'b-',freq,TLCC,'b--')
axis([9 300 0 35])
xlabel('Frequency (Hz)')
ylabel('Transmission Loss (dB)')
title('Transmission Loss of Open (-) and Closed (--) Circuit DUT')

TLportionfit;
TLimpedancefit;
TLparametersp
pause
TLparametersi
pause
return
```

Calibration.m

```
function [hcalu,hcald,hcalt]=Calibration

global rho c freq tau TLNA fmax fcrs S34 S56 S78 S910 Sd tt iii

%Calibration factors (used in reflection coefficient m-file)

calrun=[20 20 34 47 34 59 47 59 71 84 84 84 84 84 84];

calstartnum=calrun(iii);
if calstartnum<=99
   index=calstartnum;      %1
   currentrun=num2str(index);
   dircalstart=(['U:\MastersResearch\cal000',currentrun]);
   cd ([dircalstart])
end

if calstartnum>99
   disp('You need to change the Calibration.m file. \n')
   disp('Since your number is 100 or greater the cal000 \n')
   disp('needs to be cal00.');
   pause
end

numheaderlines=5;
FS=['H3, 4sv00000.txt'];
[A,B,C]=textread([FS],'%f%f%f','delimiter','\t','headerlines',...
   numheaderlines);  %first part in [] is the complete path to be read
freq=A';
tau=zeros(1,length(freq));
TLA=zeros(1,length(freq));
TLNA=zeros(1,length(freq));
TLfit=zeros(1,length(freq));

H34or=B;
H34oi=C;

index=index+1;            %2
currentrun=num2str(index);
dircalstart=(['U:\MastersResearch\cal000',currentrun]);
cd ([dircalstart])

FS=['H5, 6sv00000.txt'];
[A,B,C]=textread([FS],'%f%f%f','delimiter','\t','headerlines',...
   numheaderlines);  %first part in [] is the complete path to be read
```

```
H56or=B;
H56oi=C;

index=index+1;            %3
currentrun=num2str(index);
dircalstart=(['U:\MastersResearch\cal000',currentrun]);
cd ([dircalstart])

FS=['H7, 8sv00000.txt'];
[A,B,C]=textread([FS],'%f%f%f','delimiter','\t','headerlines',...
   numheaderlines);  %first part in [] is the complete path to be read

H78or=B;
H78oi=C;

index=index+1;            %4
currentrun=num2str(index);
dircalstart=(['U:\MastersResearch\cal000',currentrun]);
cd ([dircalstart])

FS=['H9, 10sv00000.txt'];
[A,B,C]=textread([FS],'%f%f%f','delimiter','\t','headerlines',...
   numheaderlines);  %first part in [] is the complete path to be read

H910or=B;
H910oi=C;

index=index+3;            %7
currentrun=num2str(index);
dircalstart=(['U:\MastersResearch\cal000',currentrun]);
cd ([dircalstart])

FS=['H3, 4sv00000.txt'];
[A,B,C]=textread([FS],'%f%f%f','delimiter','\t','headerlines',...
   numheaderlines);  %first part in [] is the complete path to be read

H34sr=B;
H34si=C;

index=index+1;            %8
currentrun=num2str(index);
dircalstart=(['U:\MastersResearch\cal000',currentrun]);
cd ([dircalstart])

FS=['H5, 6sv00000.txt'];
```

```
[A,B,C]=textread([FS],'%f%f%f','delimiter','\t','headerlines',...
   numheaderlines);  %first part in [] is the complete path to be read

H56sr=B;
H56si=C;

index=index+1;            %9
currentrun=num2str(index);
dircalstart=(['U:\MastersResearch\cal000',currentrun]);
cd ([dircalstart])

FS=['H7, 8sv00000.txt'];
[A,B,C]=textread([FS],'%f%f%f','delimiter','\t','headerlines',...
   numheaderlines);  %first part in [] is the complete path to be read

H78sr=B;
H78si=C;

index=index+1;            %10
currentrun=num2str(index);
dircalstart=(['U:\MastersResearch\cal000',currentrun]);
cd ([dircalstart])

FS=['H9, 10sv00000.txt'];
[A,B,C]=textread([FS],'%f%f%f','delimiter','\t','headerlines',...
   numheaderlines);  %first part in [] is the complete path to be read

H910sr=B;
H910si=C;

cd U:\MastersResearch
%Upstream calibration factor
hcalu=gethcal(H34or,H34oi,...
   H34sr,H34si,H56or,...
   H56oi,H56sr,H56si);

%Downstream calibration factor
hcald=gethcal(H78or,H78oi,...
   H78sr,H78si,H910or,...
   H910oi,H910sr,H910si);


index=index-5;            %5
currentrun=num2str(index);
dircalstart=(['U:\MastersResearch\cal000',currentrun]);
cd ([dircalstart])
```

```
FS=['H4, 7sv00000.txt'];
[A,B,C]=textread([FS],'%f%f%f','delimiter','\t','headerlines',...
   numheaderlines);  %first part in [] is the complete path to be read

H47or=B;
H47oi=C;

index=index+1;          %6
currentrun=num2str(index);
dircalstart=(['U:\MastersResearch\cal000',currentrun]);
cd ([dircalstart])

FS=['H6, 9sv00000.txt'];
[A,B,C]=textread([FS],'%f%f%f','delimiter','\t','headerlines',...
   numheaderlines);  %first part in [] is the complete path to be read

H69or=B;
H69oi=C;

index=index+5;          %11
currentrun=num2str(index);
dircalstart=(['U:\MastersResearch\cal000',currentrun]);
cd ([dircalstart])

FS=['H4, 7sv00000.txt'];
[A,B,C]=textread([FS],'%f%f%f','delimiter','\t','headerlines',...
   numheaderlines);  %first part in [] is the complete path to be read

H47sr=B;
H47si=C;

index=index+1;          %12
currentrun=num2str(index);
dircalstart=(['U:\MastersResearch\cal000',currentrun]);
cd ([dircalstart])

FS=['H6, 9sv00000.txt'];
[A,B,C]=textread([FS],'%f%f%f','delimiter','\t','headerlines',...
   numheaderlines);  %first part in [] is the complete path to be read

H69sr=B;
H69si=C;

%Hcal is calculated for the mics just upstream and just downstream for each
%freq spacing mic pair m-file
```

```
%Low freq. mic spacing
h1(1:fcrs)=H47or(1:fcrs)+j*H47oi(1:fcrs);
h2(1:fcrs)=H47sr(1:fcrs)+j*H47si(1:fcrs);

%High freq. mic spacing
h1(fcrs+1:fmax)=H69or(fcrs+1:fmax)+j*H69oi(fcrs+1:fmax);
h2(fcrs+1:fmax)=H69sr(fcrs+1:fmax)+j*H69si(fcrs+1:fmax);

%calibration factor determined here
hcalt=sqrt(h1.*h2);


%Compute Mic Pair Spacing
phase34=unwrap(angle(H34or(9*tt+1:500*tt+1)+j*H34oi(9*tt+1:500*tt+1)));
phase56=unwrap(angle(H56or(9*tt+1:500*tt+1)+j*H56oi(9*tt+1:500*tt+1)));
phase78=unwrap(angle(H78or(9*tt+1:500*tt+1)+j*H78oi(9*tt+1:500*tt+1)));
phase910=unwrap(angle(H910or(9*tt+1:500*tt+1)+j*H910oi(9*tt+1:500*tt+1)));
s34(1:9*tt)=0;
s56(1:9*tt)=0;
s78(1:9*tt)=0;
s910(1:9*tt)=0;
s34(9*tt+1:500*tt+1)=-phase34*c./(2*pi*freq(9*tt+1:500*tt+1)');
s56(9*tt+1:500*tt+1)=-phase56*c./(2*pi*freq(9*tt+1:500*tt+1)');
s78(9*tt+1:500*tt+1)=-phase78*c./(2*pi*freq(9*tt+1:500*tt+1)');
s910(9*tt+1:500*tt+1)=-phase910*c./(2*pi*freq(9*tt+1:500*tt+1)');
s34(500*tt+2:640*tt+1)=0;
s56(500*tt+2:640*tt+1)=0;
s78(500*tt+2:640*tt+1)=0;
s910(500*tt+2:640*tt+1)=0;

fl=60;
fh=500;

for i=fl*tt+1:fh*tt+1
   ras34(i)=mean(s34(fl*tt+1:i));
   ras78(i)=mean(s78(fl*tt+1:i));
   ras56(i)=mean(s56(fl*tt+1:i));
   ras910(i)=mean(s910(fl*tt+1:i));
end

S34=ras34(length(ras34)-2);
S78=ras78(length(ras78)-2);

S56=ras56(length(ras56)-2);
S910=ras910(length(ras910)-2);
```

GetHcal.m

```
function hcal=gethcal(ro1,io1,rs1,is1,ro2,io2,rs2,is2)

global freq fmax fcrs

%This function takes in the real part of the original position transfer
%function (ro), the imag. part of the orig. position transfer function
%(io), the real part of the switched position transfer function (rs),
%and the imag. part of the switched position transfer function (is).
%It then computes the spliced calibration factor.

%transfer function for original configuration

h1(1:fcrs)=ro1(1:fcrs)+j*io1(1:fcrs);
h1(fcrs+1:fmax)=ro2(fcrs+1:fmax)+j*io2(fcrs+1:fmax);

%transfer function for switched configuration
h2(1:fcrs)=rs1(1:fcrs)+j*is1(1:fcrs);
h2(fcrs+1:fmax)=rs2(fcrs+1:fmax)+j*is2(fcrs+1:fmax);

%calibration factor
hcal=sqrt(h1.*h2);

return
```

GetFiles.m

```
function [H1,H2,Su,Sd,coherence]=getfiles

global freq TLNA parameters fmax fcrs iii cc ii

   open(1,1:10)=15:1:24;
   open(2,1:10)=37:1:46;
   open(3,1:10)=60:1:69;
   open(4,1:10)=118:1:127;
   open(5,1:10)=86:1:95;
   open(6,1:10)=169:1:178;
   open(7,1:10)=145:1:154;
   open(8,1:10)=195:1:204;
   open(9,1:10)=218:1:227;
   open(10,1:10)=250;
   open(11,1)=[261 262 263 264 255 265 266 267 268 256 257 258 259 260];
   open(12,1)=252;
```

```
    open(13,1)=253;
    open(14,1)=254;
    open(15,1)=254;

    closed(1,1:10)=26:1:35;
    closed(2,1:10)=49:1:58;
    closed(3,1:10)=71:1:80;
    closed(4,1:10)=132:1:141;
    closed(5,1:10)=106:1:115;
    closed(6,1:10)=180:1:189;
    closed(7,1:10)=157:1:166;
    closed(8,1:10)=206:1:215;
    closed(9,1:10)=229:1:238;
    closed(10,1)=250;
    closed(11,1)=[261 262 263 264 255 265 266 267 268 256 257 258 259 260];
    closed(12,1)=251;
    closed(13,1)=252;
    closed(14,1)=253;
    closed(15,1)=254;

    if cc==1
       number=open(iii,ii);
    end
    if cc==2
       number=closed(iii,ii);
    end

index=int2str(number);
if number<100
    filename=['U:\MastersResearch\data000',index];
end
if number>99
    filename=['U:\MastersResearch\data00',index];
end

cd ([filename])

%some needed constants (number of header lines in the data,
%number of microphones, number of spectral lines in each measurement.)
numheaderlines=6;
FS=['Gxxsv00000.txt'];
[A,B,C,D,E,F]=textread([FS],'%f%f%f%f%f%f','delimiter','\t','headerlines',...
    numheaderlines);  %first part in [] is the complete path to be read

%Get auto power spectrums in usable form
S2=B(1:fmax);
```

```
Su4=C(1:fmax);
Su6=D(1:fmax);
Sd7=E(1:fmax);
Sd9=F(1:fmax);
if iii>9
   Su4=B(1:fmax);
   Su6=C(1:fmax);
   Sd7=D(1:fmax);
   Sd9=E(1:fmax);
end

%Combine freq spacing pairs
Su(1:fcrs)=Su4(1:fcrs).^2;
Su(fcrs+1:fmax)=Su6(fcrs+1:fmax).^2;
Sd(1:fcrs)=Sd7(1:fcrs).^2;
Sd(fcrs+1:fmax)=Sd9(fcrs+1:fmax).^2;
if iii>9
   numheaderlines=5;
end
if iii<10
   numheaderlines=6;
end
FS=['H3ysv00000.txt'];
[A,B,C,D,E]=textread([FS],'%f%f%f%f%f','delimiter','\t','headerlines',...
   numheaderlines);
r34=D;
i34=E;
if iii>9
   r34=B;
   i34=C;
end
FS=['H5ysv00000.txt'];
[A,B,C,D,E]=textread([FS],'%f%f%f%f%f','delimiter','\t','headerlines',...
   numheaderlines);
r56=D;
i56=E;
if iii>9
   r56=B;
   i56=C;
end
FS=['H7ysv00000.txt'];
[A,B,C,D,E]=textread([FS],'%f%f%f%f%f','delimiter','\t','headerlines',...
   numheaderlines);
r78=D;
i78=E;
if iii>9
```

```
   r78=B;
   i78=C;
end
FS=['H9ysv00000.txt'];
[A,B,C,D,E]=textread([FS],'%f%f%f%f%f','delimiter','\t','headerlines',...
   numheaderlines);
r910=D;
i910=E;
if iii>9
   r910=B;
   i910=C;
end

H34=r34+j*i34;
H56=r56+j*i56;

H78=r78+j*i78;
H910=r910+j*i910;

%Get transfer functions
H1(1:fcrs)=H34(1:fcrs);
H1(fcrs+1:fmax)=H56(fcrs+1:fmax);
H2(1:fcrs)=H78(1:fcrs);
H2(fcrs+1:fmax)=H910(fcrs+1:fmax);
```

ReflectionCoeff.m

```
function [r]=reflectioncoeff(ho,hcal,ud,cc)

global rho c S Sd freq TLNA parameters fmax fcrs S34 S56 S78 S910

%This function takes in an array of frequencies (freq), the uncalibrated
%transfer function, the calibration factor, ud which just lets the program
%know whether or not it is calculating upstream or downstream, and the
%maximum frequency for analysis.
%It also returns the complex reflection coefficient.
%See ASTM E 1050-90; Chung and Blaser, JASA 68(3), pp. 907-913

k=2*pi*freq/c;   %wave number array
if ud==1         %Upstream
   s1=S34;       %Spacing between low freq mic pair
   s2=S56;       %Spacing Between high freq mic pair
end
if ud==2         %Downstream
```

```
   s1=S78;       %Spacing between low freq mic pair
   s2=S910;      %Spacing Between high freq mic pair
end
len1=.3659+.05;
len2=1.1689+.05;
H=ho./hcal;      %Actual transfer function at reference mic position

%Upstream (needs to be propagated to the downsteam mic in the pair)
if ud==1
   r(1:fcrs)=(H(1:fcrs)-exp(-j*k(1:fcrs)*s1))./(exp(j*k(1:fcrs)*s1)...
      -H(1:fcrs)).*exp(2*j*k(1:fcrs)*(s1)); %reflection coeff.
   r(fcrs+1:fmax)=(H(fcrs+1:fmax)-exp(-j*k(fcrs+1:fmax)*s2))...
      ./(exp(j*k(fcrs+1:fmax)*s2)-H(fcrs+1:fmax))...
      .*exp(j*2*k(fcrs+1:fmax)*(s2)); %reflection coefficient

   rul=(H-exp(-j*k*s1))./(exp(j*k*s1)-H).*exp(2*j*k*s1);

   Ru(1:fcrs)=r(1:fcrs).*exp(2*j*k(1:fcrs)*len1);
   Ru(fcrs+1:fmax)=r(fcrs+1:fmax).*exp(2*j*k(fcrs+1:fmax)*len2);
end

%Downstream (no propagation needed)
if ud==2
   r(1:fcrs)=(H(1:fcrs)-exp(-j*k(1:fcrs)*s1))./(exp(j*k(1:fcrs)*s1)...
      -H(1:fcrs)); %reflection coefficient
   r(fcrs+1:fmax)=(H(fcrs+1:fmax)-exp(-j*k(fcrs+1:fmax)*s2))...
      ./(exp(j*k(fcrs+1:fmax)*s2)-H(fcrs+1:fmax)); %reflection coeff.
end
return
```

TransmissionLoss.m

```
function transmissionloss(ru,rd,su,sd,hcalt,cc)

global freq tau TLNA fmax fcrs TLCC tt fo

%This function takes in the upstream reflection coefficient (ru),
%the downstream reflection coefficient (rd), the auto spectrum of
%the mic just upstream of the DUT (su), the auto spectrum of the
%mic just downstream of the DUT (sd), the complex calibration factor
%between the mics used for the auto spectrum (hcal).
%The transmission loss of the DUT is outputted to a global variable.

%Chung and Blaser, JASA 68(3), pp. 907-913
```

```
rho=1.21;
c=343;
S=.0929;

tau(1:fcrs)=sd(1:fcrs)./su(1:fcrs)./(abs(hcalt(1:fcrs))).^2.*...
   (abs((1+ru(1:fcrs))./(1+rd(1:fcrs)))).^2;  %transmission coeff.

tau(fcrs+1:fmax)=sd(fcrs+1:fmax)./su(fcrs+1:fmax)./(abs(...
   hcalt(fcrs+1:fmax))).^2.*(abs((1+ru(fcrs+1:fmax))./...
   (1+rd(fcrs+1:fmax)))).^2;  %transmission coeff.

if cc==2
   TLCC=10*log10(1./tau); %Transmission Loss calculated from transmission coeff.
end

if cc==1
   TLNA=10*log10(1./tau); %Transmission Loss calculated from transmission coeff.

   TLNA(1:9*tt)=20; %Arbitrarily set to 20 dB (not valid data anyway
end

return
```

TLPortionFit.m

```
function TLportionfit;

global freq TLNA TLparametersp fmax fcrs S Sd rho c Re TLCC Zmt ii
global fClow fChigh fMlow fMhigh fo startBi endBi startLi endLi BlarrayE

w=2*pi*freq;

C=rho*c*S;
D=(Sd/S)^2;

[TLo,findex]=min(TLNA(100:2000));
fo=round(findex-1)/10+9.9
findex=round(fo*10+1)

%Assuming non-anechoic termination and compensating for it

Rmt=real(Zmt);
Imt=imag(Zmt);
```

```
Rms=(Sd/S)^2*(sqrt(((C+Rmt(findex))^2+(Imt(findex))^2)*10.^(TLo/10)-...
   (Imt(findex))^2)-(C+Rmt(findex)))

Xms=D*(sqrt(((C+Rmt).^2+(Imt).^2).*10.^(TLNA/10)-(C+Rmt+Rms/D).^2)-Imt);

Mmdarray=Xms./w;

if ii==1
   figure
   semilogx(freq(40*10+1:6401),Mmdarray(40*10+1:6401)*1000,'b-')
   title('Mmd array')
   axis([9 300 0 150])
   xlabel('Frequency (Hz)')
   ylabel('gm')
   title('High Frequency Mmd Estimate (-) With Fit (--)')
   fMlow=input('Enter in lower freq for Mmd evaluation - ');
   fMlow=fMlow*10+1;
   fMhigh=input('Enter in higher freq for Mmd evaluation - ');
   fMhigh=fMhigh*10+1;
end

Mmd=mean(Mmdarray(fMlow:fMhigh))
hold on
semilogx(freq,1000*Mmd*ones(size(freq)),'b--')

Mms=Mmd+8/3*rho*(Sd/pi)^1.5

Cms=1/((2*pi*fo)^2*Mmd)

Le=1e-3
Xe=w*Le;
invtauNA=10.^(TLNA/10);
invtauCC=10.^(TLCC/10);
%Assuming Le is known
%pos root
Blarray1=sqrt(D)*sqrt(-Re*(Rmt+C+Rms/D)+Xe.*(Xms/D+Imt)+...
   sqrt(invtauCC.*((Rmt+C).^2+Imt.^2).*(Re^2+Xe.^2)-...
   ((Xms/D+Imt)*Re+(Rmt+C+Rms/D).*Xe).^2));
%neg root
Blarray2=sqrt(D)*sqrt(-Re*(Rmt+C+Rms/D)+Xe.*(Xms/D+Imt)-...
   sqrt(invtauCC.*((Rmt+C).^2+Imt.^2).*(Re^2+Xe.^2)-...
   ((Xms/D+Imt)*Re+(Rmt+C+Rms/D).*Xe).^2));

%Neglecting impedance due to Le,
%low frequency estimate
BlarrayE=sqrt(Re*D*(sqrt(invtauCC.*((Rmt+C).^2+Imt.^2)-...
```

```
   (Xms/D+Imt).^2)-(Rmt+C+Rms/D)));

if ii==1
   figure
   semilogx(freq,BlarrayE,'b-')
   axis([9 300 0 10])
   title('Low Frequency Bl Estimate (-) With Extrapolated Fit (--)')
   xlabel('Frequency (Hz)')
   ylabel('T*m')
   startBi=input('Enter in starting freq - ');
   startBi=startBi*10+1;
   endBi=input('Enter in ending freq - ');
   endBi=endBi*10+1;
end

Blline=real(BlarrayE(startBi:endBi));
fline=freq(startBi:endBi);

%Linear fit to Bl array
P=polyfit(fline,Blline,1);
Bl=P(2)
hold on
semilogx(freq,P(1)*freq+P(2),'b--')

Bl2=Bl^2;

gamma=invtauCC.*(Imt.^2+(Rmt+C).^2)-...
   ((Rmt+C+Rms/D).^2+(Xms/D+Imt).^2);
%Once Bl is known
%pos root
Learray1=(-Bl2/D*(Xms/D+Imt)+sqrt(-(Re*gamma).^2+...
   (Bl2/D)^2*(gamma+(Xms/D+Imt).^2)+Re*gamma*Bl2/D*2.*...
   (Rmt+C+Rms/D))./(w.*gamma);
%neg root
Learray2=(-Bl2/D*(Xms/D+Imt)-sqrt(-(Re*gamma).^2+...
   (Bl2/D)^2*(gamma+(Xms/D+Imt).^2)+Re*gamma*Bl2/D*2.*...
   (Rmt+C+Rms/D))./(w.*gamma);

if ii==1
   figure
   semilogx(freq,20000*Learray1,'b-',freq,20000*Learray2,'r-')
   axis([9 300 0 1e-2*2000])
   title('Broadband Le Curve')
   xlabel('Frequency (Hz')
   ylabel('mH')
end
```

```
fs=1/2/pi*sqrt(1/(Mms*Cms))

TLparametersp(ii,6)=fs;  %[fs Cms Mms Rms Bl]
TLparametersp(ii,7)=Cms*1e6;
TLparametersp(ii,8)=Mms*1e3;
TLparametersp(ii,9)=Rms;
TLparametersp(ii,10)=Bl;


%Assuming Anechoic termination
Rmt=C*ones(size(freq));
Imt=zeros(size(freq));

Rms=(Sd/S)^2*(sqrt(((C+Rmt(findex))^2+(Imt(findex))^2)*10.^(TLo/10)-...
   (Imt(findex))^2)-(C+Rmt(findex)))

Xms=D*(sqrt(((C+Rmt).^2+(Imt).^2).*10.^(TLNA/10)-(C+Rmt+Rms/D).^2)-Imt);

Mmdarray=Xms./w;

if ii==1
   figure
   semilogx(freq,Mmdarray)
   title('Mmd array')
   axis([9 500 0 .3])

   fMlow=input('Enter in lower freq for Mmd evaluation - ');
   fMlow=fMlow*10+1;
   fMhigh=input('Enter in higher freq for Mmd evaluation - ');
   fMhigh=fMhigh*10+1;
end

Mmd=mean(Mmdarray(fMlow:fMhigh))
Mms=Mmd+8/3*rho*(Sd/pi)^1.5

Cms=1/((2*pi*fo)^2*Mmd)

Le=1e-3
Xe=w*Le;
invtauNA=10.^(TLNA/10);
invtauCC=10.^(TLCC/10);
%Assuming Le is known
%pos root
Blarray1=sqrt(D)*sqrt(-Re*(Rmt+C+Rms/D)+Xe.*(Xms/D+Imt)+...
```

```
   sqrt(invtauCC.*((Rmt+C).^2+Imt.^2).*(Re^2+Xe.^2)-...
   ((Xms/D+Imt)*Re+(Rmt+C+Rms/D).*Xe).^2));
%neg root
Blarray2=sqrt(D)*sqrt(-Re*(Rmt+C+Rms/D)+Xe.*(Xms/D+Imt)-...
   sqrt(invtauCC.*((Rmt+C).^2+Imt.^2).*(Re^2+Xe.^2)-...
   ((Xms/D+Imt)*Re+(Rmt+C+Rms/D).*Xe).^2));

%Neglecting impedance due to Le,
%low frequency estimate
BlarrayE=sqrt(Re*D*(sqrt(invtauCC.*((Rmt+C).^2+Imt.^2)-...
   (Xms/D+Imt).^2)-(Rmt+C+Rms/D)));

Blline=real(BlarrayE(startBi:endBi));
fline=freq(startBi:endBi);
%Linear fit to Bl array
P=polyfit(fline,Blline,1);
Bl=P(2);

Bl2=Bl^2;

gamma=invtauCC.*(Imt.^2+(Rmt+C).^2)-...
   ((Rmt+C+Rms/D).^2+(Xms/D+Imt).^2);
%Once Bl is known
%pos root
Learray1=(-Bl2/D*(Xms/D+Imt)+sqrt(-(Re*gamma).^2+...
   (Bl2/D)^2*(gamma+(Xms/D+Imt).^2)+Re*gamma*Bl2/D*2.*...
   (Rmt+C+Rms/D))./(w.*gamma);
%neg root
Learray2=(-Bl2/D*(Xms/D+Imt)-sqrt(-(Re*gamma).^2+...
   (Bl2/D)^2*(gamma+(Xms/D+Imt).^2)+Re*gamma*Bl2/D*2.*...
   (Rmt+C+Rms/D))./(w.*gamma);

if ii==1
   figure
   semilogx(freq,Learray1,'b-',freq,Learray2,'g-')
   axis([9 500 0 1e-2])
   title('Le array root 1 (blue), root 2 (green)')
end

fs=1/2/pi*sqrt(1/(Mms*Cms));

TLparametersp(ii,1)=fs;  %[fs Cms Mms Rms Bl]
TLparametersp(ii,2)=Cms*1e6;
TLparametersp(ii,3)=Mms*1e3;
TLparametersp(ii,4)=Rms;
TLparametersp(ii,5)=Bl;
```

TLImpedanceFit.m

```
function TLimpedancefit;

global freq TLNA TLparametersi fmax fcrs S Sd rho c Re TLCC Zmt ii
global fClow fChigh fMlow fMhigh b a fo

Rmt=real(Zmt);
Imt=imag(Zmt);

w=2*pi*freq;
C=rho*c*S;

TLo=TLNA(round(fo*10+1));

f=freq(9*10+1:500*10+1);
findex=round(fo*10+1);

Rms=(Sd/S)^2*(2*C*10^(TLo/20)-2*C);

Zm=(Sd/S)^2*(Rms+j*sqrt((2*C)^2*10.^(TLNA/10)-(2*C+Rms*(S/Sd)^2)^2));

phase(1:findex)=-1*angle(Zm(1:findex));
phase(findex+1:6401)=angle(Zm(findex+1:6401));

Zm=abs(Zm).*exp(j*phase);
Z=abs(Zm).*exp(j*phase)-Rms;

wt=1./freq(9*10+1:300*10+1)./(Z(9*10+1:300*10+1).^2);
[b,a]=invfreqs(Z(9*10+1:300*10+1),w(9*10+1:300*10+1),2,1,wt);
Zfit=freqs(b,a,w);
[junk,fsi]=min(Zfit);
foimp=w(fsi)/2/pi;
Mmd=b(1)*1e3;
Mms=Mmd+1e3*8/3*rho*(Sd/pi)^1.5;
Cms=1/b(3)*1e6;
fs=1/(2*pi)*sqrt(1/(Cms*Mms/1e9));
Bl=0;

TLparametersi(ii,1)=fs; %[fs Cms Mms Rms Bl]
TLparametersi(ii,2)=Cms;
TLparametersi(ii,3)=Mms;
TLparametersi(ii,4)=Rms;
TLparametersi(ii,5)=Bl;
```

```
%Assuming non-anechoic termination and compensating for it
Rms=(Sd/S)^2*(sqrt(((C+Rmt(findex))^2+(Imt(findex))^2)*10.^(TLo/10)-
(Imt(findex))^2)-(C+Rmt(findex)));
Zm=(Sd/S).^2.*(Rms+j*sqrt(((C+Rmt).^2+(Imt).^2).*10.^(TLNA/10)-
(C+Rmt+Rms*(S/Sd)^2).^2)-Imt);

phase(1:findex)=-1*angle(Zm(1:findex));
phase(findex+1:6401)=angle(Zm(findex+1:6401));

Zm=abs(Zm).*exp(j*phase);
Z=abs(Zm).*exp(j*phase)-Rms;

wt=1./freq(9*10+1:300*10+1)./(Z(9*10+1:300*10+1).^2);
[b,a]=invfreqs(Z(9*10+1:300*10+1),w(9*10+1:300*10+1),2,1,wt);
Zfit=freqs(b,a,w);

Mmd=b(1)*1e3;
Mms=Mmd+1e3*8/3*rho*(Sd/pi)^1.5;
Cms=1/b(3)*1e6;
Bl=0;
fs=1/(2*pi)*sqrt(1/(Mms*Cms/1e9));

figure
subplot(211)
semilogx(freq,abs(Zm),'b-',freq,abs(Zfit),'b--')
axis([9 50 0 100])
ylabel('Mechanical Ohms')
title('Magnitude of Complex Reactance Curve Fit')
subplot(212)
semilogx(freq,angle(Zm),'b-',freq,angle(Zfit),'b--')
axis([9 300 -4 4])
xlabel('Frequency (Hz)')
ylabel('Radians')
title('Phase of Complex Reactance Curve Fit')

TLparametersi(ii,6)=fs;  %[fs Cms Mms Rms Bl]
TLparametersi(ii,7)=Cms;
TLparametersi(ii,8)=Mms;
TLparametersi(ii,9)=Rms;
TLparametersi(ii,10)=Bl;
```

VITA

Brian E. Anderson

Brian E. Anderson was born on August 27, 1977 to Vance N. Anderson and Carla D. Peterson Anderson in Santa Clara, California. He earned a Bachelor of Science Degree in General Physics from Brigham Young University. This thesis has been submitted as part of the requirements for the Master of Science Degree in Physics (Acoustics Emphasis) from Brigham Young University. He served as an officer in the Society of Physics Students (SPS) in the BYU student chapter. Brian has worked on the technical support staff at Larson Davis, Inc. in Provo, UT. As a graduate student at BYU, Brian also worked on research projects in the areas of Musical Acoustics, Noise Control, and Architectural Acoustics. He was the chairman of the Brigham Young University student section of the Audio Engineering Society. Brian is currently beginning his service as a member of the Student Council for the Acoustical Society of America representing the Technical Committee on Noise Acoustics. Currently, he is pursuing his a Doctorate of Science Degree in Acoustics at the Pennsylvania State University.